SQUEEZING THROUGH THE GUT: MICRO-MANUFACTURING OF SMART CAPSULE

A thesis presented in partial fulfilment of the requirements for the degree of

Master of Engineering

in

THE SCHOOL OF FOOD AND ADVANCED TECHNOLOGY

at Massey University, Palmerston North,

New Zealand.

Martin Christopher Allen

2025

Contents

List of Tables

List of Figures

Abstract

Capsule robotics has been an important part of medical evaluation of conditions within the Gastro-intestinal (GI) tract since their inception in 1957. As technology improved, their functionality expanded to explore the entirety of the GI tract such as; taking images; measuring chemical and mechanical properties; delivering drugs; performing biopsies; and retrieving samples of microbiome. This has led to a significant increase in adoption with over 130,000 procedures conducted annually; however, approximately 1,400 of these procedures result in capsule retention, which requires surgery to remove the capsule. This risk is significantly increased, with patients suffering from inflammatory bowel diseases such as Crohn's disease being approximately 8 times more likely to retain capsules. This thesis investigates how to improve the safety and motility of microrobotic capsules, especially for those with intestinal complications, to ensure equal access to this technology and improve patient outcomes, increasing access to the information needed to better treat these ailments. This project covers multi-disciplinary subject areas ranging from biomedical technology, mechanical characterisation, robotics, and electronics. Including the design and manufacture of capsule exteriors down to the microscale and the development of new testing equipment for them, such as a synthetic intestine tensile testing platform and robotic intestine testing system for quantifying capsule performance inside an intestinal-like environment. In addition, a precise testing procedure is provided with the created equipment so that experiments can be easily replicated and accurate data are collected. The best capsule design determined is a three-dimensional resin printed capsule using surgical guide resin with a six-ridged segmented design. Determined using force response data from pulling capsule designs and measuring the excess power draw to push them through a synthetic intestinal constriction. This also demonstrated the functionality of the testing equipment developed during this research project. In the future, these capsule design considerations are expected to be used to increase the adoption of this field of technology and improve patient outcomes. Also, it is hoped the testing equipment is used and developed further by my research group to improve their respective project outcomes; and by any external group looking to test their capsule prototypes.

Dedication

To my loving parents, Roy and Heidi Allen, for their unwavering support throughout my education; and in memory of my beloved great-aunt, Annette Helliwell (1934-2025), whose strength and kindness I will always miss.

Acknowledgements

First and foremost I will acknowledge my parents Roy and Heidi Allen for being the most supportive and amazing people I could ever hope to have as parents. Through all the highs and the lows they never gave up on me, so I never gave up on myself, and for that I will always love them and be truly thankful.

This thesis is dedicated to the memory of my lovely Aunty Net (Annette Helliwell), who passed away the day before I submitted my thesis. She was a constant source of love and support throughout my education, especially during the tough times when I would take the train to visit her in Paraparaumu. I will always remember her kindness and generosity - the world feels so much bleaker without her.

I am extremely grateful to my supervisors, Ebu Avci, Volker Nock, and David Thomas; my panel of experts behind my thesis. Without Ebu, this project would never have happened and the support for fully funding this research project meant that I never had to go hungry. His expertise and passion for microrobotics is infectious; and I have always enjoyed our conversations while walking and running. His immense support through the closure of the engineering department at Massey University helped me land on my feet and finish this thesis, which I will always be grateful for. Volker Nock gave me a new home for my project at the University of Canterbury (UC) after the closure and has done an amazing job establishing our research group down south. His generosity in educating me and providing me with some of the best facilities in the country will always be appreciated. Last but not least, I am grateful for David Thomas, who for little benefit of his own, did the paperwork necessary for my Masters programme, and attended group meetings. Also for reading my thesis while attending a pet food conference.

The next acknowledgement goes to the hard-working former workshop technicians in the engineering department at Massey in Palmy, who provided amazing technical and practical advice throughout my study. Special thanks go to Simon Lookmire, who was like an unofficial supervisor to me. This also extends to the workshop technicians of the ECE wing, Nigel Pink and Paul Agger, because talking with you guys always filled me with inspiration and cheer needed to finish my thesis. Another special thanks to Oscar Torres for helping with tensile testing at the Material Testing Laboratory at

the Mechanical Engineering Department at UC. Since they are too numerous, I will also thank all remaining staff (academic, technical, and administrative) in the former School of Food and Advanced Technology (SFAT), if I needed help from anyone, I could just walk into any lab or office and consult whoever I needed. I also thank the remaining staff of the ECE wing for giving me anything from electronic equipment to zip ties.

A special acknowledgement to my Uncle Rob (Robert Allen), who has the patience of a saint through all the difficulties I faced with relocation to UC. He gave me a free room in Lincoln and many fun and memorable adventures in hunting, fishing, hiking, and gold prospecting. He ensured that I could have fun despite the fact that I do not have a car. His guidance as a retired academic has also been valuable during my education. It has been a privilege to paint your fence and roof for you.

In addition, I thank my sister Natalie for letting me stay in her Auckland apartment while visiting for unrelated academic and personal activities, which I hope she will have an amazing honours year in. I also thank my sisters Emily and Antonia for being a source of fun in Palmy; and my sister Elke with her partner and lovely children. Extra thanks to all other family including my oma, opa, tantes, onkles, aunties, uncles, half-siblings, nieces, nephews, cousins.

Another special acknowledgement has to go to my best friend Reagan (Qianxing Zeng). It felt like a short time ago that we buddied up for a physics lab session at summer school in 2019 at the very start of our tertiary education and that by some miracle through pandemic and subsequent de-syncing of our education programmes we still remain strong friends; and it was an honour to have you for Christmas when stuck in NZ due to border restrictions. We had a great time learning together. I also thank my other best friend David Tastard, whose old laptop was very loud. You always supported me through those difficult group projects and continued to be a good friend through my Masters. I also thank my friend Shaun Garea for all the laughs we shared together at GRAIL with the crew; and Evan Ritchie at UC for the fun hikes, beach trips, and skiing trips. I hope I am as fast as you one day.

Thanks to the MacDiarmid Institute and MESA members. This organisation has made post-graduate research fun and engaging. I love the times we got to travel together, go to conferences, symposiums, camps, and other fun activities. You guys keep innovation alive in New Zealand.

I thank all the post-graduate members of the former Massey Microrobotics Group for providing constant academic support, a good yarn, and staying tight during the difficult times in chronological order: Muhammad Rehan, Phillipa Kate-Andrew, Nicholas Carlisle, Farzaneh Baserisalehi, Atusa Ghorbani Siavashani, Angus Quigly, and Adam Carlisle.

I thank all the former students at Massey engineering who I had some great parties and friendships with, and the post-graduate students at ECE UC for those wonderful lunch breaks. I thank Chris Hann for doing so much for UC engineering post-grads, and helping me with 3-minute thesis. I also thank Dianne Stock and the others at The Centre / Te Wairoa Massey for their guidance, lunch, piano, and pancakes. Also for all the fun had with the following clubs: TECHENSOC; Massey Tabletop; Massey Surf, Ski, & Skate; MUAC; Massey Hunting & Fishing Club; SAGA Inc; CUSSC. Lastly, a thanks to everyone who was subjected to my questionable writing for D&D.

Lastly, although this predates uni, I thank Whaea Risalie at Murupara Area School, the best maths teacher I could ever hope for; and Mrs Taylor at Galatea School, without whom I would never have left reading recovery and become literate enough to do a Masters thesis.

Funding

This Masters project was funded by the New Zealand Ministry of Business, Innovation and Employment (MBIE) MAUX2205 and the Ken and Elizabeth Powell Bursary Fund.

Abbreviations

2.5D - Two-Point-Five-Dimensional
3D - Three-Dimensional
4L-PEG - 4L-Polyethylene Glycole
ABS - Acrylonitrile Butadiene Styrene
BMI - Body Mass Index
CMOS - Complementary Metal-Oxide-Semiconductor
CAD - Computer Assisted Drawing
CD - Crohn's Disease
CNC - Computer Numerical Control
CR - Capsule Robot
CT - Computed Tomography
DC - Direct Current
DLP - Direct Laser Photo-polymerising
GI - Gastro-Intestinal
HCl - Hydrochloric Acid
HMP - Human Microbiome Project
IBD - Inflammatory Bowel Disease
IBS - Irritable Bowel Syndrome
IV - Intravenous
MDF - Medium Density Fibreboard
MRI - Magnetic Resonance Imaging
PC - Personal Computer
PEEK -Polyether Ether Ketone
PMMA - Poly Methyl Methacrylate
PLA - Polylactic Acid
RMS - Root Mean Square
SLA - Stereo-Lithography
UHF - Ultra-High Frequency
US - Ultrasound
UV - Ultraviolet

Symbols

O_2 - oxygen
fps - frames per second
Ø - diameter
° - degrees

Chapter 1

Introduction

With the recent development of innovative microfabrication techniques, the possibilities of microrobotic technology have expanded at an accelerated rate. This has resulted in new sensing and actuation capabilities, allowing microrobotics to explore previously unreachable areas of science [1]. The field of medical robotics is a primary benefactor of these advancements, allowing a wide range of prostheses and exploratory robotics to be developed, with interest in this research space growing exponentially. Capsule robotics is the least explored category of medical robotics with less than 70 publications in 2020, compared to more than 5,000 articles in total [2]. Meaning, there is great potential to develop novel solutions to unique problems encountered in this area.

The leading application of Capsule Robots (CR) is in the field of endoscopy, where a camera device is passed through the Gastro-Intestinal (GI) tract to allow high-quality imaging from within the small intestine. This process is significantly less invasive than traditional endoscopy and can inspect areas of the small intestine that were previously difficult to reach [3]. Recently, there has been interest in expanding the functionality of these devices to perform more complex operations such as drug delivery [4], sampling, and biopsies [5]. Among the various sampling procedures, an intriguing avenue is microbiota sampling which can help scientists understand these biomarkers within the gut. It helps identify the connections between the microbiome and general body health; and how to apply treatment accurately to the medical aliments associated with it [4, 5].

Currently, more than 130,000 capsule endoscopes are deployed annually. With the continued development of more advanced capsules with greater functionality, this number is set to continue to grow, especially when other CR types such as sampling capsules are commercially used in the future. However, with limited power capacity and possible capsule retentions, it is important to ensure that CR can transit the GI tract safely and efficiently. So operations can be successfully completed, improving patient experience, and increasing adoption by medical organisations [6].

1.1 Research Topic

The aims of this research is to improve the safety and motility of micro robotic capsules that pass through difficult areas within the small intestine of the GI tract; and to create the materials, robotics, and experimental procedures necessary to evaluate the safety and motility of micro robotic capsules.

1.2 Research Objectives

The objectives of this research are as follows:

1. Create a process for rapidly fabricating a synthetic intestinal environment.
2. Develop a test rig that uses a synthetic intestinal environment with a tensile testing machine to evaluate the performance of CR under static conditions.
3. Develop a robotic intestine to replicate peristaltic movement using a synthetic intestinal environment to evaluate the performance of CR under dynamic conditions.
4. Experiment with a wide range of shapes, materials, and manufacturing methods for CR exteriors using self-developed testing equipment; and collecting robust quantitative data on their performance.
5. Find an optimal design for the exterior of the CR which minimises the factors that cause transit to slow down and prevents retention.

1.3 Scope of Research

This research focuses on understanding the physical properties of different capsule designs after fabrication with different methods; measuring the response they have while being pulled through a static environment with a tensile testing machine; and measuring the response they have as they are pushed with peristalsis in a dynamic environment. The following parameters and processes used in this study are listed below with the range for which the measurement range in brackets.

- Analyse the surface topography of capsules from 1 to 1000 µm using contact profilometery to measure its shape and surface roughness (0.01 to 10.00 µm).
- Measure the force response of the capsules from 0.01 to 3.00 N as they are pulled through a synthetic intestine testing rig; to measure work done (0.001 to 0.050 J), average force (0.01 to 1.00 N), peak force (0.01 to 2.00 N)

- Measure the current drawn by the stepper motors that drive the robotic intestine from 0.950 to 1.05 A, with and without capsules; to calculate excess power draw for each capsule (-0.005 to 0.035 W) and the work done (0.01 to 8.00 J).

Data are collected from the School of Food and Advanced Technology at Massey University, Palmerston North; the Department of Electrical and Computer Engineering at University of Canterbury, Christchurch; and the Department of Mechanical Engineering at University of Canterbury, Christchurch. This project was conducted from the 1st of July 2023 until the 28th of February 2025.

The exclusions for this research are as follows:

- **Computer Simulation:**
  This is a thesis of practical experimentation only, which focuses on physical prototyping and experimentation. No computer simulations will be performed.
- **Environmental Variations:**
  The synthetic intestinal environment used in each experiment will be kept constant. No investigation will be conducted on how this change affects capsule performance.
- **Motor Behaviour Beyond Specified Range:**
  Capsule performance will not be evaluated when the robotic intestine is operated beyond the specified range of 0.950 to 1.05 A. Including high current scenarios, thermal effects, and degradation of motor performance.
- **Material Degradation and Long-term Effects:**
  The long-term durability and degradation when exposed to chemical conditions in the GI will not be investigated.
- **External Influences:**
  The impact of temperature fluctuations, humidity, and chemical interactions (if any) will not be examined.
- **Alternative Profilometery:**
  Methods other than contact profilometery, such as optical profilometery, scanning electron microscopy, atomic force microscopy, and other methods; will not be used to analyse surfaces.
- **Project Timeline:**
  Research activities beyond the set project period (1st of July 2023 to 28th of February 2025) will not be considered, including follow-up studies or extended data collection.

This scope has been set to ensure that the project can be reasonably completed within the time frame of a Master of Engineering degree. Computer simulation of capsule behaviour within the GI tract would complement and strengthen understanding of results but would take too much time to model and investigate within a practical project. This project will deliver new testing methods for CR evaluation and information on how to optimise their design.

1.4 Thesis Structure

This thesis is structured into five chapters:

- **Chapter 1:**
  Introduces basic contextual information from the literature to establish the focus and purpose of the thesis. The aim is stated, along with each objective being clearly listed, and the scope with necessary exclusions established providing clear expectations for the thesis below.

- **Chapter 2:**
  Covers all contextual information required to understand the issues and challenges facing the field of capsule robotics. The basic principles of human digestive system biology are explored and related to the challenges of identifying issues within the GI tract using conventional technology. It is determined how CRs overcome these difficulties but create new difficulties in the process and the literature gap within this space is identified.

- **Chapter 3:**
  Describes the prototyping process used to develop new types of capsule exteriors; the development behind the synthetic intestinal platform; and the design and development of the robotic intestine system. Each experiment is carried out within the scope of this project and has a clear procedure with all materials, equipment, and software required to complete it. All experimental aims and variable types are stated.

- **Chapter 4:**
  All data collected from experimentation are presented graphically and the relationships between variables are identified. Each experiment's results have their own discussion subsections interpreting meaning from the data using literature. All discussion is summarised at the end, stating the important determinations.

- **Chapter 5:**
  Conclusions are made on how each objective was achieved in the project and

what impact these results might have within the research group and beyond. Recommendations are made on how to proceed with this project.

Chapter 2

Literature Review

This section covers the background knowledge required to understand the context in which medical CRs operate with respect to the physical characteristics of the body. Alternative CR methods are analysed and their respective shortcomings are identified to build the case for CR usage. A wide range of existing CRs are investigated, including both commercially available designs and experimental devices from articles to understand the current state of existing technology and what could be further improved. To fully identify these problems, the risks associated with CRs are evaluated and the effects they could have on the quality of the collected data. Lastly, the information is contextualised to microbiome sampling capsules (the focus of this thesis), and the literature gap is explicitly stated.

2.1 Gastrointestinal Physiology

2.1.1 General GI Physiology

The human digestive system contains distinct sections with different conditions for medical robots. The pharynx and oesophagus require CRs to enter without mastication and mixing with saliva. The oesophagus (which is 18 to 26 cm long) uses peristaltic contractions to push objects along it while also preventing breathing, making it crucial that CRs do not get stuck. Following this, the stomach presents the most challenging environment for the CR due to strong hydrochloric acid (HCl), and muscle contractions breaking down materials over 90 to 120 min, pose additional difficulties for the CR's transit. A capsule will then travel through the small intestine through peristalsis (the focus of this thesis) and into the large intestine, where the contents are slowly churned and propelled to the colon, where it exits the GI tract [7].

2.1.2 Small Bowel Physiology

The small intestine is approximately 700 cm long and divided into the duodenum, jejunum, and ileum. The small intestine has a highly complex surface designed to maximise digestion and absorption of nutrients, resulting in a total surface area of 250 to 400 m^2 [8]. However, other sources dispute this figure and with a total surface area of only 32 m^2 thought to be more realistic [9]. The average diameter of the small intestine in an adult is 2.5 cm, and it is the narrowest section of the GI tract on average [9]. A primary feature of the small intestine are villi, cylindrical projections that increase the absorption area by ten times and secrete mucin (Mucin 2) that lubricates the system and provides a habitat for the microbiota, as shown in Fig. 2.1. These secretions are made from carbohydrates (80%) and contain polysaccharides that can also be found in other organic matter (some of which can be ingested) [10, 11]. Microvilli on the surface of each villi increase the area of the small intestine by another twenty times. The crypts at the base of the villi produce cells and hormones that increase digestive capacity. The duodenum is a 25 cm section of the small intestine where gastric juices are neutralised and enzymes are added to aid digestion. The jejunum and ileum are 5 metres long with extra folds in the mucosa to increase nutrient absorption [8, 12].

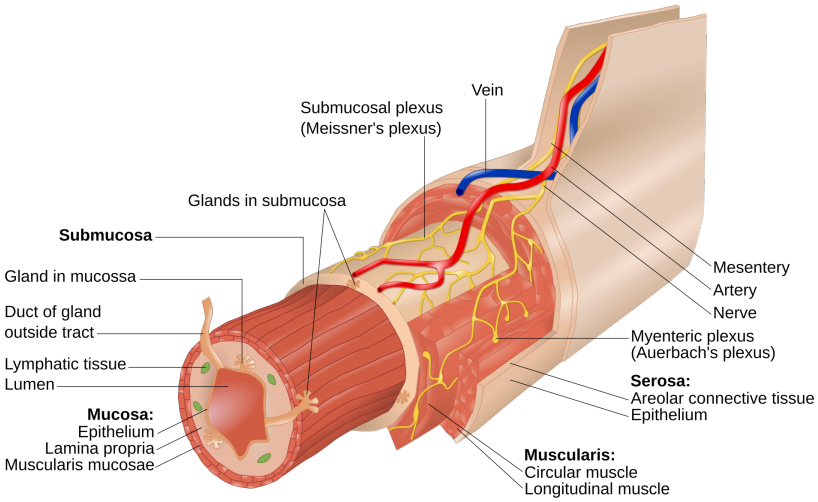

Figure 2.1: Each layer of the small intestine is as follows: The lumen where there are cylindrical projections of the villi and pocket-like crypts where nutrients are absorbed; The mucosa and submucosa where the network of blood vessels carry nutrients away and protect the body from unwanted incursions of bacteria; The circular and longitudinal layers of muscle which create the peristaltic motion to move digested material; The serosa which is a membrane separating the small intestine from the rest of the body and surrounding mesentery tissue. Goran tek-en, CC BY-SA 4.0.

2.1.3 Small Bowel Physiology During Peristalsis

As mentioned earlier, the small intestine consists of layers, with the one between the mucosa and serosa comprising circular and longitudinal muscles that cause peristalsis. Peristalsis is invoked when objects such as a capsule or a food bolus cause distention in the intestine, which stretches the surface of it and sends a signal to the nervous system. This signal causes the circular muscles before the bolus (oral direction) to contract, pushing it forward while the longitudinal muscles contract and shorten the intestine. Inhibitory reflexes just after the bolus (aboral direction) cause the circular muscles to relax. The bolus is moved a few centimetres by each peristaltic wave before the process is repeated again. Peristalsis does not lead to a consistent net transit along the GI tract, as it can reach a quieter segment or an area of high pressure in the intestine that causes content to stop. Otherwise, the process would take minutes instead of the several hours it normally takes, which would provide insufficient time for absorption to occur [13, 14].

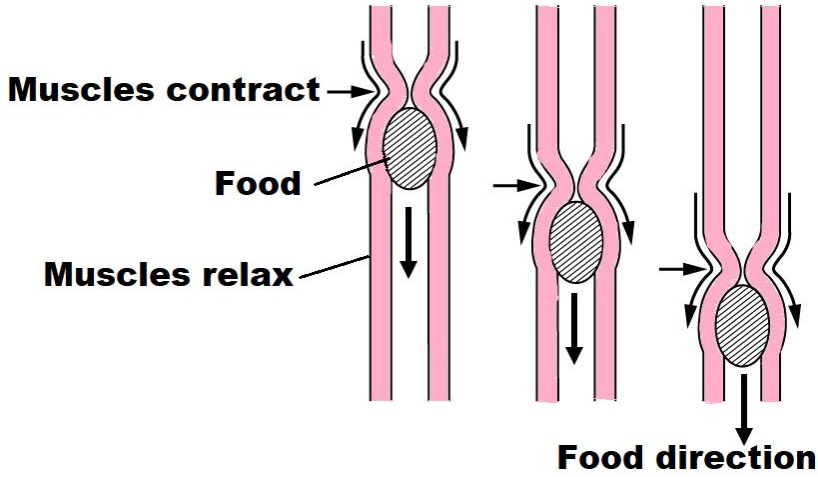

Figure 2.2: Peristalsis pushes material inside the GI tract using muscular contractions. OpenStax College, CC BY-SA 3.0

2.2 Microbiome

The human body is a complex system that operates in symbiosis with trillions of microorganisms located primarily in the intestine, affecting weight, digestive function, and mood [15, 16]. These microorganisms are commonly referred to as microbiota, and the collection of genetic material that they carry is referred to as the microbiome. The microbiome is significantly different from that of the free-living microbes in the environment, indicating a level of co-evolution to survive in the gut. The microbiome can be collected from the surrounding environment and other humans (mainly parents)

during the early years of childhood. The human microbiome consists of 3.3 million active genes, which significantly outnumbers the 22,000 genes of the human body [15].

The human genome project successfully sequenced all genes in the human body, discovering approximately 20,000 protein-encoding genes, no more than a fruit fly, prompting the search for other sources of genetic variance. A natural successor to this project is the Human Microbiome Project (HMP), which aims to characterise all the genomes in the microbiome of the human body. The ultimate goal is to be able to link differences in microbial communities with differences in metabolic function / disease, allowing more successful diagnoses and treatments [17]. Many studies have begun to establish links between the microbiome and health; for example, there was an accuracy of 90% in classifying individuals as lean or obese according to Christensenella abundance in the microbiome, which is negatively correlated with Body Mass Index (BMI). In addition, there are links between Lactobacillus and memory formation. Microbiome perturbation, particularly in early life, can lead to the development of Irritable Bowel Syndrome (IBS), diabetes, allergies, and asthma in later life [15]. The microbiome is an important factor in determining human health and identifying the causes of diseases; therefore, it is of the utmost importance to safely extract and analyse the microbiota from the human body to build an understanding of it, in line with the aims of the HMP.

2.3 Small Bowel Gastroenterology

Gastroenterology is the study of diseases and medical conditions that affect the digestive system. These diseases present unique challenges when navigating the small intestine.

2.3.1 Celiac's Disease

Celiac's Disease is a rare systemic immune-mediated disorder that is triggered by gluten ingestion in susceptible people. It affects 0.6 to 1.0% of people globally, and can vary greatly between different regions and ethnicities for unknown reasons. A significant proportion of people with Celiac disease go unrecognised, with European studies suggesting an incidence of around 79%. Genetic background plays a significant role in the risk and development of the disease, as certain genes are associated with Celiac disease, some found in up to 90% of patients [18]. Common symptoms include chronic diarrhoea, weight loss, and abdominal dilation. It can also cause abdominal pain, chronic fatigue, and iron deficiency. Blood serum analysis is fundamental for the detection of this disease by identifying specific associated antibodies; however, a biopsy is required to confirm diagnosis. An increased count of lymphocytes, crypt elongation, and partial to total villus atrophy (as shown in Fig. 2.5) can confirm the presence of Celiac disease [18, 19].

2.3.2 Inflammatory Bowel Disease (IBD)

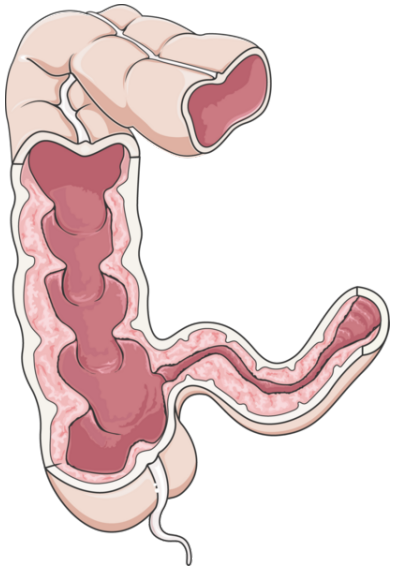

Figure 2.3: Inflammatory bowel disease in the colon and ileum, leading to significant wall thickening. Laboratoires Servier, CC BY-SA 3.0

IBD presents in two distinct forms, ulcerative colitis in the ileum and Crohn's disease (CD) as shown in Fig. 2.3, which can develop anywhere within the small intestine, but most likely within the ileum. Ulcerative colitis is common among young adults and causes the mucosa to become inflamed, changing blood flow, and creating patches of new connective tissue. This results in diarrhoea and blood passage with increasing frequency as the disease develops. CD causes irregular lesions to form throughout the intestine, thickening and constraining the bowel, resulting in inflammation. Long fissuring ulcers form in the mucosa, causing it to develop a cobblestone-like appearance. Symptoms include diarrhoea, abdominal pain, weight loss, fever, and rectal bleeding [20, 21]. IBD is characterised by an abnormal immune response within the mucosa that can be influenced by microbial factors [22]. In addition, IBD (particularly CD) leads to stiffening of intestinal tissue, changing its mechanical properties [23].

2.3.3 Tumours & Cysts

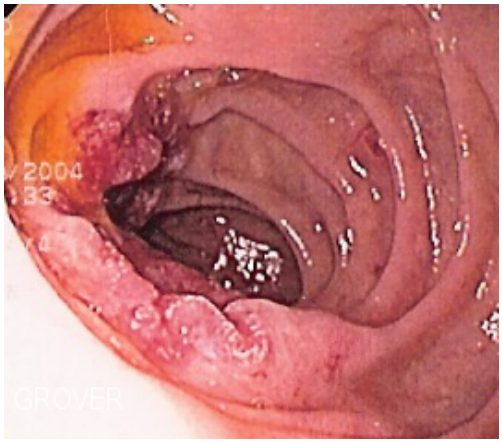

Figure 2.4: Tumours growing within the duodenum of the small intestine. Samir, CC BY-SA 3.0

Cancer can develop anywhere within the GI tract as shown in Fig. 2.4; however, the small intestine is very resistant. Only 3 - 6% of all tumours and 1% of all malignant tumours are found within it, likely due to the sterility of the contents and the rapid transit times of carcinogens, which reduces exposure. Most tumours develop in the duodenum and proximal jejunum and are associated with other conditions such as CD. Tumours can cause bleeding, abdominal pain, and obstruction forming

in the intestinal wall or within the surrounding lymph nodes [20, 21]. Similar polypoid growths can appear in the small intestine due to Pneumatosis cystoides intestinalis that causes gas-filled cysts to develop in the submucosa causing similar symptoms [21]. However, this disease is rare and the cause is not well understood. Theories range from surgical damage, to the production of gas from bacteria, indicating the need for a deeper analysis of the small intestine [24].

2.3.4 Bacteria & Parasites

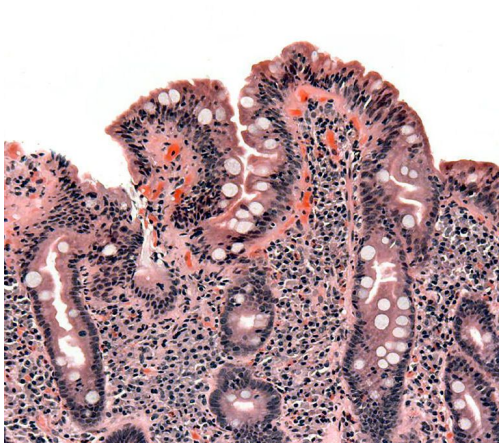

Figure 2.5: A cross-section of small intestinal surface affected by Celiac disease, causing the villus to partially atrophy. Bacterial overgrowth affects the small intestine in a similar way. Samir, CC BY-SA 3.0

Bacteria play a key role in the environment of the GI tract; however, harmful microorganisms can move into the small intestine. Bacteria such as Campylobactor or Giardia can produce enterotoxins that can damage the wall of the small intestine, causing the villus to atrophy as shown in Fig. 2.5, resulting in loss of fluid and electrolyte (not to be confused with Celiac disease, which causes the same effect hereditarily). Bacteria can also infiltrate the mucosa and lymphoid tissues causing lesions to form mainly in the jejunum and ileum, and in severe cases causing necrosis and haemorrhage. Some viruses also cause similar damage and symptoms. Parasites can live in the small intestine, causing abdominal pain and increased peristalsis due to their mass, and also causing diarrhoea and blood loss [20, 21].

If normal peristaltic movement is frequently interrupted or large diverticula (sacks in the small intestine formed in defects in the muscular wall) are formed, it can encourage rapid bacterial growth. Increasing the concentration of bacteria from 10^6 to 10^{10} per mL [20, 21]. Patients can suffer from mild symptoms to chronic diarrhoea causing weight loss. This is caused by mucosal wall thinning and atrophy of the villus, as well as inflammation that further develops the disease [25].

2.4 Conventional GI Tract Exploration

2.4.1 External Imaging

The small intestine is a difficult part of the body to physically reach using medical tools due to its length, complexity, and mobility. Therefore, many technologies have been developed to analyse it non-invasively. These includes; Computed Tomography (CT), Ultrasound (US), Magnetic Resonance Imaging (MRI), and Nuclear radiology [26].

Computed Tomography (CT)

CT requires four main components to operate; a rotating table, an X-ray source, an X-ray detector, and a data processing unit. CT emits photons through the plane of an object at different angles, causing some to become absorbed, transmitted, or scattered. The transmitted photons are collected and computed as an image of the interior of an object [27]. CT is very effective in diagnosing obstruction within the small intestine. It is also sensitive to changes in the thickness of the small intestinal wall and the mucosal structure. Recent advances in dual-energy CT, allows 0.1 mL of fluid to be detected in cases of GI bleeding or cutoff of the blood supply [26].

Ultrasound Sonography (US)

Ultrasonic generally refers to sound waves with a frequency of more than 20 kHz, and sensors that use them (ultrasonographs) typically operate from 2 to 18 MHz. Diagnostic US is an imaging technique for viewing internal body structures (including the small intestine) for potential pathology or lesions, which is very effective in soft tissues. It produces images by sweeping a beam of ultrasound across the body, reflecting back sound waves to build 2D images [28]. US is often used for long-term monitoring as it is inexpensive, accessible, and does not produce ionising radiation. US is very useful for characterising certain conditions such as CD. In addition, it can monitor the thickening of the small intestine, the mucosal structure, and blood vessels to a high sensitivity within the small intestine [26].

Magnetic Resonance Imaging (MRI)

MRI uses a strong external magnetic field to align nuclei within the human body parallel or antiparallel to that field, creating a net magnetisation, causing excitement. Once the field is turned off, the nuclei relax, with the relaxation time changing between different types of tissues. This creates an echo signal that can be processed into a cross-sectional image of the body [29]. MRI primarily uses magnetic resonance enterography to evaluate the small intestine. Compared to CT, it has less ionising radiation, allowing

safer and more frequent use. The patient does not require intravenous contrasts, as fluid buildup and inflammation can be evaluated with different imaging techniques. However, MRI is more expensive; has longer examination times; lower resolution; and more artefacts [26].

Nuclear Radiology

Nuclear radiology is based on the external mapping and detection of radiotracers administered to the body. Unaltered radionucleids or radioisotopes such as Iodine-123, Technicium-99, or Pertechnetate (Tc-99m-O4) are commonly used. The normal approach is to combine it with a physiologically active compound and administer it intravenously, orally, or by direct injection. If perctechnetate is combined with an imino-diacetic acid derivative; it can be used for a biliary scan that shows blood cells, antibodies, peptides, glucose, and fatty acids [30]. Within the small intestine, nuclear radiology can be used to analyse the structure by using Gallium-68-based analogues for the identification of neural system tumours or fluorodeoxyglucose for the identification of CD and other inflammatory bowl diseases [26].

2.4.2 GI Endoscopy

Endoscope Description

Endoscopes are highly versatile tools that can be used for many different operations within the human GI tract. These flexible devices use fibre optics and charge-coupled devices to capture imagery far into the GI tract, as shown in Fig. 2.6. These images can be magnified and altered to closely examine the structure of the intestine wall. Some systems also have valves to deliver air to targeted areas of the intestine or to provide suction, allowing manipulation. To use these functions, a long insertion tube consisting of a soft polymer exterior and steel mesh interior is pushed into the body, with a guided tip manipulated by wires pulling it up or down. Below the insertion tube is a control section with the required knobs, locks, switches, and valves to perform operations at the tip connected to a umbilical tube transferring fluid and information. Endoscopes have different accessories that can be added to the tip including; biopsy forceps, brushes, injection needles, and fluid flushing devices [31, 32].

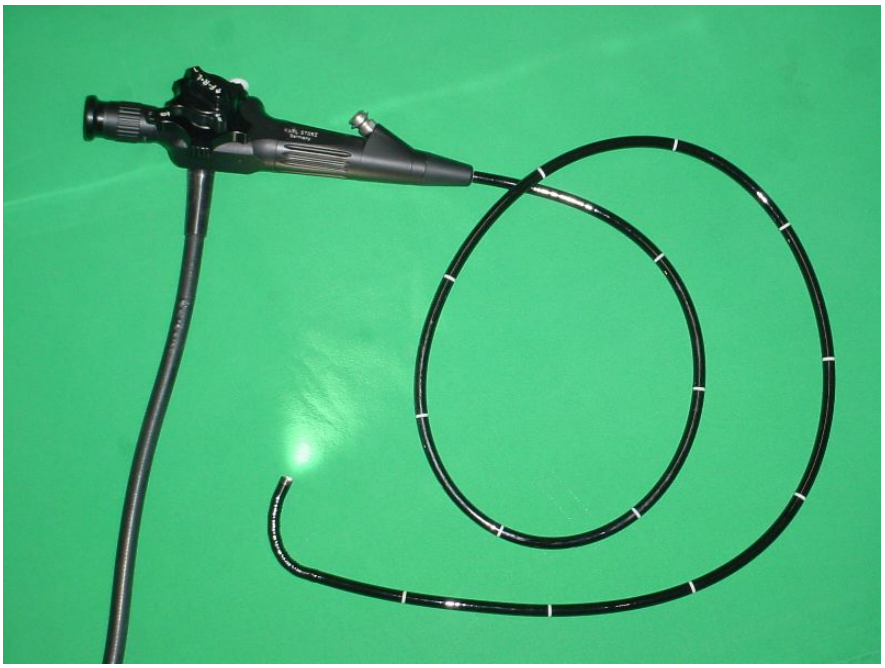

Figure 2.6: The key functional components of a typical medical endoscope. With the controls in the top left, the flexible long body, and the camera with light near the bottom. de:Benutzer:Kalumet, CC BY-SA 3.0

Endoscopic Procedures

Upper endoscopy refers to performing an endoscopic operation from the patient's mouth. The patient is fitted with a bite guard and rests on their side throughout the operation. Most operations (due to advances in technology) are vision-assisted, allowing the doctor to navigate down the oesophagus, through the stomach, and into the duodenum by viewing the position of the tip of the endoscope through the camera. Upper endoscopy requires a high degree of caution as it passes through many delicate sections of the GI tract, with a complex pathway to the duodenum. Endoscopic operations can also begin from the anus or colon, which is easier to navigate f. Getting into the ileum is more difficult as it requires precise manoeuvring to enter the narrow ileocecal valve and potential insufflation to open it up. Once inside the tip, it can explore up to 30-50 cm inside the ileum, requiring gentle movements due to its more delicate surface compared to the colon [31].

Patient Risks & Preparation

Before an endoscopy, a patient should not eat food for 6 to 8 hours or drink fluids for 2 to 4 hours prior to the procedure, with medicine often given to speed up the digestive process (prokinetic drugs). It is important to consider bleeding disorders if

they are suspected or known with relevant blood tests, so corrective measures are taken before the procedure. Special instructions are also required for patients taking diabetes or anticoagulant medication. For obstruction, external imaging is recommended to understand how the object or food bolus is lodged in the GI tract, to carefully plan removal. During waiting, prokinetic drugs can be used to move the bolus; however, the operation should not be delayed due to this. Patients with bleeding from the upper GI tract require extensive preparation to clear the digestive system and remove excess blood to provide a clear view of the site, with adequate airway protection. Lower GI bleeding is semi-urgent with some operations starting without preparation, while some administer 4L-Polyethylene Glycole (4L-PEG) 4 hours beforehand [31, 32].

There are multiple adverse events that can impact the success of an endoscopic procedure. Hypoxia (caused by an inadequate O_2 supply) must be constantly monitored and treated quickly. Foreign material may be accidentally inhaled, especially by those individuals with food residue and bleeding. Bleeding can occur from existing sources or is caused by the operation during or after endoscopy. Perforation is the most concerning complication which is the opening of a hole in the GI tract, it is rare but must be minimised with gentle movements under direct vision. Patients with infections such as salmonella pose a high risk to doctors and require strict cleaning and disinfection during and after operations, as well as the risk of infecting patients who are immunosuppressed. There is an extremely small risk of disturbance in heart rhythm from endoscopy and requires immediate expert treatment after recognition. Local blood clots can form from the intravenous (IV) supply, which is not dangerous. However, if spreading inflammation occurs, it should be treated seriously [31].

2.5 Capsule Robotics

Wireless CRs were first developed in the 1950s but could only record basic data like temperature, pressure, and pH. However, in 2000, Medtronic® developed a wireless capsule endoscope to transmit images from the small intestine. This was a previously difficult area to reach with traditional endoscopy, indicating that "the discomfort of internal gastrointestinal examination may soon be a thing of the past" [33]. An example of a capsule endoscope is shown in Fig. 2.7.

2.5.1 Capsule Endoscopy

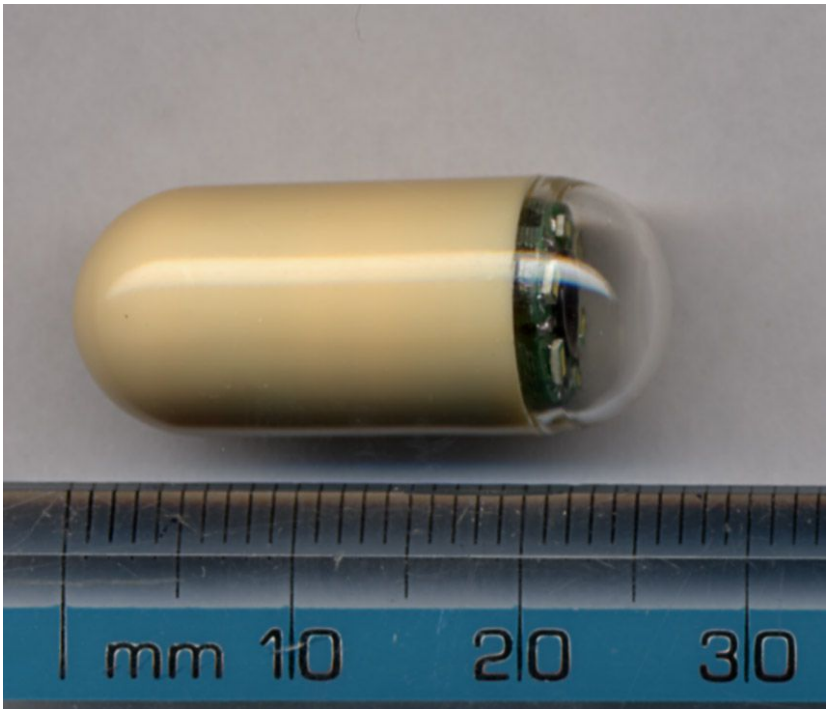

Figure 2.7: A endoscopic capsule. Public Domain, https://commons.wikimedia.org/wiki/File:CapsuleEndoscope.jpg

PillCam®

One of the first commercially developed CR was PillCam SB® which has been in use since 2001, with more than 600,000 deployments from 2001-2008 [3] and 2,000,000 from 2001-2015 [6]. The PillCam SB® system consists of three main components: the physical CR, the receiving antenna, and a custom Personal Computer (PC) work station. The capsule itself is Ø11 mm x 26 mm at 3.64 g, with a complementary metal-oxide semiconductor (CMOS) chip, a short focal lens, 6 white lights for illumination, 2 watch batteries, and a Ultra High Frequency (UHF) transmitter. The camera can detect features down to 0.1 mm, and captures at 2 fps (frames per second) over the 8 hour battery life [3]. The newer PillCam SB3® has some improved features such as a; longer battery life of more than 11 h, a viewing angle of 156°, decreased mass of 3.00 g, and adaptive frame rate of 2 - 6 fps if the capsule is accelerated by peristalsis. However, the efficacy of this system has not been demonstrated, and there are no significant improvements in overall completion or findings (usually a few percent better over a small sample size) [34].

Endocapsule®

Endocapsule® was first released by Olympus® in 2008 and has recently been developed into a newer version (Endocapsule 10®). It is similar in dimensions (Ø11 mm X 26 mm at 3.30 g) and operation as Pillcam SB3®, however, it features a wider viewing angle of 160° and a longer battery life of 12 hours. Otherwise, it runs at 2 fps [3, 34].

Mirocam®

Mirocam® has dimensions similar (Ø10.8 mm X 24.8 mm) to other capsules with a maximum weight of 4.7 g. Its unique feature is the use of electric field propagation over standard radio transmission. The human body acts as a conductor to transmit imagery to electrodes placed on the body. This technology is more efficient, allowing for a longer battery life of 12 hours at a higher fixed frame rate of 3 fps. It also has a wider viewing angle of 170° [34].

OMOM Capsule®

OMOM Capsule2® is a second generation CR from Jiashan Science and Technology, with dimensions similar (Ø11.0 mm X 25.4 mm) to other current generation capsule endoscopes. It has a heavier weight of 4.5 g and a shorter minimum battery life of 10 hours, but it has a variable frame rate of 2- 6 fps with a wider viewing angle of 165° [34].

CapsoCam®

CapsoCam SV-1® was developed by Capsovision® in 2013 and takes a very different approach to image capture and retrieval compared to its competitors. CapsoCam SV-1® has 4 cameras in the middle mounted 90° to each other, providing a full 360° viewing angle. In addition, it captures footage at a significantly higher framerate of 12 - 20 fps while still conserving limited battery life. This is achieved by storing images locally, which requires the capsule to be retrieved later after passing through the GI tract [34]. This design was more successful in detecting lesions within the body, although it had a slightly higher complication rate [35]. Despite concerns about self-retrieval of these capsules, only a 2% failure rate has been observed due to using a toilet outside the home. Another 5% of the time, the capsule has remained in the stomach too long and has run out of power. In general, patients were successful in using and retrieving them from home, indicating that this methodology is suitable for practical use [36].

2.5.2 Other Sensing Capsule Robots

Endoscopic capsules are a form of advanced sensing capsule that allows the operator to capture images within the GI tract. However, images cannot convey all the information

necessary to ensure a correct diagnosis of GI diseases. Therefore, advanced sensing capsules have been developed to measure attributes within the GI tract, including pH, temperature, pressure, and gas sensing [37].

pH Sensing

pH imbalances can cause a high level of digestive discomfort in patients, and these imbalances can occur anywhere within the GI tract. Gastro-oesophageal reflux disease can cause irritation in the upper GI tract from stomach acid or bile in the food pipe. Traditional catheters are uncomfortable, which is why CRs can be fixed to the oesophagus wall to provide constant pH monitoring for several days, improving the feasibility and safety of testing for this disease. High stomach pH levels due to insufficient HCl have been detectable by the Heidelberg pH capsule since the 1960s, which is held in the stomach and attached to the mouth. The pH is continuously measured while sodium bicarbonate is released (neutralising stomach acid), and the time it takes for the stomach to become acidic again is measured to determine health. Some diseases (such as IBD) require the monitoring of pH throughout the GI tract, and wireless capsules such as SmartPill® (Medtronic®, USA); can measure pH, temperature, and pressure. These can be used to calculate the transit times of the GI in humans and animals, with some CRs capable of measuring intestinal parameters for up to 10 days [37].

Temperature Sensing

The healthy body temperature for a human is between 35°C and 40°C, and going outside this range can put the welfare of that individual at risk, highlighting the importance of accurate monitoring to determine the appropriate treatment. External measurements through thermometers and infrared pyrometers are inaccurate, resulting in the development of CRs that can measure the core temperature within the digestive system [37]. The first temperature capsules were developed in response to improving the safety of astronauts who are exposed to temperature extremes by providing live monitoring of their core temperature, and became commercially available in 1988. The capsule contained a quartz crystal sensor that vibrated relative to body temperature, allowing a transmitted signal to measure the temperature at $1/10^{\text{th}}$ of a degree Celsius. In 2001 and later, high-performance athletes adopted this technology to protect against heat stroke [38].

Pressure Sensing

The peristaltic forces required to complete the digestive process can malfunction; for example, achalasia restricts the lower esophageal muscles from allowing food into the stomach. The diagnosis of these conditions was initially achieved with tethered devices.

However, wireless CRs can measure peristaltic forces with improved comfort over a longer period of time. Some capsules have up to 233 hours of battery life, allowing the entire GI tract to be measured. Current commercial capsules measure total pressure in sections of the GI tract. Recent prototypes implement two additional sensors to nullify heart rate and breathing disturbances, improving the accuracy of the data [37].

Gas Sensing

Gases can be found within the GI tract; which can originate from swallowed air, fermentation, bacterial overgrowth, malabsorption, and irregular intestinal movement. These gases can be used to detect conditions such as IBS, carbohydrate malabsorption, and bacterial overgrowth. Traditionally, breath tests were used for their non-invasive method; however, it is difficult to find the origin of these problems. CRs have been developed to measure hydrogen, oxygen, and carbon dioxide within human patients, providing precise locations on gas generation [37].

2.5.3 Other Capsule Robots

The demanding physiological challenges to reach certain areas within the GI tract have provided unique opportunities for CRs to perform difficult operations in a safe and efficient manner [37].

Targeted Drug Delivery

. The first example of a CR for the delivery of targeted drugs was developed in Germany in the 1980s that could release chemicals into the GI tract [39]. This was achieved via a radio-frequency that melts a thread, releases a needle, and pierces a balloon, allowing the stored chemical to be released passively around a targeted site. Other systems can release a needle into the intestinal wall, allowing frequent injections in an intestinal area based on the change in pH level associated with the small intestine. Passive systems lack precision and practicality to target specific locations, which is why active systems with actuation are required. There are multiple approaches to achieving control that can be externally powered and manipulated through magnetic fields or activated through radio transmission [39]. An example of a magnetically driven capsule; uses induction into coils at each end of the capsule to drive a magnetic piston that ejects drugs into the targeted surrounding area [40]. A more interesting approach uses external magnets on a bi-stable mechanism to reconfigure the shape of the capsule into a sphere through soft-robotics. It cannot progress beyond the stomach, which causes it to steadily release drugs into the stomach and duodenum [41].

Biopsy

The development of biopsy capsules has been ongoing since 1957 when the Crosby capsule was created with a spring-activated rotating blade to collect a sample of mucosa, drawn into the capsule with suction. The prototype was tethered outside the body, limiting its exploration capabilities [42, 43]. After the development of wireless endoscope capsules in 2005; a wireless biopsy capsule was proposed which used a similar spring loaded mechanism that is activated by a signal with a battery to melt the wax and release the razor. However, limitations in battery capacity required the use of an external power supply [44]. The functionalities of these proposed devices were significantly expanded, with cameras that observed the intestinal surface; an anchoring mechanism; rotational actuation to align with the biopsy site; and razors to cut off the tissue. However, battery technology has not been developed enough to support these complex operations [45]. Other advanced biopsy capsules are based on magnetic fields to externally power them, using coils to induct electricity to the actuators. These actuators cause the entire capsule (with a soft body) to collapse inward, causing the needle to puncture a targeted lesion within the stomach. This capsule is retrieved with a tether through the oesophagus to avoid contamination [46].

2.5.4 Capsule Size

The size and shape of a CR can have a great effect on its transit through the GI tract. Larger capsules allow for more advanced electronics and actuator mechanisms to be housed inside it. However, this increases the risk of retention, which could result in obstruction of the GI tract [47]. A study on foreign body ingestion was conducted in a children's medical centre in Taiwan from 2001 to 2015 in 484 patients under 18 years of age. Regular-shaped objects (similar to the shape of CR) typically pass through the GI tract safely within 72 hours if their diameter is less than Ø1.95 cm. The average diameter of regular objects that spontaneously passed was Ø1.63 cm. The diameter had a directly proportional effect on the transit time, which was on average [median (IQR)] 69 (36.75-117) hours when greater than Ø1.5 cm; 36 (24-48) hours when less than Ø1.5 cm; and 25 (24-47) hours when less than Ø1.0cm [48]. Healthy GI transit times when digestible material passes should range from 10 to 73 hours [49]. Therefore, a hard cutoff for the maximum capsule size should be 1.5 - 1.63 cm since it should be safe for a wider range of cases than in the average scenario.

2.5.5 Conventional Materials & Methods

CRs have strict requirements to be viable for use within the GI tract. This involves the material being biocompatible so that it does not harm the living tissues of the body

it is in contact with, or the living samples collected within it, and must be chemically resistant to the wide range of naturally occurring chemicals in the body; which vary the pH from as low as 1.0 to as high as 7.9. Furthermore, a capsules size typically ranges from Ø11 to Ø13 mm in diameter with a length from 24 to 31 mm long. This requires the material to be sufficiently strong to resist the mechanical pressure of the GI tract while having relatively thin wall thickness to maximise capsule capacity. Passive CRs propelled by peristalsis must minimise resistance from friction against the wall of the GI tract to ensure efficient transit; which requires capsules to be fabricated in high resolution with functional materials to minimise the risk of complications during operations [50].

Three-Dimensional (3D) printing

3D printing is classified as an additive manufacturing technique and is available in a wide variety of forms. The general process used to create an object using 3D printing involves creating a 3D model in a Computer-Aided Drawing (CAD) software package and converting it into an STL file format. The model is broken down into Two-Point-Five-Dimensional (2.5D) slices that are built layer by layer in a machine that is calibrated to produce that object from the desired material. After that, the supporting structures are removed and post-processing can be used to enhance the physical properties of the objects [51].

The approach many additive manufacturing processes use involves high amounts of thermal energy to melt a 3D shape together. Either by partially or fully melting the material into the desired shape or holding the powder in the target shape with a temporary material and using a furnace to set it. However, these processes can suffer from low spatial resolutions or a potentially high level of thermal distortion from changes in temperature, making them suboptimal for creating small high-quality capsules. 3D sheets can also be laminated layer by layer from sheet material; however, the layer thickness is much higher than any other method, which is not suitable for capsules which typically have thicknesses in the millimetre scale. Vat photo-polymerisation, otherwise known as Stereo-Lithography (SLA), is the most attractive method with the best surface finish and accuracy of all additive manufacturing processes and is used extensively in dental and medical devices. Additionally, this is well suited towards rapid prototyping; however, there are limitations on material choice which can be overcome through experimentation. A more recent method is two-photon photo-polymerisation, which uses two photons to create a radical which causes polymerisation. This allows fabricated feature sizes down to 0.2 µm or smaller to be manufactured, which is considerably finer than standard SLA; however, this is considerably more time consuming to use and requires access to specialised equipment and facilities [51, 52].

Injection Moulding

Injection moulding is a process that uses thermoplastic polymers that are melted into a high-viscosity fluid and injected into a mould to form the shape of the desired object. It typically involves feeding in pellets of a material and compressing them down while they are heated, and collection in front of a no-return valve until there is sufficient quantity and pressure to fill the mould. The valve is released pushing the molten polymer at 700 - 2,000 bar into the mould as it is left open, maintaining pressure while it cools into a solid shape. Typical thermoplastics include: low-density polyethylene, high-density polyethylene, polypropylene, and polystyrene. Edible materials such as specific types of starch and gelatin can be used to make capsules for medicine. For shaping the capsule, two moulds are required for the cap and the rest of the body. Small dimensions can be used in the design, with features as small as 0.1 mm and potential wall thicknesses of even less. Since this process is easily repeatable and automated, it is highly suitable for commercial production, making it desirable for future commercial CR products [53, 54].

Machining

There are two main machining processes that can be used to create complex geometries. Milling involves using a rotating tool to cut into the material, each tooth of the mill removing small arched segments known as chips. It can be used to create curved shapes such as capsules, but requires a special configuration with rounded-off tools. End mills can also be used to grind holes into the bodies of objects. Another common process that can be used is turning (or lathing), which involves holding the worked material in a chuck and turning it around rapidly. A tool is held statically and is moved towards the centre of the object cutting away a cylindrical (or possibly more complex) shape from the worked material, removing long spiralled chips [55]. In the case of plastics the fundamentals behind machining it are similar, with more caution on regulating the temperature during cutting as frictional forces can heat up the plastic near its melting point causing many thermal distortions. Despite the inherent brittleness of some polymers, under optimum cutting conditions, turned objects of high resolution without cracks can be easily fabricated. Milled objects are also easily feasible using polymers [56]. When using small-scale tools (100 - 500 µm) for milling operations, high-quality surfaces with low surface roughness (20 - 30 nm) can be achieved if the thermals are properly regulated by using sufficient coolant and steady placement [57]. Although it involves more complex operations and more fabrication steps to create capsule shapes with machining processes, it is still a viable option to assess. It allows for a wider range of materials to be used, rather than being restricted to sets of photo-polymers and thermostats used in printing and injection moulding, respectively.

2.5.6 Capsule Robotics Risks

Capsule Retention

Capsule retention is a significant well-documented risk associated with capsule endoscopy and is defined as an endoscopic pill (or CR) that remains indefinitely stuck inside the body for a period of more than two weeks. The effects of capsule retention are usually asymptomatic, but can lead to acute bowel obstruction that requires emergency surgery. In fact, the most common resolution to capsule retention is invasive surgery (particularly if the capsule is retained in the small intestine, which is the most common scenario), which is the primary difficulty that CRs are supposed to avoid; however, in some situations, endoscopy can be used to remove the capsule. From 2001 until 2018, four different case studies (as shown in Table 2.1) were conducted in the USA, South Korea, and Sweden, associated with multiple universities and medical professionals. In total, this data set represented 8,406 patients, 90 of them experiencing capsule retention, representing a retention rate of approximately 1.1%. This risk is greater in patients with known CD, with retention rates ranging from 2.9% to 13.0% (this variability is likely due to the limited number of patients with known CD being tested) [58, 59, 60, 61].

Table 2.1: Case Studies on Capsule Robotics

Literature	[58]	[59]	[60]	[61]	Total
Total Cases	1,000	2,300	2,401	2,705	8,406
Capsule Retentions	14	31	25	20	90
Retention Rate (RR)	1.4%	1.3%	1.0%	0.7%	1.1%
Reported RR with Known CD	13.0%	12.2%	2.9%	N/A	8.4%

A standard method to identify potential complications in successfully passing a CR involves the use of patency capsules. Patency capsules are simple devices that consist of a dissolvable exterior with a radio frequency identification tag, so if it is retained due to stenosis, the capsule will dissolve, allowing the contents to leave the body. A study was conducted in 27 patients with known or suspected strictures in the intestine, 15 of them successfully passed the patency capsule and later underwent a successful capsule endoscopy. In the remaining 12, 10 of them passed a fully or partially dissolved capsule, indicating that they were not suitable for capsule endoscopy. However, 2 of them had retention of the patency capsule requiring emergency surgery to remove it, representing an RR of 7.4%. This is not ideal, as the purpose of these capsules is to reduce this risk in CR trials, however, the risk of these capsules is still relatively high

compared to the values in Table 2.1 [58].

Capsule Robot Components

Risks are associated with the components within CRs. Batteries are a high-risk component, and the nature of the risk varies between different sizes. Most batteries inside CRs are silver oxide, which is preferred over lithium ion batteries because of the lower perceived risk. Most silver-oxide batteries provide approximately 25 mW power; however, more advanced CR features may require up to several hundred mW of power [62]. A case study analysed 130,000 cases of children who ingested button batteries. Four main risks were identified: electrical discharge, pressure necrosis, alkaline leakage, and metal toxicity [63]. For CRs, pressure necrosis can be ignored as all batteries have to be smaller than the diameter of the capsule, and significant poisoning has not been recorded since the mercury ban for use in batteries in 1996. The electrical discharge risk is proportional to the voltage of the battery, with lithium batteries having higher voltages than silver-oxide batteries. Higher voltage allows for a greater current to be released when the negative pole contacts conductive tissues in the body, causing corrosive tissue damage and generating hydroxide which causes necrosis. Silver-oxide batteries can discharge strong alkalies into the digestive system when damaged, also causing necrosis [63, 64]. A minor risk comes from the heavy metals contained in the electronics inside the capsule. Usually, prolonged exposure to them can affect the immune system, hormone balances, and DNA structure. However, this is not likely due to the limited number of electronics in a CR if it were to fracture. Extra care should be taken when performing CR operations in pregnant women and adolescents, as it can have a pronounced effect on developmental growth [65]. If the CR contains a thermally heated component, care must be taken to ensure that it does not heat up significantly beyond normal body temperature, which requires appropriate thermal isolation. If the CR is compromised, a heated component could cause internal burns in the intestine, highlighting the importance of fully disconnecting the CR's circuitry when compromised [66].

Other Risks

A significant yet easily apparent risk with CRs is related to difficulty swallowing the capsule. Patients who have a preexisting swallowing disorder are contraindicated from using CR; however, 1.5% patients without any of these disorders may still have difficulty swallowing the capsule (probably due to its larger typical size). Devices have been developed to help patients swallow capsules by deploying them into the stomach using endoscopic tools [67]. The shape of the capsule can introduce extra risk to the patient, especially with protruding features such as anchoring, surgical, sampling, or

locomotion devices; which can cause physical strain on intestinal tissue and possible perforations. These risks can be minimised by ensuring that appropriate materials and capsule designs are used to minimise these risks [62].

2.6 Microbiome Sampling Capsules

With the miniaturisation of the CR components and a greater understanding of the microbiome, sampling capsules were developed to collect the microbiome from the targeted areas of the small intestine; an area that was previously unreachable within the GI tract. During the past few years, various prototypes and concepts have been published in the literature to optimise the safe collection of microbiome [37]. A simple method to obtain a sample is to use a biodegradable coating to create an opening where the surrounding digesta can flow into the capsule that is resealed by an expanding hydrogel [68]. Although this is a very compact, simple, and safe design, it primarily lacks the ability to target specific areas within the body, which limits its data collection abilities. A similar design can also take a sample of the surrounding digesta, but is activated by an external magnetic field that bisects the device, allowing a sample to be safely captured and resealed in the centre of the capsule [69]. An interesting alternative design samples the surrounding digesta with magnetic actuation. However, it has three separate chambers that can be filled by changing the inlet-port alignment in-vivo. Allowing separate samples to be collected, improving data quality [70]. However, previous designs miss most of the microbiome that mainly grows on the surface of the small intestine, around the microvilli [10]. A solution to this problem is achieved by integrating an active sampling mechanism that can remove the microbiome from the surface of the intestine without damaging it. This example uses a shape memory alloy spring to lift a levered scraper from the side of the capsule, which is powered by a small lithium-ion battery and activated by a wireless radio-frequency transmission. Providing safe extraction of a sample from a specific location in the GI tract without contamination or leakage into the capsule electronics [66].

2.7 Literature Gap

There is a wide variety of CRs on the market; however, all appear to have a similar uniform appearance that is the same fundamental design as standard capsules. However, unlike standard capsules, these do not dissolve and are designed to explore the intestine, rather than reach it. Looking through the literature, there is no information on how changing the shape, texture, mechanical properties, or materials can affect the transit of a capsule through the entire GI tract. Case studies that examine existing capsules indicate that there is a clear risk of retention of 1 - 2%, which can result in

worse outcomes for patients and reduces the reliability and scope of data collection. This can have a great impact on projects that aim to understand how the gut and its microbiome work with the rest of the body, limiting the amount of data that can be collected while excluding individuals from the dataset, which may result in biased results that do not reflect everyone.

2.8 Literature Summary

The physical properties of the digestive system are explored, including physiology, microbiology, and gastroenterology; to better understand how the GI tract functions when healthy and unhealthy. Various methods are identified to explore the GI tract, such as external imaging techniques (such as CT, US, MRI, and nuclear radiology) and GI endoscopy. All available CRs are identified, including capsule endoscopes, sensing capsules (for pH, temperature, pressure, and gas sensing), targeted drug delivery, and biopsy. In addition, the effect of the size and shape of the CR on capsule transit is discussed. In addition, conventional manufacturing techniques are used to make them, including 3D printing, injection moulding, and machining. The risks CRs pose to the body are also discussed, from retention to the physical components inside and other related issues that may occur. Lastly, specific microbiome sampling capsules are discussed to relate with the objectives and goals of the sponsors of this project. Using this information, the literature gap is identified which is used to set the aim (Section 1.1), objectives (Section 1.2), and scope (Section 1.3). In the following chapter on the materials and methods of this project, the information from the literature is used to develop new equipment, technology, and experimental procedures to fulfil the objectives of this thesis.

Chapter 3

Materials & Methods

This section covers the design and development process behind the optimisation of the exteriors of CRs, the synthetic intestine, and the subsequent robotic intestine system. In Section 3.1.1, the conceptualisation of new exterior capsule structures and the different materials and manufacturing techniques used to create them are included. Following this in Section 3.1.2, the difficulty in evaluating capsule designs is identified and a solution is proposed by developing a synthetic intestinal system that can safely and easily assess capsule performance. The exact techniques used to create the synthetic intestine are described in detail and further modifications are proposed to replicate some of the disorders identified in the literature review. In Section 3.1.3 an application of the synthetic intestinal system is proposed in the form of a robotic intestine that can simulate intestinal peristalsis. This includes describing the development of the linear actuation system for longitudinal peristalsis and a novel aperture mechanism to replicate circular peristalsis. These mechanisms are integrated into a unified robotic system which is controlled using Computer Numerical Control (CNC) to set the position of the actuators by using trigonometric principals to model then approximate motion. An overview of the systems electronic and programming architecture is provided. In Section 3.2.1 the experimental procedure for the tensile testing setup is described that evaluates the static interaction the capsule design has with an intestinal-like surface. This method is applied to all capsule designs evaluated in this thesis. In Section 3.2.2 and Section 3.2.3 the experimental procedure is described for collecting quantitative data on the energy required to move the final group of capsule designs via peristalsis and their surface profiles in terms of actual shape and roughness.

3.1 Design & Manufacture

3.1.1 Capsules

Early Concepts

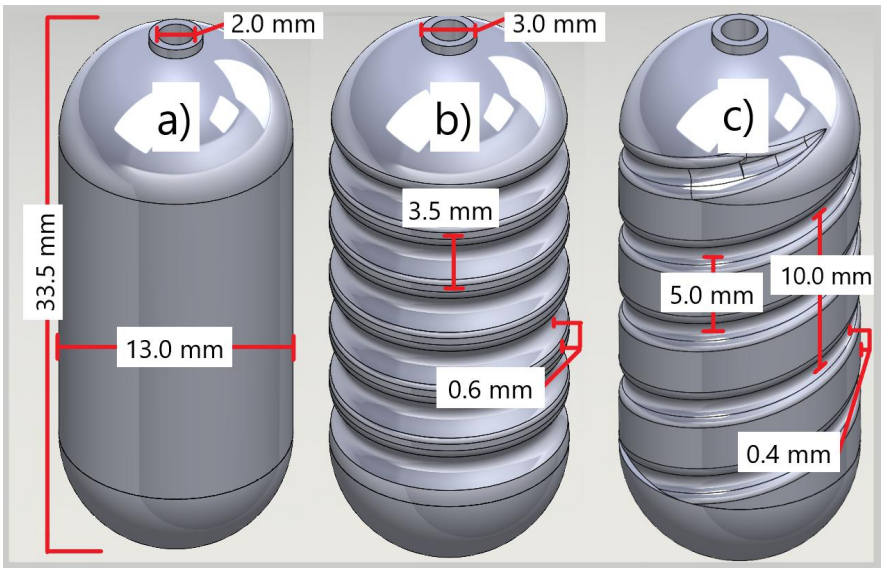

Figure 3.1: The dimensions of different capsule designs, all of which have a base 0.75 mm wall thickness. Designs include a smooth surface (a)), a segmented surface (b)), and a spiral surface (c)).

Three different surface designs are tested for the exterior of the CR. The control design Fig. 3.1 a) has a smooth surface with a diameter of 13.0 mm, a length of 35.0 mm, and a wall thickness of 0.75 mm (used in all designs). In addition, a 2.0 mm diameter hole with a wall thickness of 1.0 mm is located at the top of each capsule to allow it to be attached to a string for tensile testing. Each capsule design has the same end cap opposite the hole to allow objects to be placed inside it. In Fig. 3.1 b), a segmented surface is applied to the exterior with a wavelength of 3.5 mm and a peak-to-trough depth of 0.6 mm, moving inward from the 13.0 mm diameter. In Fig. 3.1 c), a double spiral is applied to the exterior of the capsule, each spiral does 1 revolution around the capsule every 10.0 mm, with a depth of 0.4 mm into the 13.0 mm diameter of the capsule.

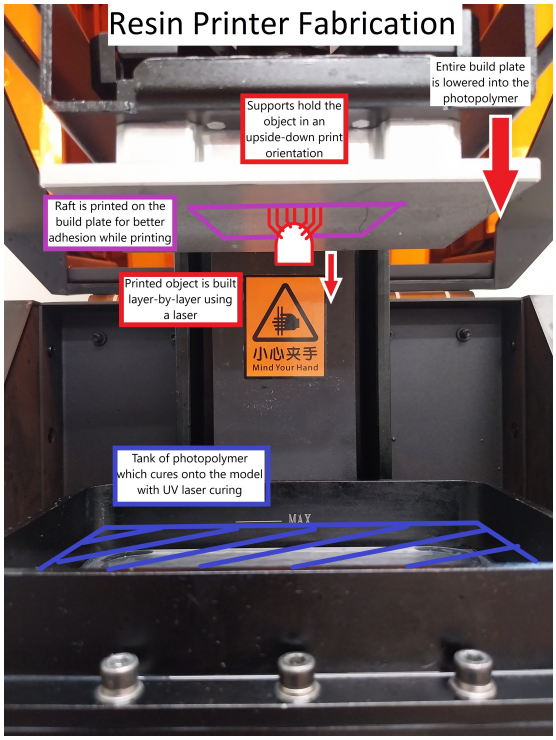

Figure 3.2: How an object is printed with a Flashforge Hunter® resin printer, demonstrating how it is built layer-by-layer from the plate which is repeatedly lowered into a vat of photopolymer resin.

The capsule exteriors are printed using a Flashforge Hunter® Direct Laser Photo-polymerising (DLP) resin printer (Flashforge® Hunter, Flashforge Technology Co., Ltd, Jinhua, China), as shown in Fig. 3.2. The rigid capsules use Flashforge® FHD-1200 biocompatible green resin (FHD-1200, Flashforge® Technology Co., Ltd, Jinhua, China), the soft capsules use 3DResyns® Bioflex A50-MF (3DResyns® Bioflex A50 MF, Resyner Technologies S.L., Barcelona, Spain), and the semi-soft capsules have soft Bioflex A50-MF bodies with rigid FHD-1200 end caps. The models for the capsules are created in a 3D Computer Assisted Drawing (CAD) package and imported as STL's into Flashforge®'s proprietary software for adding the required support structures and slicing the STL model. Once sliced, it produces an svgx file, which is used by the resin printer to fabricate the designs layer-by-layer.

Optimising for Shape

Nine variations of the segmented surface design in Fig. 3.1 b) are tested including the control in Fig. 3.1 a). All capsule designs have an external diameter of 12.0 mm, a length of 30.5 mm, and a wall thickness of 1.0 mm. In addition, a 2.0 mm diameter hole with a wall thickness of 1.0 mm is located at the top of each capsule to allow it to be attached to a string for tensile testing. Each capsule design has the same end cap opposite the hole to allow objects to be placed inside it. In Fig. 3.3, the segmented design parameters are adjusted, including varying the quantity of ridges (or the peak-to-peak distance) from 4 to 6 (4.5 mm / 3.6 mm / 3.0 mm) while the peak-to-trough (depth) is varied from 0.5 mm to 0.125 mm. The control has an entirely smooth surface, as that is the standard shape used commercially.

The capsule exteriors are printed using a Flashforge Hunter® DLP resin printer, as shown in Fig. 3.2. The exteriors are printed using Flashforge® FH-1200 green resin (FH-1200, Flashforge® Technology Co., Ltd, Jinhua, China). This was selected as the

material most similar to FHD-1200 (which is no longer commercially available) to use for reference to previous experiments. This material will not be investigated further in later testing as it does not meet the requirements for safe use inside the human body. The models were created using a CAD package and sliced into a svgx file (the same as before).

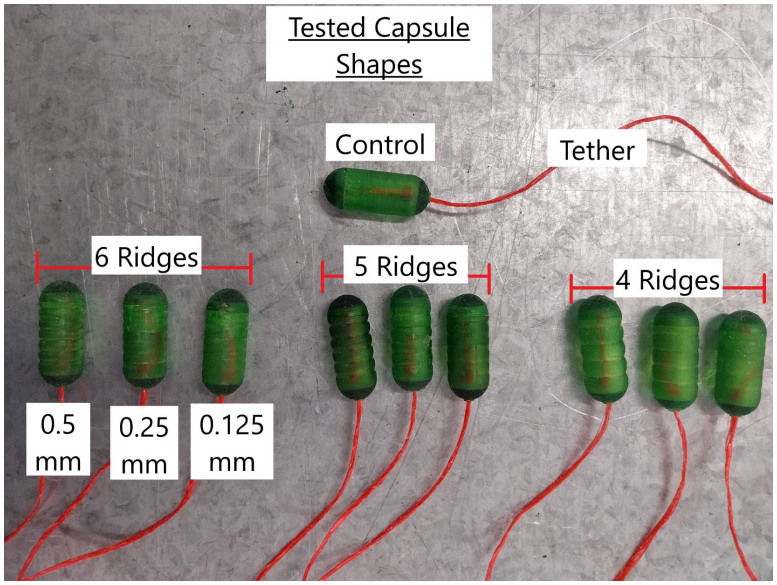

Figure 3.3: Different designs derived from the most successful design in Fig. 3.1 b) with a) being the control.

Optimising for Materials and Manufacturing

The best variation of the segmented capsule design in Fig. 3.4, are used in further experimentation. All capsules have an external diameter of 12 mm, a ridge-depth of 0.125 mm, and a ridge distance of 3.0 mm. It also retains the same hole at the top so that a string can be attached for tensile testing and to pull it back to the starting position for the robotic intestine; and the same wall thickness of 1.0 mm.

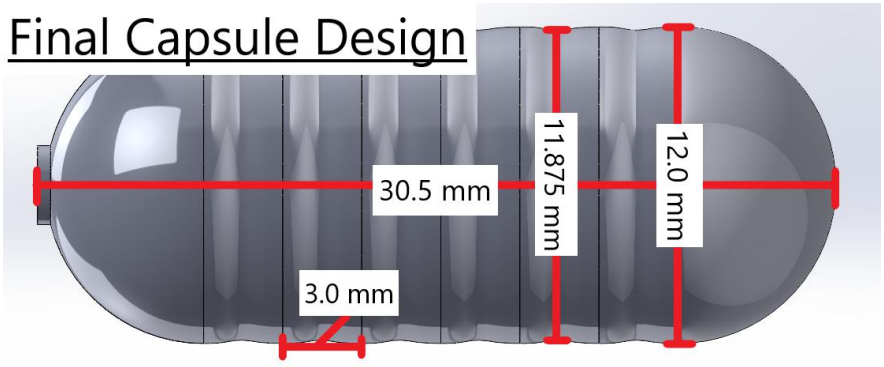

Figure 3.4: The final selected design for the CR exterior. It has an external diameter of 12 mm, a ridge-depth of 0.125 mm, and a ridge distance of 3.0 mm. The overall length of the capsule is 30.5 mm.

The design in Fig. 3.4 is manufactured with the following materials and respective manufacturing techniques below, with bio-compatibility cited next to the materials, and the output shown in Fig. 3.5:

- Power Resins® Surgical Guide resin manufactured according to ISO 13485:2016 standards [71] (Ethoxylated Bisphenol-A Methacrylate (40-60%), Methacrylate Ester (10-20%), Photoinitiator (1-5%), Hexanediol Dimethacrylate (1-5%), Hydroxyethyl Methacrylate (1-5%)) using a Flashforge® Hunter DLP printer.
- Acetal plastic (polyoxymethylene) [72] using a Boxford® CNC lathe (MT2 CNC Lathe, Boxford®, Halifax, United Kingdom).
- Teflon plastic (polytetrafluoroethylene) [73] used on a Boxford® CNC lathe.
- Teflon plastic (polytetrafluoroethylene) [73] was processed using a Minitech® CNC micromill (Mini-Mill/GX, Minitech® Machinery Corporation, Norcross, GA, USA) using Sutton Tools® 3.0 mm and 1.0 mm ball nose end mills (Ball nose end mill, Sutton Tools Ltd., Thomastown, Australia).
- Polyether Ether Ketone (PEEK) plastic [74] using a Boxford® CNC lathe.

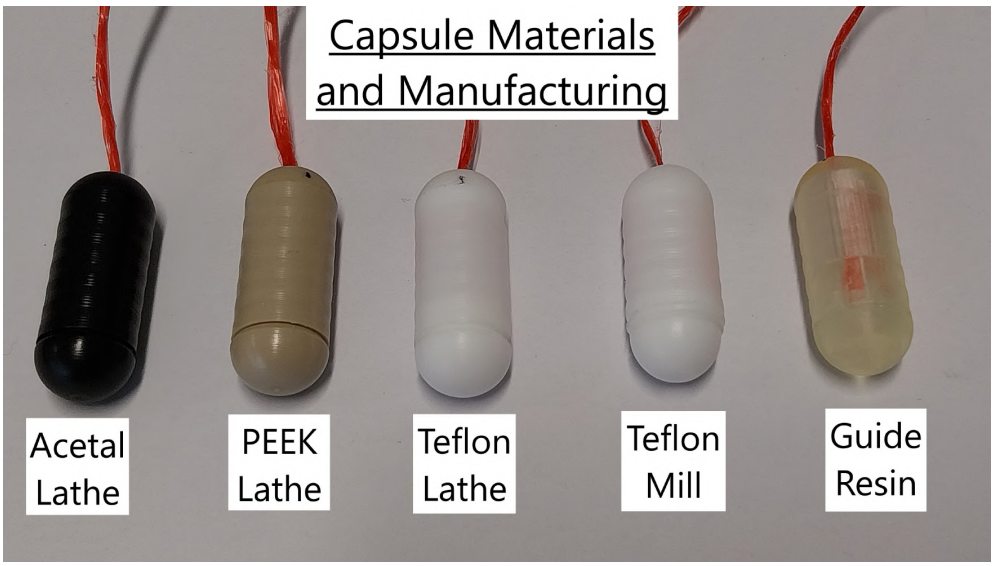

Figure 3.5: The group of capsules made with different materials and manufacturing methods used in this round of experimentation.

Creating capsules with the Minitech® CNC micromill requires several steps. A 3D model of the object is created and then the G-code is generated using SolidCAM® (SolidCAM®, SolidCAM Ltd., Yehuda, Israel) to plan the milling path. The G-code is loaded into the Mach-3 software® (Mach3, Artsoft Consult, Cluj-Napoca, Romania)

to interface with the micromill. A round of material at least 1 mm greater in diameter and 25 mm longer than the planned object is placed inside the rotary chuck, as shown in Fig. 3.6. When tightened, the coordinate space will be set before each separate operation, which is hollowing, shaping, and finishing. The hollowing operation is used only in the body of the capsule, milling a 10 mm diameter pocket with a 3.0 mm diameter endmill from the bottom of the capsule body; this is done first to prevent the capsule from wobbling if it was done after the shaping process. The shaping process cuts the excess material from the capsule body and end cap leaving its approximate shape behind, also using the 3.0 mm in diameter endmill. Lastly, the endmill is swapped to a 1.0 mm diameter one, and used to finish the surface by removing a small amount of material at a high speed. The shaping and finishing operations use a four-axis operation by rotating the chuck, allowing it to cut a round body as shown in Fig. 3.6; and the pocket is milled using a three-axis operation to cut from above.

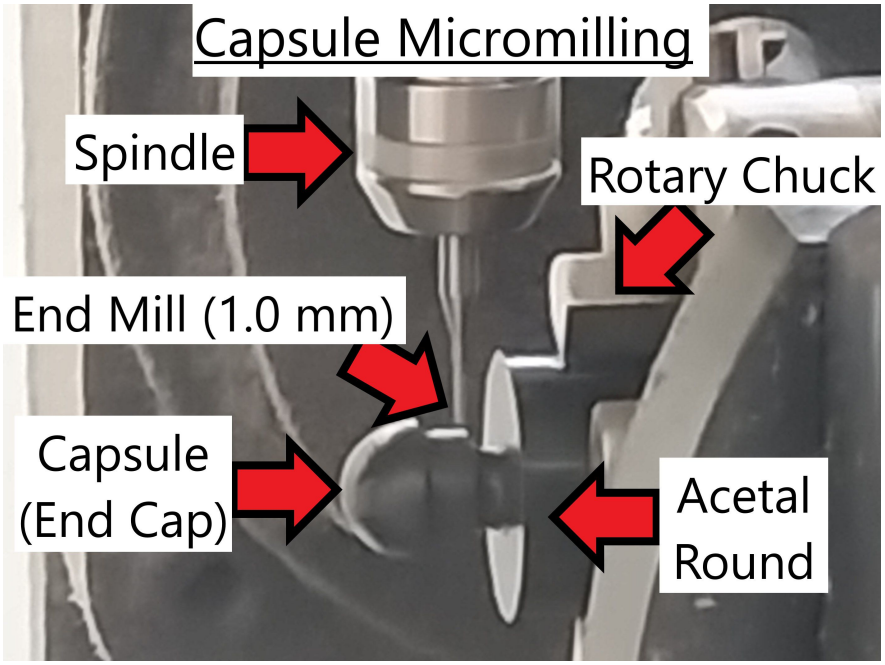

Figure 3.6: How capsule bodies are produced using the Minitech® micromill using Sutton Tools® 3.0 and 1.0 mm end mills.

The lathed capsules were manufactured by the workshop technicians in the Mechanical Workshop of the Department of Electrical and Computer Engineering, University of Canterbury, Christchurch. The G-code was generated by the workshop technicians and cut using the same hollowing, shaping, and finishing steps on the Boxford® CNC lathe. The capsule is hollowed with a boring bar, shaped and finished with a turning tool, and separated from the round using a parting tool. Each tool change is automatically performed with a tool turret carousel. The process is shown in Fig. 3.7, where

the turning tool is placed in the round (held by a rotary chuck) which is being turned rapidly, removing the material and creating the capsule's body. A stem is left behind, which is parted off at the end of the lathing operation.

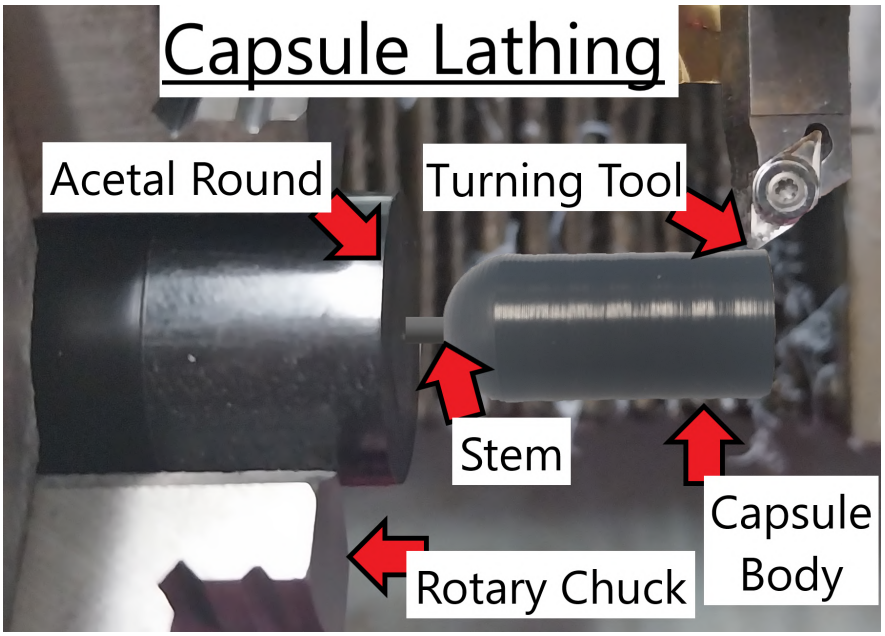

Figure 3.7: How capsule bodies are produced using the Boxford® CNC lathe.

3.1.2 Synthetic Intestine

Alternative Testing Methods

Any new capsule designs must be measured and compared quantitatively in an experiment. However, there are a wide range of methodologies for collecting data. In this research, clinical trials and animal trials are ruled out because of the difficulty in accessing them within the scope of the research. Another possibility is to use dissected intestine in ringer solution to measure capsule performance. However, the narrow time frame for which the intestine remains alive and the required conditions to keep it alive increase the difficulty of experimentation. In addition, the unique properties and conditions of different intestinal samples make it difficult to keep factors under control during experimentation, causing variance in the collected data [66]. Silicone resin can be moulded to replicate the mechanical properties of human tissues [75], which means that a mechanically similar synthetic intestine could be made of it. This creates a consistent environment to test capsule designs inside of, which can be customised to create any scenario required for experimentation. For these reasons, in this research, a synthetic silicone intestine is used.

Proposed Method

The synthetic intestine should be based on the dimensions of a section within the human GI tract. An interesting area to replicate would be the ileum or lower area of the small intestine, as the small intestine has the smallest internal diameter and the ileum has a higher susceptibility to IBDs such as CD. This is likely to be the area that is the most difficult for a CR to pass through successfully [50]. The ileum has an approximate diameter of Ø21.7 mm, an interfold distance of 17.91 mm, and a fold height of 1.6 mm [50]. These values will be used to create the synthetic intestinal mould demonstrated in Fig. 3.8. This mould has a core based on the previous dimensions and is 160 mm long. The core is encapsulated by an outer mould that is 3.0 mm wider in diameter, giving the synthetic model a wall thickness of 1.5 mm. The outer mould is split into two halves and is fastened together with a flange that is held together by six M5 bolts (reducing silicone leakage). There is also an inverted conical volume above the modelling area to store excess silicone and to compensate for any leakage that does occur. The mould itself if filled from the bottom-up via a spout which is 5 mm long and 5 mm in diameter, which is slightly tapered.

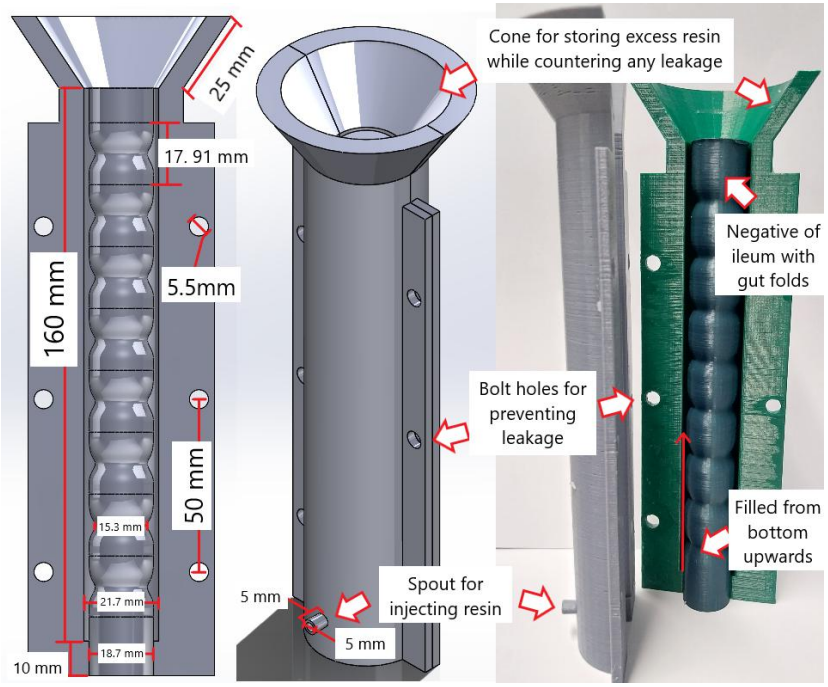

Figure 3.8: The dimensions and construction of the synthetic intestine mould.

The material used to create the synthetic intestine is a silicone rubber resin (Ecoflex® 00-50 Platinum Cure Silicone Rubber Compound, Smooth-on, Inc., Macungie, PA, USA) that is supplied in two liquid components. When these components are mixed,

they are set under exposure to Ultraviolet (UV) to form a solid rubber of Shore's hardness 50A; in other examples of synthetic intestinal tissue, 30A is used [76]. However, IBD causes stiffening of the intestinal tissues [23], which means 50A was used instead. To prepare the resins for the synthetic intestine moulds, parts A and B were poured in a 1:1 volume ratio into an open plastic syringe and vigorously stirred to ensure that all the resins set properly. However, this introduces air bubbles that are difficult to remove passively before the resin sets fully, causing them to become a part of the solid. This affects the mechanical properties and introduces weaknesses in the synthetic model. To address this, the syringe is placed in a vacuum chamber until most bubbles are removed from the liquid. After this, the syringe plunger can be added back to the top of the syringe and is ready to be injected into the mould, which is shown in Fig. 3.9.

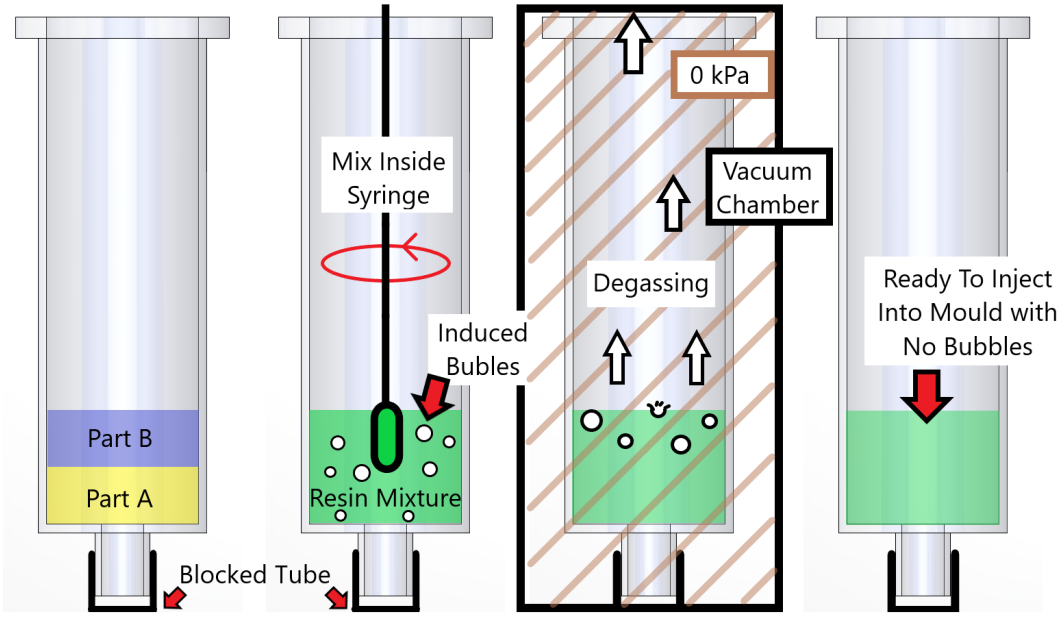

Figure 3.9: The preparation process used to make the silicon resin used in moulding the synthetic intestine.

The prepared syringe has an open tube attached to its end and is connected to the spout of the mould. Force is applied to the plunger that pushes against the air gap between the plunger and the resin that pushes the resin into the mould without causing any mixture. This resin fills the mould from the bottom up, allowing the air inside to escape through the top. This is important as pouring the resin from the top would cause large bubbles of air (especially at where the gut folds go) to become trapped, causing large sections of the synthetic intestine to not be moulded. The syringe will have 40 mL of mixed resin inside to completely fill the intestine area and to overfill the inverted conical space. Once filled, the tube is removed, and the spout is blocked off

with a plug and left to stand for several hours (longer than is normally required due to the enclosed space inside it) until gradual ambient UV exposure causes all the resin to set. The two outer mould halves are unbolted and separated from each other (care is taken not to puncture the set silicone while using blunt tools), revealing the exterior of the synthetic intestine, with extra silicone that leaked through the flange and overfilled being clipped off. After this, the core of the mould is pulled out, leaving behind an artificial intestinal model that is ready to use for experimentation, which is shown in Fig. 3.10.

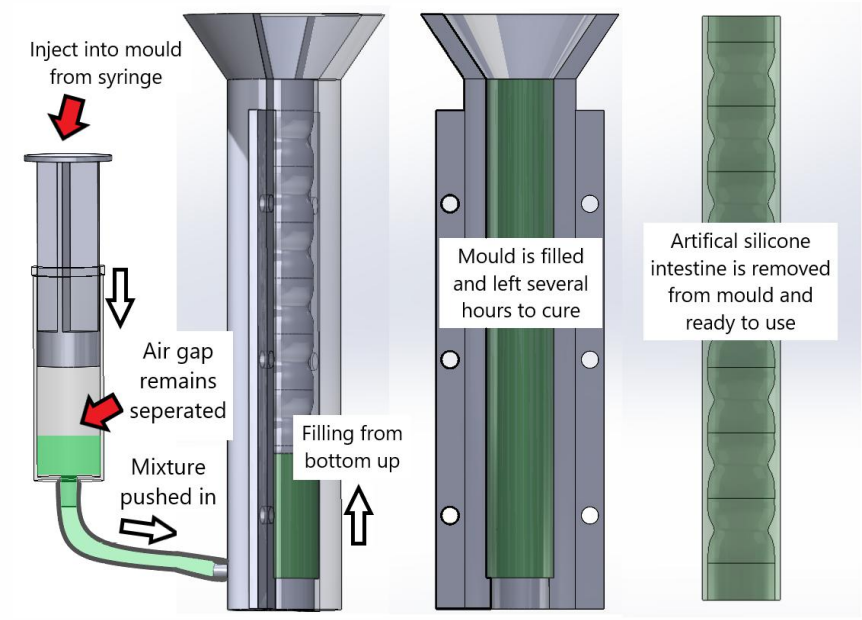

Figure 3.10: How moulds are filled with silicone resin from a syringe and left to cure to create a synthetic intestine.

Stenosis Replication

The process of adding diseased sections to the synthetic intestine involves all the same standard steps as before except changing the core of the mould. As shown in Fig. 3.11, the core has been narrowed to approximately Ø11 mm in a technical CAD package and further modified in an artistic CAD package to add the cobblestone-like appearance associated with CD shown in Fig. 3.12. This core is inserted into the mould and the silicone resin is set around it; however, the core cannot be pulled out, so it must be broken at its narrowest point and pulled from both ends. Leaving behind a custom synthetic intestine for experimentation.

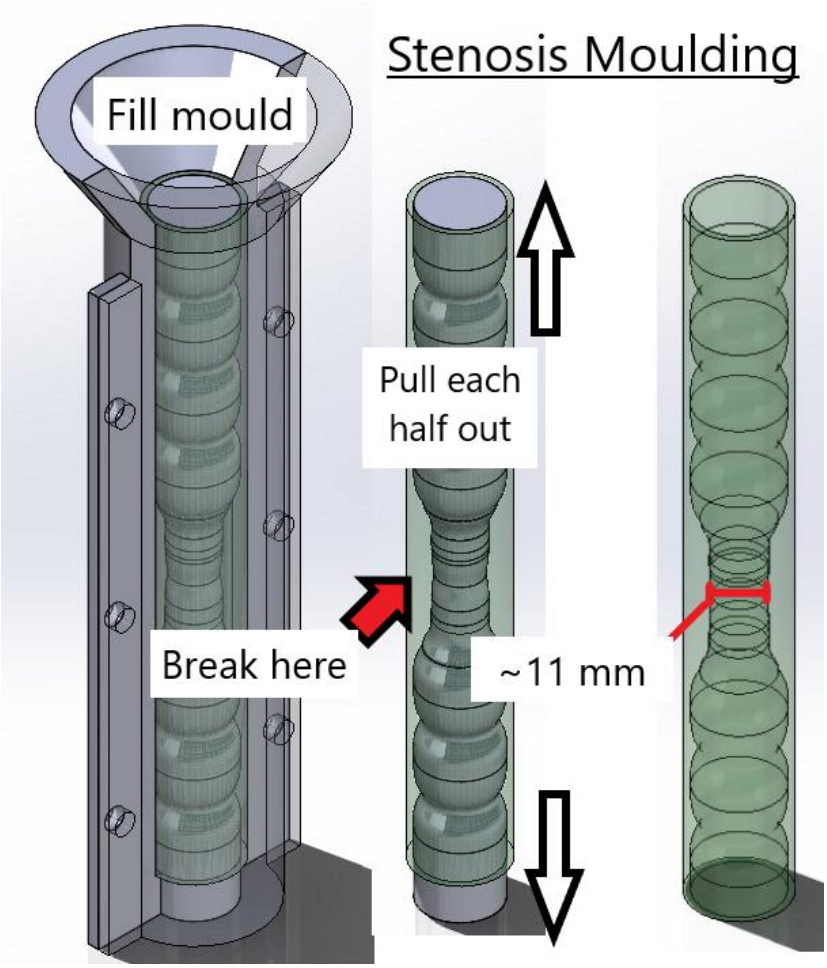

Figure 3.11: How to mould a synthetic intestine with stenosis.

Figure 3.12: The textured surface that was added to the technical model using sculpting tools in a CAD package.

3.1.3 Robotic Intestine

To test and evaluate the performance of CRs in this research project, they must navigate conditions similar to those of the small intestine. The testing in clinical trials on the intended users of these capsules is a difficult process to set up and is too early in development for this level of testing. Animal testing is more viable due to established connections and completed paper work with the School of Agriculture and Environment at Massey University, Palmerston North. However, animal testing is a slow process which only provides a small quantity of data within the time-frame of a Masters project. Animal testing may be useful for the validation stage, but there needs to be a platform which can be used extensively for the development of CR prototypes without risking living animals in experimental designs. Therefore, a robotic platform has been developed to replicate the forces, mechanical, and fluid properties found within the small intestine. It will be necessary to replicate both circular muscle contractions that squeeze objects in a direction and longitudinal muscles that translate this motion down the length of the small intestine. Creating an accurate simulation of peristaltic contractions that can be subjected to any design placed within it, providing extensive data on the motion and forces experienced by the capsule.

Linear Actuation

To provide the linear movement that represents the longitudinal muscles in peristaltic motion, an existing platform is modified, allowing focus to be concentrated on the novel parts of the robot. The platform used is the Poseidon Syringe Pump system developed by Pachter Lab at Caltech [77] shown in Fig. 3.13. This project uses many of the same components for the linear actuator with everything except the base of the design and the carriage being unchanged. The system uses a Nema 17 stepper motor which is coupled to a 5 mm threaded rod that drives the carriage back and forth using an M5 nut which is encapsulated inside the carriage. The carriage also runs along two fixed, 6 mm steel rods with a 6 mm linear bearing encapsulated in the sides of the carriage, providing structural support. All standard purchasable parts for the entire system are listed in Appendix A.1.

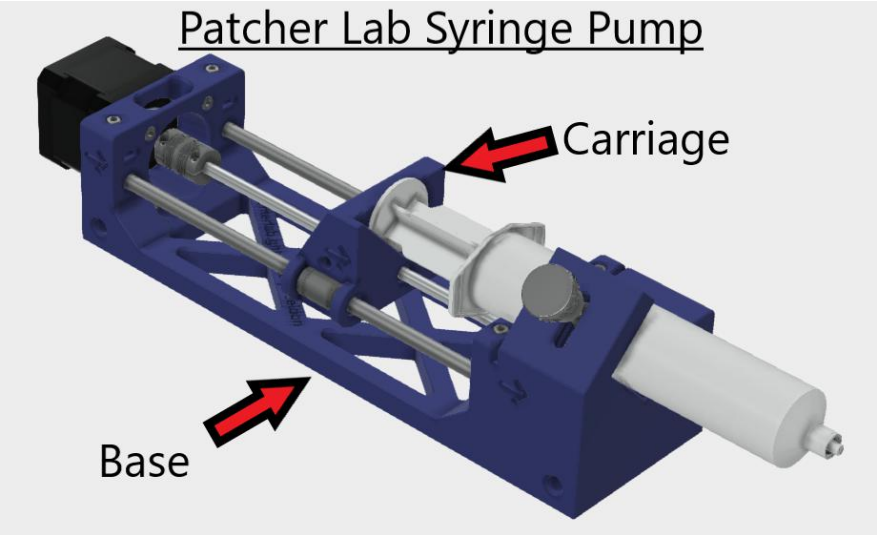

Figure 3.13: The original design of the Pachter Lab Poseiden Syringe Pump [77], highlighting the parts that are altered in this projects design.

The changes made to the pump base from the original model are shown in Fig. 3.14. In the back, the space where the body of the syringe was placed is filled and extended upward. The extension has a slot with four pins in it to hold the silicone synthetic intestine and its holder in place approximately 75 mm above the lead screw, so it aligns to where it will be squeezed by the robotic circular muscles. This slot is mirrored on the other side of the base in a raised section so that the synthetic intestine is level. The component is 3D printed (according to the recommendation of Pachter Lab [77]) using a Creality® 3D printer (218253 Ultimaker S5 (AU), Creality®, Shenzhen, China) and a 2.85 mm white Acrylonitrile Butadiene Styrene (ABS) filament. This exact printer was used as a larger print volume (330 x 240 x 300 mm) was required to build the modified pump base.

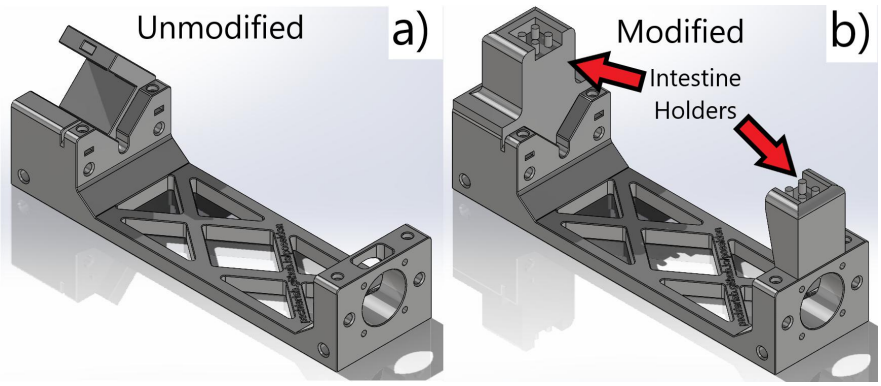

Figure 3.14: Changes made to the pump base of the Poseiden Syringe Pump [77] as shown in a), which has been raised on the front and back end with slots to place the intestine holders of the synthetic intestine as shown in b).

The carriage in the Poseidon Syringe Pump [77] has been extensively modified to be suitable for an intestinal robot, as shown in Fig. 3.15. Three M3 bolt holes have been added to the body of the carriage above the lead screw and rod holes. They provide a space to mount an attachment to the carriage which will be for the mechanism which replicates the circular muscle contractions which is part of peristaltic motion. There is a wider cutaway above the bolt holes so that the same length of bolt (20 mm) can be used. On the left side an extension has been added to support a Nema 17 stepper motor, so it can be fastened in place using three 10 mm M3 bolts (only three as one of the holes is obscured by the attached mechanism) with a cutout so that the motor sits flush against the carriage. There is a hole in the centre so the motor shaft can come out on the other side. The carriage is printed with a Bambu Lab® 3D printer (Bambu Lab® A1 Mini, Bambu Lab®, Shenzhen, China) with a 0.2mm orange Polylactic Acid (PLA) filament.

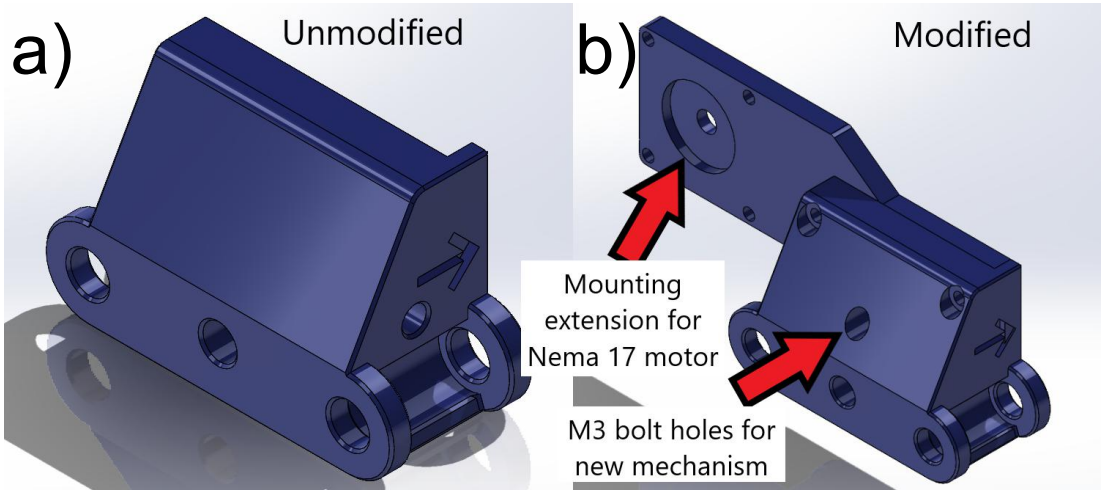

Figure 3.15: Changes made to the carriage of the Poseiden Syringe Pump [77] as shown in a), which has three M3 bolt holes added to support a new mechanism and an extension of the left side to bolt on a Nema 17 stepper motor while allowing its motor shaft to go through as shown in b).

Mechanism Design

Creating a continuous range of motion for the longitudinal muscles is a straightforward process with established methods of actuation like using a lead screw coupled to a stepper motor which is more than sufficient. Replicating the compression of the circular muscle in the synthetic intestine is a more complex process. Existing methods use a series of actuators that are fixed in place at consistent intervals to mimic the motion of the peristalsis using electronic or pneumatic compression [76, 78, 79]. However, this motion is not continuous, which causes aliasing, and the thickness of the actuators

makes it impossible to completely eliminate it. The proposed solution uses a custom actuator that compresses the synthetic intestine while moving its length up and down using the linear actuator of the Poseidon Syringe Pump [77]. The first step was finding examples of actuation that could achieve this motion, the most promising option came in the form of a simple aperture design which is used similar to a camera aperture, shown in Fig. 3.16. The design was modified with the red blades replaced with slider-crank mechanisms, translating the rotational motion into linear motion on all sides, allowing for an even grip at the centre. These arms are reinforced with a bracer that sits flush against the slider-crank slot. The green linkages were also reduced in length to accommodate the added features.

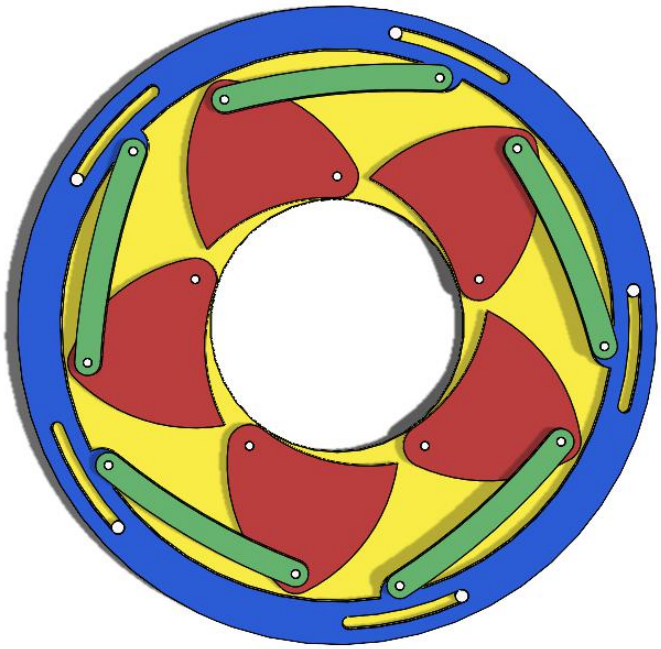

Figure 3.16: The original concept the aperture mechanism was based off. The primary changes involve swapping the red blades for slider-crank arms, shortening the linkages, and adding structural support in the centre for firm grasping. The original model is accredited to Bieber Alexis: https://grabcad.com/library/mechanical-iris-5

The modifications made to the model in Fig. 3.16, created version 1 as seen in Fig. 3.17. This design was printed using a Creality® 3D printer (Creality® Ender-3 V3 SE, Shenzhen Creality 3D Technology Co.,Ltd., Shenzhen, China) with a PLA filament. The design was assembled with mainly M2 bolts and some M3 bolts. This proof-of-concept demonstrated that the type of motion desired was achievable using this kind of mechanism. However, its range of motion was limited because the arms seize up once they reach a 90° angle with themselves. The rough surface due to the layering of the filament also made the mechanism difficult to move because of the high

friction resistance. Its size was also much larger than necessary and could be made more compact to better integrate with the rest of the robotic intestine robot. These issues are addressed in version 2 with the entirety of the mechanism constructed from 3 mm sheet Poly Methyl Methacrylate (PMMA), which is machined to shape using a CNC mill. The aperture radius and arm length were reduced so that the overall diameter was reduced from 150 mm in version 1 to 130 mm in version 2. All bolts used in the body of this design are M3, as they are easier to source and are better at reinforcing the structure. Since this is cut from sheet the base layer and slots for the slider-crank arms are separated. They are then tightly bolted together with the redesigned bracer to form the static part of the assembly. At the end of the arms an M2 threaded hole is tapped, allowing for an M2 4 mm shoulder bolt to be attached, with roller beads printed from the Creality Ender-3 3D printer using PLA filament. These roller wheels theocratically allow the mechanism to move down the length of a surface without being caught due to friction, and the exposed bolt thread would cut into the grasped material. However, the threads for the M2 shoulder bolts were too short and easily became undone; and the roller wheels were too small, making the mechanism stick. In version 3 the arms were redesigned to fit the entire 4 mm bolt thread and sanded down to the hole, minimising the contact the arm had with the material. The diameter of the wheels was increased and a grippy pattern was applied to the surface. The sliding outer part of the mechanism in version 2 is extended out 2 mm and a 3D printed gear profile (for a timing belt) is attached to it using M3 bolts allowing the mechanism to become motor driven.

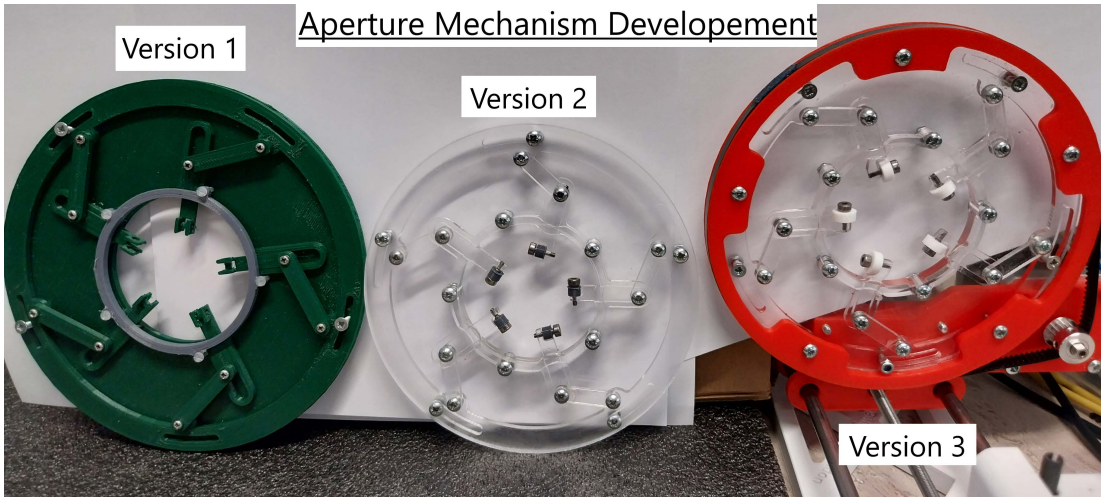

Figure 3.17: The physical prototyping done on the aperture mechanism, starting with a basic proof-of-concept in version 1 to the final prototype in version 3.

The final design is depicted in Fig. 3.18 and is assembled from components in Appendix A.1. The aperture mechanism is fixed to the carriage of the Poseidon Syringe

Pump using the previously made modifications and on the bottom right a Nema 17 stepper motor is fixed to the carriage with the motor shaft coming through to the front. The motor shaft has a 6 mm wide 16-tooth GT2 timing belt pulley which has a 6 mm wide GT2 timing belt running through it. This belt drives the rotation of the red 3D printed GT2 gear profile which is fastened to the outer slider, which is guided by M3 bolts. When it rotates clockwise it causes the linkages to rotate clockwise at both ends, causing the arms in the centre to move inward. This reduces the effective internal diameter of the aperture, allowing it to evenly squeeze the synthetic intestine, replicating the circular muscles of the small intestine. The range of motion has a maximum diameter of 30.5 mm and a minimum diameter of 11.7 mm.

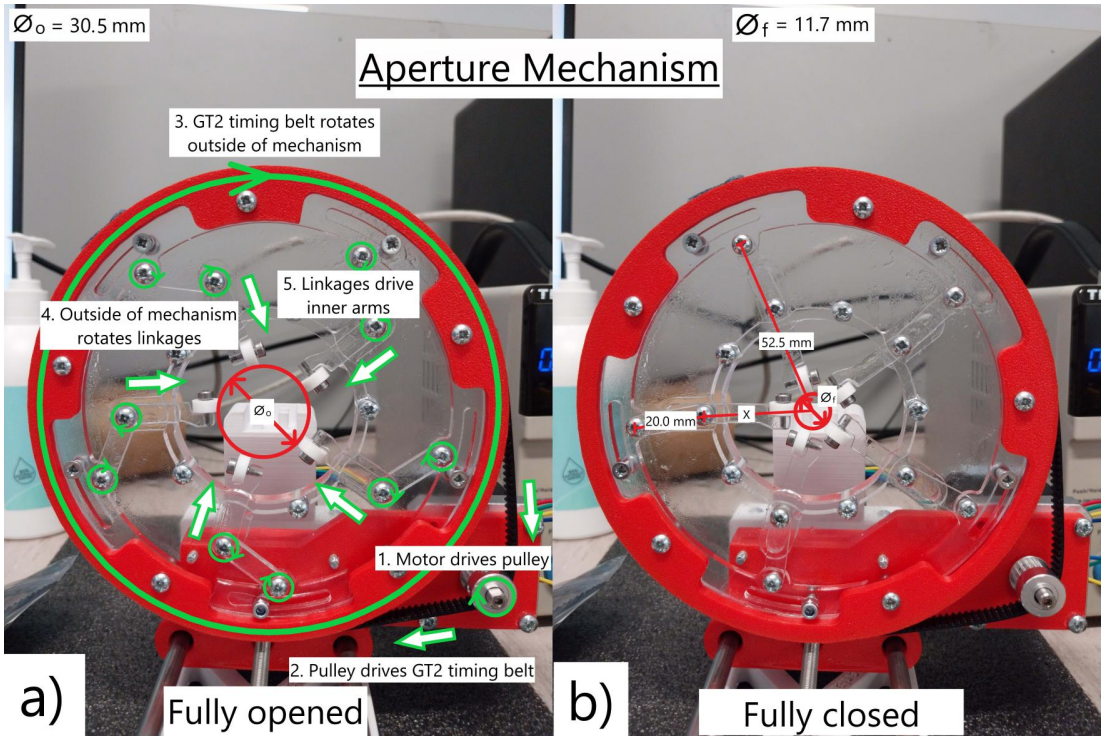

Figure 3.18: How the final prototype moves from the driving motor to the driven inner arms, along with the total range in motion. a) shows the mechanism fully dilated, while b) shows the mechanism fully contracted

Theoretical Motion

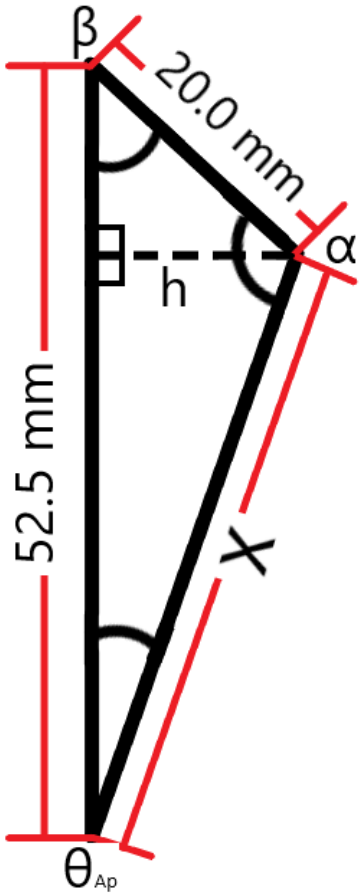

Figure 3.19: A simplification of the motion of the aperture mechanism. It shows how one arm moves with respect to the fixed lengths from center to top (52.5 mm), and the linkage itself (20.0 mm), with the movement of the arm represented by 'X'. The driving angle is θ_{Ap} and the driven angles are α and β.

The aperture mechanism has a theoretical range of motion that is calculated to allow for control at the end of the roller wheels at the end of the robotic arms. The motion of the mechanism shown in Fig. 3.18 can be simplified to a triangle in the diagram in Fig. 3.19. The distance from the first bolt of the linkage to the centre of rotation is constant at 52.5 mm. The length of the linkage itself is also constant at 20.0 mm long. The distance from the centre of the second bolt to the centre of rotation is a variable defined as 'X'. When the stepper motor causes the mechanism to rotate via the GT2 timing belt, this causes the angle between the 52.5 mm line and 'X' to change by the same rotation, which is represented by θ_{Ap}. The other angles change in response to θ_{Ap} and are defined in Fig. 3.19 as α and β. To determine how θ_{Ap} causes 'X' to change an intermediate value 'h', represents the distance from the 52.5 mm line to α and is used to decompose the triangle into two right angle triangles, simplifying the trigonometry. The equations used to find 'X' from θ_{Ap} are defined below:

$$\frac{\sin\theta_{\text{Ap}}}{20} = \frac{\sin\alpha}{52.5} \tag{3.1}$$

$$\alpha = (\arcsin(2.625\sin\theta_{\text{Ap}}) - 180) * -1 \tag{3.2}$$

$$\beta = 180 - \theta_{\text{Ap}} - \alpha \tag{3.3}$$

$$\beta = 180 - \theta_{\text{Ap}} + \arcsin(2.625\sin\theta_{\text{Ap}}) - 180 \tag{3.4}$$

$$\beta = \arcsin(2.625\sin\theta_{\text{Ap}}) - \theta_{\text{Ap}} \tag{3.5}$$

$$h = 20\sin(\beta) \tag{3.6}$$

$$h = 20\sin(\arcsin(2.625\sin\theta_{\text{Ap}}) - \theta_{\text{Ap}}) \tag{3.7}$$

$$x = \frac{h}{\sin\theta_{\text{Ap}}} \tag{3.8}$$

$$x = \frac{20\sin(\arcsin(2.625\sin\theta_{\text{Ap}}) - \theta_{\text{Ap}})}{\sin\theta_{\text{Ap}}} \tag{3.9}$$

After calculating for 'X', the result needs to be adjusted to compensate for the length of the robotic arm and roller wheel. The measured arm length from its centre of rotation at the bolt to the linkage to the end of the roller wheel is approximately 27.2 mm on average. Therefore, the formula for determining the effective diameter at which the aperture mechanism squeezes the synthetic intestine is as follows:

$$\theta_{\text{Ap}} = 2(x - 27.2) \tag{3.10}$$

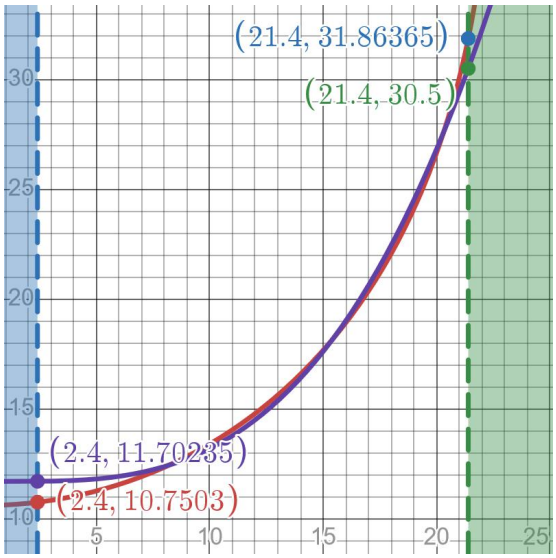

Figure 3.20: The difference between the theoretical formula (in red) which uses sines to solve for the aperture movement and the approximation formula (in purple) which uses a cubic formula. The cubic formula is $\varnothing_{\text{Ap}} = 0.00235(x - 1.4)^3 + 11.7$. The difference between the curves is 0.3 mm or less with adjustments at the limits to align with the measured values.

However, this formula is difficult to reverse to find θ_{Ap} from 'X', computationally expensive, and does not align well with the actual motion it ranges. Solving for 'X' across the range of motion from 2.4° to 21.4° gives a minimum $\varnothing_{\text{R}}$ of 10.7 mm and a maximum $\varnothing_{\text{R}}$ of 31.9 mm. This is different from the measured range of motion from 11.7 mm to 30.5 mm. Therefore, a cubic formula is used to approximate the non-linear motion of the aperture mechanism:

$$\theta_{\text{Ap}} = 0.00235(\theta_{\text{Ap}} - 1.4)^3 + 11.7 \tag{3.11}$$

This formula is easier to implement in software to control the position of robotic arms. The y-values at the limits of the formula have been adjusted to align with the measured range of motion. In the middle of the formula the error between it and the theoretical formula is 0.3 mm or less, which is less than the difference between the two minimums and maximums.

Electronic Systems

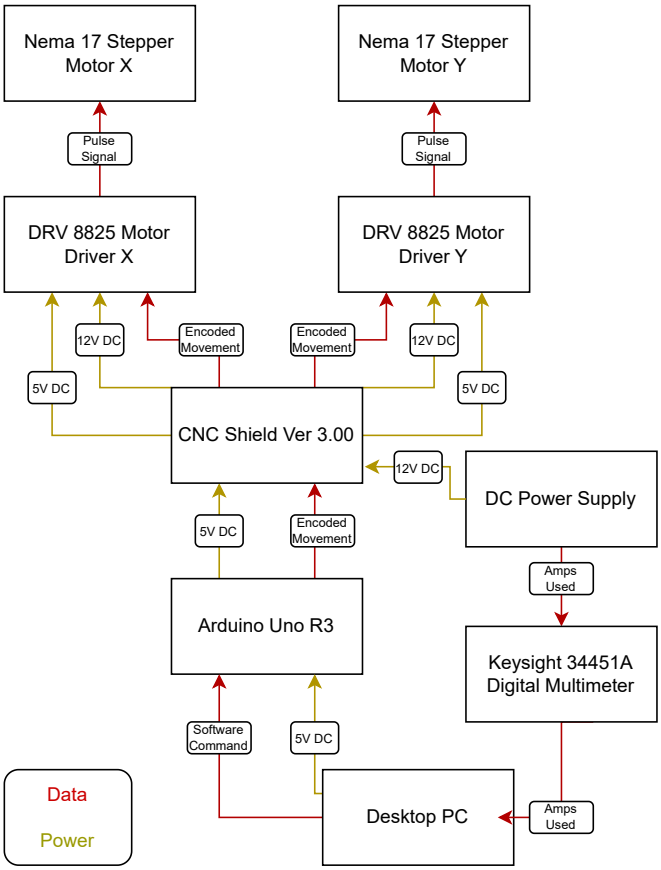

Figure 3.21: The layout of electronic components and power systems used to drive the robotic intestine.

The robot itself is driven by Nema 17 Stepper motors for circular and longitudinal movement. Since circular movement uses less than a full revolution of the stepper motor, it has been microstepped to a 1/32 ratio for finer control on synthetic intestinal compression. In addition, the linear motor has been microstepped to the same level so that it can operate quietly. The stepper motors are driven with a pulse signal sent from DRV 8825 motor drivers which are inserted into a CNC shield Ver 3.00 that plugs into a microcontroller (Arduino® R3, Arduino®, Monza, Italy). A variable Tenma® Direct Current (DC) power supply (72-2690 DC Power Supply, Tenma®, Kita-ku, Japan) is used to power the robotic system that is recorded by a Keysight® 34451A digital multimeter (34461A Digital Multimeter, Keysight®, Santa Rosa, CA, USA). Commands to control robot movement are sent from a desktop computer that also receives the amps used to move objects inside the robotic intestine, which can be used to derive how much excess work is done by the motors.

Control and Communication

The robotic system is programmed in two different environments, a C++ environment on the Arduino Uno and acts as the firmware which directly controls the motors and software written in Python. The Arduino Uno is connected to a PC using a USB cable and communicates with it using a communications (COM) port. Software written in the Python environment allows the user to interface with the system using commands

that are easy to understand.

The firmware assigns which pins on the microcontroller are driving the stepper motors through the CNC shield and initialises serial communications with the PC. The firmware has a main loop that continually checks the serial port for data, then extracts it into a string, and processes the string into a command for the motors. The string is broken into three sub-strings, saying; which motor is to be driven (X/Y), how many steps the motor should move, and which direction it should go (forward (F)/reverse (R). An example of a command is as follows 'Y640000F' which translates to move motor Y 640,000 steps forward. It takes this information and sends it to the moveStepper function, writing to the corresponding pins for the targeted motor, configuring it to the correct direction, and then creating a loop to move it to the appropriate number of steps. This loop writes the stepping pin high and low to move it one step which has a delay of 150 µs between each pin write to make it move 1.5 cm/min [50], the speed at which the intestine moves. If invalid commands are sent at any point, an error message will be written to the serial.

The software (programmed in the Python language) performs the calculations required to manipulate the positions of the edge of the roller wheels relative to the machine's initial position. Open-loop control is used for its simplicity and due to the space the CNC motor shield occupies on the Arduino board. The software makes use of two imported modules for communications, including Serial to open, read, and send information into the COM port, and the Time module to allow time for initialisation. The software is initialised in the main function, which opens the serial port and returns an error if it cannot be opened. Both motors are jogged back and forth by 400 steps to validate that the robot is operational and to prepare it for operation. A while loop is started, which prompts the user for an input into the control terminal of the software. It will ask the user to set the position of motor X (circular) or motor Y (linear) in millimetres, with motor X restricted between 30.5 and 11.7 mm. The position of motor Y can also be reset, or the software can be closed in the terminal. If a position command is sent, it will be broken down into which motor to drive and how many millimetres it must move. The required steps to move will be calculated based on which motor is driven, if motor X is moved this will involve the previously calculated formula to convert it to motors steps through the required amount of revolutions. In the software, it is always assumed that the motor X is starting at 30.5 mm, so it must be manually adjusted to the maximum dilation before it is operated. Motor Y relies on simple calculations using the pitch of the lead screw to convert the set position into the required revolutions of the motor. To ensure that the motors are likely left in the consistent positions to start with, when the program is terminated, both motors will return home which is 0 mm on motor Y and its starting position on motor X.

3.2 Testing

3.2.1 Tensile

Early Testing

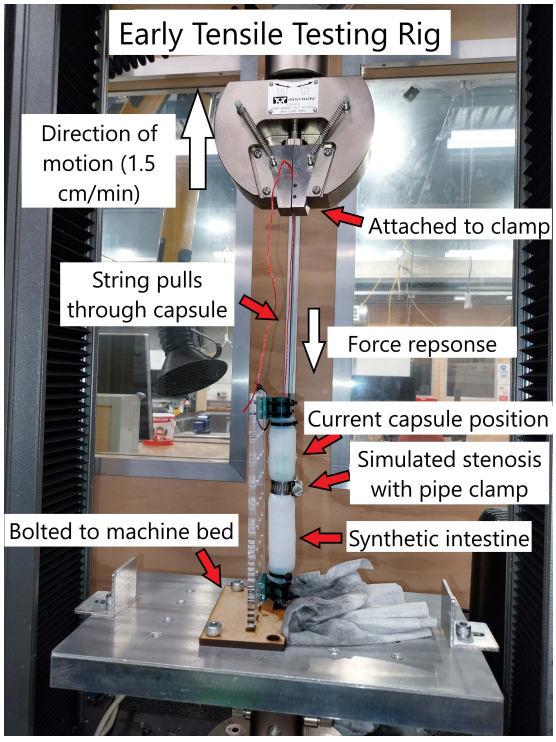

Figure 3.22: The tensile testing configuration used in early prototype evaluation. The machine is an Instron® 5967 tensile testing machine that is pulling capsule designs through a Ø20.8 mm constriction on the outside of the synthetic intestine (made by the pipe clamp) at a speed of 1.5 cm/min [50] and recording the force response across distance travelled.

This experiment aims to measure the tensile force generated when various capsule designs (Fig. 3.1) pass through a simulated narrowing in a synthetic silicone intestinal testing rig in Fig. 3.22. The materials and equipment used for this experiment include the following:

- **Plastic Capsule:**
  Fabricated using a Flashforge® Hunter resin printer with FHD-1200 resin (Acrylated monomer 50%, Methacrylic resin 47%, Additives 2%, Photoinitiator 1%) and Bioflex resin (composition is proprietary information).
- **Synthethic Intestine:**
  Fabricated using the methodology described in Section 3.1.2.
- **Tensile Testing Machine:**
  A tensile testing machine (Instron® 5967 30 kN, Instron®, Norwood, MA, USA) with a grip attachment on the upper half and a base plate with M10 bolt threads (as shown in Fig. 3.22).

- **Attachments:**
  Synthetic intestine holders printed from a 3D printer (Prusa® Mk 3, Prusa Research, Prague, Czechia) using PLA filament with four Ø4.5 mm holes spaced 10 mm apart; 6 mm thick Poly Methyl Methacrylate (PMMA) base board cut using a laser cutter (Fusion Pro 48, Epilog Laser®, Golden, CO, USA) with 2 sets of the four Ø4.5 mm holes on the intestine holders and an array of Ø5.0 mm holes for manipulation of intestine position; 6 mm thick Medium Density Fibreboard (MDF) cut from sheet using a laser cutter with an interlocking pattern to perpendicularly attach to the bottom of the base board with Ø10 mm holes to fasten it to tensile testing machine.

- **Synthetic Mucus:**
  A 0.1% (w/w) solution of xanthan gum and water to replicate the viscosity of bodily mucus secretions (similar to that found in the small intestine) [80].

- **Pipe Clamp:**
  A 13 - 26 mm pipe clamp for simulating stenosis (Breeze® 300 Series S.S., NORMA Pacific Australia, Dandenong South, Australia)

- **Containers and Syringes:**
  Any plastic syringe with with mL markings for injecting 5 mL of synthetic mucus, and any glass jar to prepare and store synthetic mucus.

- **String:**
  Narrow diameter household twine to pull capsules (Jobmate Household twine 61 m, Mitre 10, Auckland, New Zealand)

The experiment was carried out in a workshop environment, using a tensile testing machine at Massey University, Palmerston North, New Zealand. An assembled testing rig (a static intestinal environment to evaluate capsule performance) using the synthetic intestine combined with fabricated attachments and pipe clamp was used in the following experimental procedure:

1. Add the grips to the top half of the tensile testing machine and a base plate to the bottom half with evenly spaced M10 bolt holes.

2. Fasten the synthetic intestine test rig to the base plate of the tensile testing machine using M10 bolts and centre it in the middle of the intestine below the grips.

3. Take out the capsule design, pass the twine through the top hole of the capsule body and tie a knot on the other side, pulling the knot down to the hole to ensure

it cannot pass through and enclosing it with the end cap. Cut to a sufficient length to reach the grips.

4. Pass the cut end of the length of twine through the grips and tighten until it is firmly held in place.
5. Push the capsule manually down the synthetic intestine testing rig until it is past the pipe clamp, adjust the z-height of the tensile testing machine if necessary.
6. Apply 5 mL of synthetic mucus to the synthetic intestinal testing rig.
7. Set the tensile testing machine to move upward at a speed of 1.5 cm/min [50] in a 'quick-test' routine and observe it while recording the current tensile force applied by the capsule.
8. When the force begins to climb above 0.1 N, inject an additional 5 mL of synthetic mucus into the synthetic intestine to maintain lubrication as the capsule passes through the pipe-clamped area.
9. Stop the test once the force drops below 0.1 N for 5 s, which will automatically log all the collected data.
10. Reset the z-axis back to the initial starting position on the tensile testing machine and manually push the capsule below the pipe clamp.
11. Repeat steps 6-10 twice more to collect replicates to validate the data collected.

Independent Variable:
The shape of the capsules and their material composition are tested.

Dependent Variables:
The force (N), the maximum force (N), and the work done (J) by the capsule as it passed through the pipe-clamped area.

Controlled Variables:
The diameter and fabrication method of the capsules; the concentration and quantity of xanthan gum solution used; the dimensions, shape, and materials used in the synthetic intestinal testing rig.

Data are collected automatically using proprietary software used by Instron® tensile testing machines. Then it is exported to separate CSV files for each capsule experimented with (with each replicate in the same file) at a resolution of 0.1 N (the software records 0.001 N, but it forcibly exports to 0.1 N). Each replicate is trimmed

to within 5 s before and after the capsule enters the pipe-clamped area and aligned chronologically to when the capsule starts entering the pipe-clamped area. Each replicate is averaged together, providing the average result for each capsule. Each set of capsule data is combined into a single table and imported into Minitab® statistical analysis software (Minitab® 22, Minitab, LLC, State Collage, PA, USA). The software calculates the effect of the independent variables on each of the dependent variables individually and determines the optimal parameters to use. In addition, the data are graphically analysed to qualitatively understand the capsule's behaviour. Graphs are also generated using Matlab® (Matlab®, Mathworks Inc, Portola Valley, CA, USA).

Shape Variants Testing

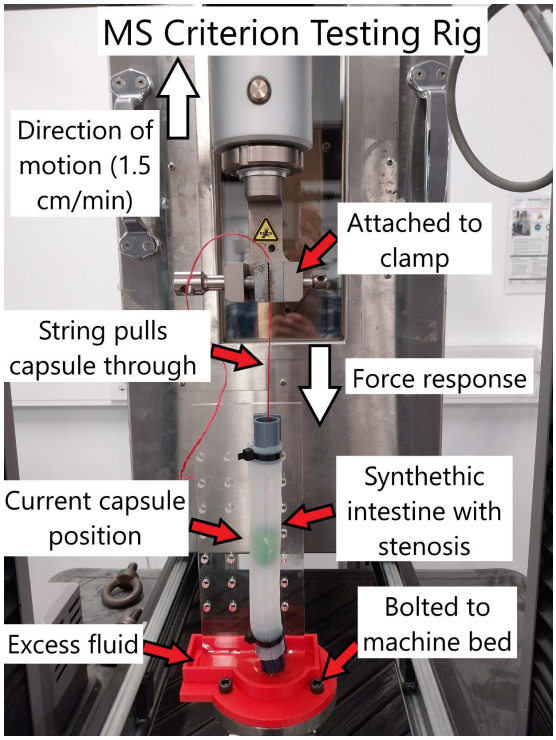

Figure 3.23: The tensile testing configuration used in later testing. The machine is an MTS Criterion model 43 that is pulling capsule designs through an approximately Ø11 mm moulded stenosis at a speed of 1.5 cm/min [50] and recording the force response across distance travelled.

This experiment aims to measure the tensile force generated when various capsule designs in Fig. 3.3, pass through a narrowing in a synthetic silicone intestinal testing rig in Fig. 3.23. The differences in materials and equipment used for this experiment include:

- **Plastic Capsules:**
  Fabricated with a Flashforge® Hunter resin printer with FH-1200 resin (Polyurethane acrylate resin 50%, Acrylated monomer 40%, Toner 5%, Photoinitiator 5%).
- **Synthethic Intestine:**
  Fabricated using the methodology described in Section 3.1.2 with stenosis and CD texture.
- **Tensile Testing Machine:**
  A tensile testing machine (MTS® Criterion Model 43, MTS systems®, Eden Prairie, MI, USA) with a 100 N load cell (LPB.102 E) and with grip attachment and an M10 threaded base plate (as shown in Fig. 3.23).

- **Attachments:**
  Synthetic intestine holders printed from a 3D printer (Creality® Ender-3 V3 SE, Shenzhen Creality 3D Technology Co.,Ltd., Shenzhen, China) using Polylactic Acid (PLA) filament with four Ø4.5 mm holes spaced 10 mm apart; 6 mm thick PMMA base board cut using a laser cutter (Fusion Pro 48, Epilog Laser®, Golden, CO, USA) with two sets of the four Ø4.5 mm holes on the intestine holders and an array of Ø5.0 mm holes for manipulation of intestine position; 6 mm PLA base board printed using a Bambu Lab® 3D printer (Bambu Lab® A1 Mini, Bambu Lab®, Shenzhen, China).

- **Pipe Clamp:**
  Not Used

This experiment was carried out at the Materials Testing Laboratory at the University of Canterbury, New Zealand. The methodology for the experiment is nearly the same except that an MTS® tensile testing machine is used and configured to run at 1.5 cm/min [50] and is controlled with the run and stop buttons. There is no pipe-clamp which is replaced with a moulded-in stenosis section within the synthetic intestine.

This experiment was carried out in the Materials Testing Laboratory, using a tensile testing machine in the Department of Mechanical Engineering, University of Canterbury, Christchurch, New Zealand. An assembled testing rig (an intestinal environment to evaluate capsule performance) using the synthetic moulded-in stenosis intestine combined with fabricated attachments was used in the previous experimental procedure outlined in the Early Testing subsection of Section 3.2.1.

Independent Variable:
The shape of the capsules tested.

Dependent Variables:
The force (N), the maximum force (N), and the work done (J) by the capsule as it passed through the moulded-in stenosis area.

Controlled Variables:
The diameter, material, and fabrication method of capsules; The concentration (0.1% w/w) and quantity of xanthan gum and water solution used; the dimensions, shape, and materials used on the synthetic intestine testing rig.

Data are collected automatically using proprietary software used by MTS® tensile

testing machines. Then it is exported into separate text files for each capsule experimented with (with each replicate in the same file) at a resolution of 0.001 N. Each replicate is trimmed when it rises above 0.1 N and falls below 0.1 N. Each replicate is averaged together, providing the average result for each capsule. Each set of capsule data is combined into a single table and imported into Minitab® statistical analysis software. The software calculates the effect of the independent variables on each of the dependent variables individually and determines the optimal parameters to use. In addition, the data are graphically analysed on charts to qualitatively understand the behaviour of the capsules. Graphs are also generated using Matlab®.

Materials Testing

This experiment aims to measure the tensile force generated when the final capsule design in Fig. 3.4 is fabricated with different rigid biocompatible materials and manufacturing techniques in Fig. 3.5. This experiment will use the exact same materials, equipment, and testing procedure from the previous subsection (Shape Variants Testing) with materials and respective manufacturing techniques described in the Optimising for Materials and Manufacturing subsection in Section 3.2.1.

Teflon was lathed and milled as its higher flexibility caused uncertainty about whether it would be possible to lathe or not. Since it was made successfully with the lathe, both capsules were tested to see if there is a significant difference between the two.

3.2.2 Capsule Peristalsis Propulsion Testing

In this experiment, the capsules developed for the Materials Testing subsection in Section 3.2.1 will be evaluated in the robotic intestine developed in Section 3.1.3 shown in Fig. 3.24. This robotic intestine uses a similar synthetic intestinal design with moulded-in stenosis, except the texture is removed to lower the difficulty of transit, as there were issues with capsules becoming stuck. This creates an obstacle to navigate through that can be compared with previous data. The system is lubricated with an aloe vera gel which shares properties similar to intestinal mucus [81]. This experiment aims to measure the work required to pass through the constriction by pushing force instead of the pulling force used in Section 3.2.1. It will analyse capsules made from different materials and manufacturing methods in Materials Testing. The materials and equipment used for this experiment include the following:

- **Plastic Capsules:**
  The same five capsules as the previous Materials Testing subsection within Section 3.2.1 shown in Fig. 3.5.

- **String:**
  Narrow diameter household (Jobmate) twine to pull capsules

- **Synthethic Intestine:**
  Fabricated using the methodology described in Section 3.1.2 including stenosis replication without CD texture.

- **Robotic Intestine:**
  As described in Section 3.1.3.

- **Synthetic Mucus:**
  Thursday Plantation® aloe vera (Thursday Plantation®, Homart Wellness Australia Pty Ltd., Rydalmere, Australia).

- **Power Supply:**
  A Tenma® DC power supply.

- **Data Logger:**
  A Keysight® digital multimeter.

- **USB Stick:**
  A generic USB storage device with at least 10 MB of storage.

- **Leads and Wires:**
  Generic power supply test leads and electronic jumper wires.

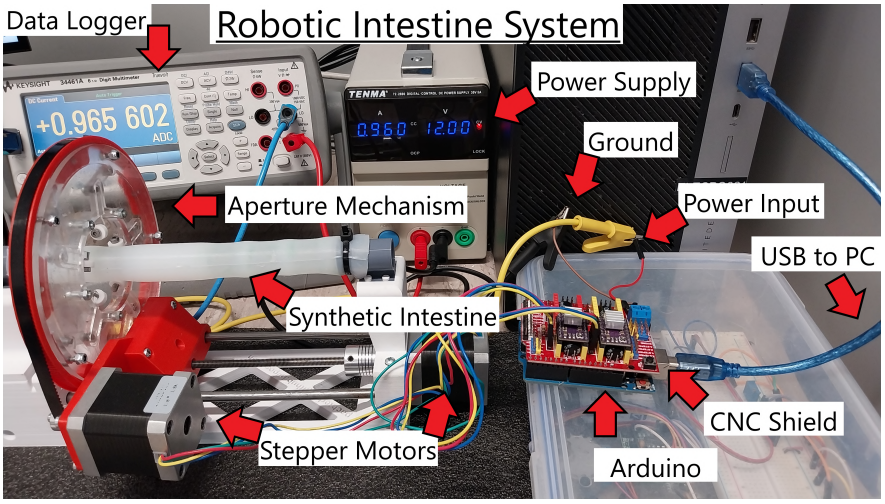

Figure 3.24: The testing setup used for operating and collected data from the robotic intestine system. Power is supplied at 12 V using a Tenma® desktop DC power supply with a Keysight® digital multimeter data logger placed in series to record the amperage as the robot pushes the capsule with peristalsis.

The experiment was carried out in the Postgraduate Study Area at the Department of Electrical and Computer Engineering, University of Canterbury, Christchurch, New Zealand. The robotic intestine is fully assembled and connected to a DC power supply using test leads and jumper wires with the data logger placed in series before the 12 V connection to the CNC motor shield. The test is performed on five capsules in the following experimental procedure:

1. Turn on the power supply and set it to 12 V at a maximum current of 1.6 A, turn on the data logger, set it to DCI mode, and display the data on a trend chart. Put a USB drive into the data logger.

2. Connect USB A to USB B cable from Arduino® to desktop PC. Run Python-based software on the desktop PC and ensure that it communicates successfully with the robot.

3. Apply 2 mL of aloe vera gel to the side of the synthetic intestine where the capsule will be placed and spread it down its length using a solid object (in this case a spare capsule).

4. Ensure that the linear motor position is set to zero approximately the capsule length (30 mm in this experiment) behind the moulded-in stenosis of the synthetic intestine and the aperture mechanism is fully dilated.

5. Wipe the capsule until clean and dry with a string already attached. Put it inside the synthetic intestine just past the aperture mechanism.

6. Set the aperture position to 11.7 mm in motor X and pull the capsule back with the attached string until it is in front of the simulated peristaltic contraction.

7. Simultaneously set the linear position to -75 mm (or + 75 mm if operating from opposite side in Fig. 3.24) and press the clear readings button on the data logger.

8. Once movement completes, press the acquire button on the data logger and save readings to the USB drive. Set the aperture position to 30 mm and then the linear position to 0 mm.

9. Repeat steps 4 - 8 until 10 replicates are collected for the tested capsule to average out natural variability in the power supply, then repeat step 3 once.

10. Repeat step 9 for each capsule tested in the experiment and once again using no capsule to measure the baseline current draw.

Independent Variables:
The material and manufacturing processes used to make the capsules.

Dependent Variable:
The current drawn by the stepper motors from the CNC shield (A).

Controlled Variables:
The diameter and target shape of the capsules; The amount of aloe vera gel applied before each capsule; The dimensions, shape, and materials used in the synthetic intestine testing rig; The starting position of the robotic intestine and capsule; The distance the robot is linearly actuated for each trial; The voltage applied to the stepper motors.

Data are collected by saving the logged current data in the short-term memory of the data logger onto a USB stick. It is saved as a CSV file with a resolution of 10 nA. The elapsed time was manually recorded for the experiment at 184 s and divided between all data points collected, providing time stamps. The base current (the current draw without the motors doing work) is determined for each trial by finding the minimum value in the first and last 15 data points and calculating the slope between them. A linear trend is put between these two points, and the difference between this line and the current draw is calculated. The current is summed, then multiplied by 12 V and the time slice of 0.404 s to calculate the work done in a trial. The median and quartiles are calculated then the median baseline work (work done without capsule) is subtracted from the result for each material type. In addition, the current difference for the 10 replicates is averaged and the average baseline current is subtracted from each material type and multiplied by 12 V to give the excess power consumption graphs for each material type. All calculated data are then drawn into graphs and box-and-whisker plots using Matlab®.

3.2.3 Contact Profilometery

To understand what the actual surface is that is produced using different manufacturing methods, the surface of the capsules must be assessed quantitatively. There are two methods of measuring the surface profile of objects, contact profilometery which uses a probe to measure displacement as it is physically dragged down the length of the object and non-contact profilometery which uses beams of light to measure the distance through reflection off the object [82]. Since some capsules are made with transparent resin, it will likely interfere with the reflection of light; therefore, the best method to use is contact profilometery.

This experiment aims to measure the surface profile of five different capsule surfaces

in the Materials Testing subsection of Section 3.2.1 in Fig. 3.5. The materials and equipment used for this experiment include the following:

- **Plastic Capsules:**
  The same five capsules as the previous Materials Testing subsection within Section 3.2.1 shown in Fig. 3.5.
- **Contact Profilometer:**
  A Intra Touch contact profilometer (Intra Touch, Ametek®, Berwyn, PA, USA).
- **Platform:**
  A custom-made platform with rotary stage.
- **Adhesive Putty:**
  2 g of adhesive putty at each end of the capsule to hold the position on the stage.
- **Marker:**
  A generic black marker.

The experiment was carried out in the Characterisation Laboratory at the Department of Electrical and Computer Engineering, University of Canterbury, Christchurch, New Zealand. Contact profilometery is performed on five capsules in the following experimental procedure:

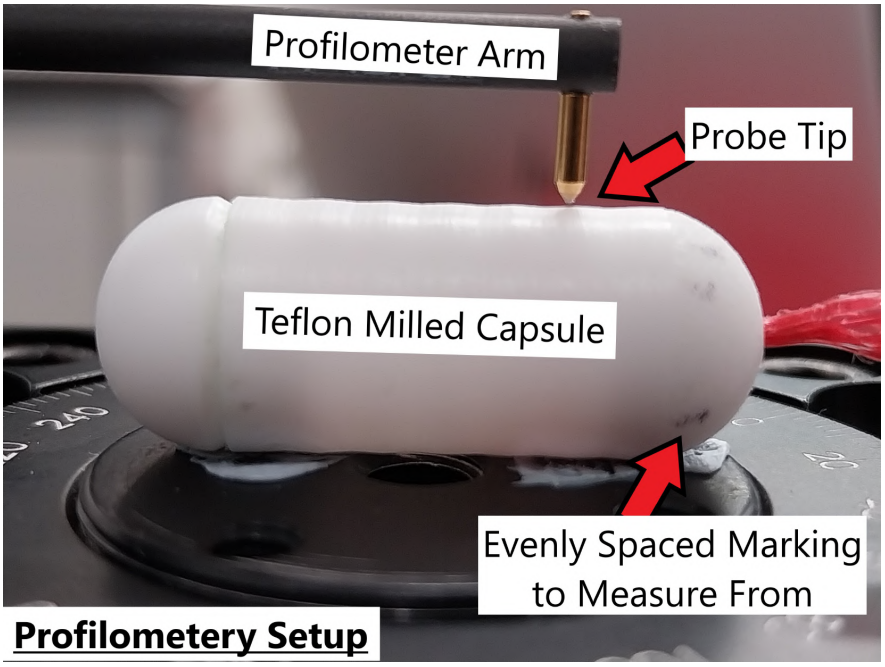

Figure 3.25: The contact profilometery process when a cantilever arm is in contact with the capsules surface and is translated down its length recording its vertical displacement as it travels. The capsule is marked into quarters to sample from each side of it.

1. Use a black marker to divide the circumference of each capsule into quarters to provide a reference from where sampling should begin.
2. Attach the probe to the contact profilometer and open the computer software to communicate and log data from the profilometer.
3. Apply 1 g of adhesive putty to the rotary stage at each end of where the capsule will go, to ensure that the capsule is held in place during measurement.
4. Press the capsule into the putty until it is held in place and ensure that one of the black marks is orientated upward.
5. Place the platform underneath the probe and use the rotary platform to align the capsule with the profilometer arm so that they are parallel.
6. Lower the probe until it contacts the surface of the capsule, as indicated in the software.
7. Move the probe 10 mm down the capsule's surface and save data to the computer.
8. Raise the probe, clean the adhesive putty from the surface of the capsule to prevent interference with the probe, and rotate it 90°.
9. Repeat steps 4 - 8 until all 4 sides of the capsule are measured.
10. Repeat step 9 on each of the five capsules. Export the profiles after levelling the data in the software to compensate for misalignment.

Independent Variables:
The material and manufacturing processes used to make the capsules.

Dependent Variable:
Vertical displacement along the surface of the capsule (µm).

Controlled Variable:
The planned shape of the capsule.

Data are collected using the proprietary software used by Intra Touch profilometers, an operation within the software automatically calculates the Root Mean Square (RMS) surface roughness. Then it is exported into separate text files for both the profile and the summary of the surface roughness for each measured surface, down to a resolution of 1 pm (probably sensitive to 1 nm [82]). The profile of each side is trimmed so that the peaks and troughs are aligned and 9 mm of recorded length is left. The mean of all

four sides is calculated, creating the average profile for each capsule and the average surface roughness. The profile data are graphically analysed against the planned shape of the capsule by generating graphs using Matlab®.

3.3 Summary

A wide range of fabrication methods are explored to create capsules, including 3D SLA printing, CNC micromilling, and CNC lathing; and multiple materials are identified. In addition, a process for creating a synthetic intestine is developed from silicone resin, which is used in tensile testing setups and a novel robotic intestine system. Experimental procedures are described to measure the capsules created; to conduct tensile testing with capsules at Massey University and the University of Canterbury; and how to experiment with the robotic intestine. Data can be collected from these experiments, which is presented and discussed in the next chapter.

Chapter 4

Results & Discussion

This section covers the results and data collected from the experimental procedures described in the previous chapter; discussion of the implications of these results; how they relate to literature; and what limitations were in the experiments conducted.

In Section 4.1, the results are presented on the measured profiles of each capsule in Fig. 3.5 and their respective calculated RMS surface roughnesses. The 3D SLA printer is discussed to have produced the most accurate capsule shape but had a high roughness of 5.41 µm due to process layering, with the milled capsule even higher at 6.42 µm due to teflon flexure. The lathe achieved a lower surface roughness of 2.94 to 4.04 µm, suggesting a microscale-capable lathe could outperform the SLA printer. A significant difference between lathed and non-lathed capsules is identified, requiring further investigation for its impact on later experiments.

In Section 4.2, the results on the force response of all capsules produced for this thesis are presented in multiple tensile testing experiments. In the discussion, it is identified that the best tensile testing results came from the capsule printed with surgical guide resin using the segmented design, requiring 0.0228 J, and an average and peak force of 0.485 and 0.860 N, respectively. Closely matching that of a similar milled capsule (0.0223 J and 0.478 N) but with a higher maximum force (0.926 N). The 20 µm difference between lathed and non-lathed capsules significantly affected the force response, suggesting that the shape of the capsule plays a critical role in transit through constricted intestinal environments. Testing in a more realistic setting is needed to understand the effects of the surface.

In Section 4.3, the results of the robotic intestine testing are presented for capsules in Fig. 3.5, using the design in Fig. 3.4. The best results of the robotic intestinal test are discussed as coming from the capsule printed with surgical guide resin using the segmented design, showing the lowest mean work (2.33 J) and power consumption (-0.005 to 0.015 W) to pass the constriction. Its performance was also more consistent between trials. The shape of the capsule had the greatest impact on the results, while

the type of material influenced the passage due to differences in roughness (2.94 to 6.42 µm) and mass (1.60 to 4.42 g).

In Section 4.4, the various discussion sections are summarised, including the interpretation of results and the identification of limitations in experiments.

4.1 Contact Profilometery

4.1.1 Surface Data

The results in Fig. 4.1 are from data collected using the contact profilometery process demonstrated in Fig. 3.25. Data are collected using the previously outlined testing procedure in Section 3.2.3. The purpose of these graphs is to compare the planned shape of the capsules down to the microscale with what was actually fabricated. The graph is divided into two subplots; graph a) shows the differences between the manufacturing types experimented with; and graph b) shows the difference between materials within the same manufacturing type. Graph a) exhibits the strongest differences with the resin-printed capsule closely following the planned shape with some variation of the peaks and a lot of high-frequency variation across the surface. On average, the milled capsule follows the planned shape but has large random deviations throughout its length, making it less accurate overall. The least accurate method is the lathing process which follows at 40 µm triangular waveform instead of the 62.5 µm sinusoidal wave form that was planned. To ensure that this was not variation based on the materials used instead of the fabrication type, two more materials were lathed into capsules on graph b). Of these materials, teflon was the most different with increased jaggedness, but overall all 3 materials were very similar to each other, indicating that lathing is very precise but never accurate to shapes at this scale.

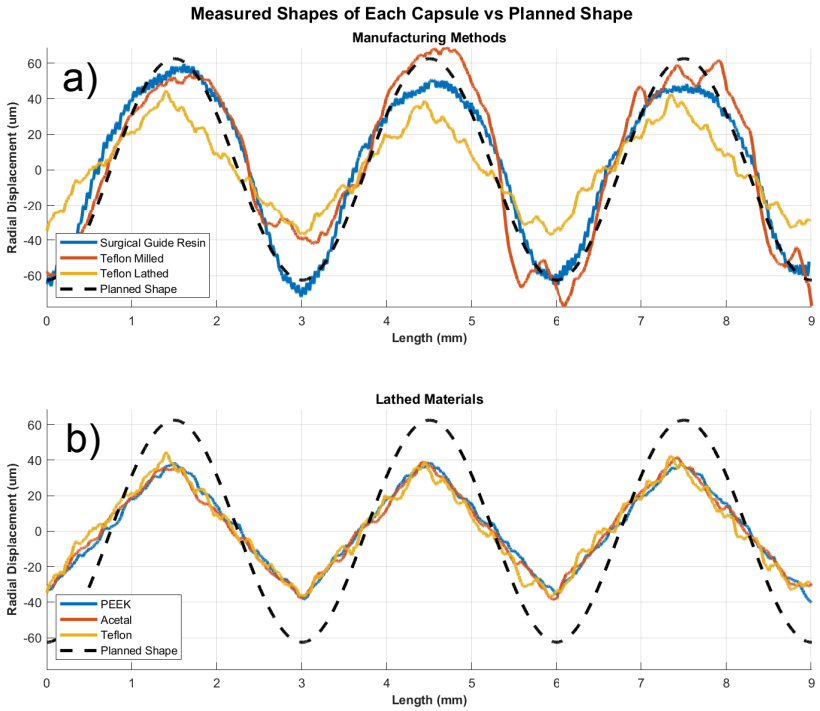

Figure 4.1: The true shape of each capsule that is fabricated for the materials testing and peristaltic propulsion tests. Graph a) highlights the differences between different manufacturing methods; and graph b) shows the differences between each material used on the lathe. The black dashed line on both graphs represents the intended shape of the capsule. The lines on the graphs are made with a moving average of three data points.

The bar chart in Fig. 4.2 analyses the amount of small-scale variation on the surface of the capsules rather than its general precision in calculating the planned shape. Each capsule type is compared with the surface roughness measured by the RMS approach. The milled teflon capsule has the highest surface roughness of 6.42 µm with a high level of variation between each measured side of the capsule, which is much more compared to all other types. This is likely due to the large spikes in the measured profile at the peaks and troughs of the capsule's shape. The surgical guide resin also had a higher RMS roughness of 5.41 µm, which is likely due to the increase in noise along its surface, which is not of high magnitude but occurs frequently along its length. All lathed capsules have lower surface roughnesses of 2.94 - 4.04 µm, which reflects the high precision that this manufacturing process has. Only the lathed teflon capsule is higher than 4.0 µm which is due to its increased noise level along its length.

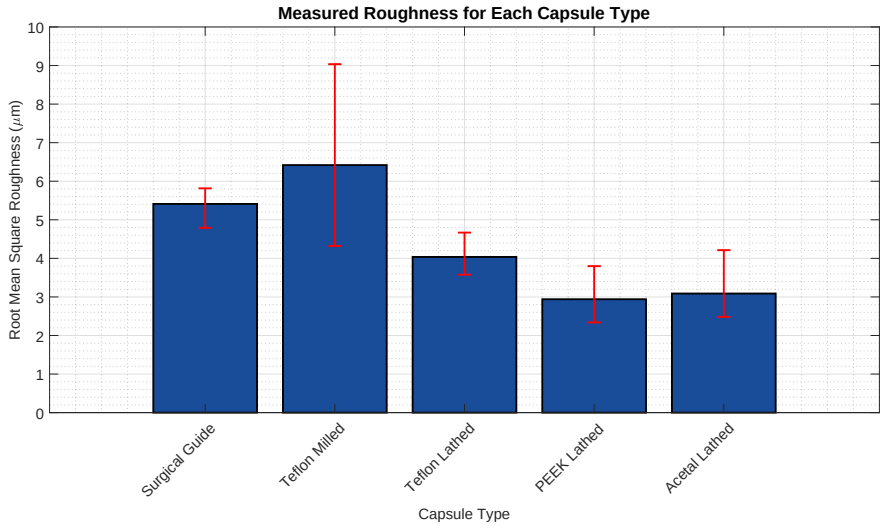

Figure 4.2: The RMS (Root Mean Square) average surface roughness for each capsule type made from its respective material type and fabrication method. The error bars are for four data points.

4.1.2 Discussion

In Fig. 4.1 and Fig. 4.2, it is apparent that there is a significant difference in capsule shape based on the respective manufacturing methods. The printed and milled capsules had the most accurate shapes, but higher roughness, while the lathed capsules were highly inaccurate with lower roughness. This can be explained by how each manufacturing method physically shapes the capsule during the process.

For 3D printing with Flashforge® SLA printer, each layer is additively built 0.05 mm at a time. This process is the most accurate, especially since the XY resolution of the SLA printer is able to go to the microscale. However, like all additive processes, the plastic bulges outwards between layers, causing a consistent noise to form throughout the length of the capsule. This effect causes the RMS surface roughness to increase, causing it to be a higher but more consistent value than other methods. The small amount of differences between the printed capsule's shape and the actual shape could be explained by the curing process, which may have caused some partially set polymer to shift to the bottom of the print (which is to the left of the graph), leading to an approximate 5 µm decrease in amplitude for every 3 mm in length as it goes to the right [51, 52].

The milling process has a more chaotic profile than 3D printing, resulting in random spikes in displacement along the length of the capsule. These features seem to align with the burr that is typically left behind on the surface of an object after machining. There are a variety of reasons that can cause these formations, ranging from inadequate milling parameters leading to suboptimal chip load or thermal distortions due to inadequate

cooling [55, 56, 57]. Looking at the graph, it seems that going from 0 mm to 9 mm length causes it to become more chaotic, which aligns with the exact process used to mill the capsule. In order to cut its body out, a 2.0 mm stem had to be left behind to support the capsule while the surface was finished with the smaller 1.0 mm tool. However, because of the flexibility of the teflon, it may have caused the capsule to wobble while being milled, causing the surface to become rougher and less accurate the further away from the stem (right of the graph) the tool travels. This is reflected in the milled teflon capsule having the highest surface roughness with the highest variability.

Compared to other manufacturing methods, the accuracy of lathed capsules is much lower, with significant deviations from the planned shape. Since this manufacturing method was repeated three times on different materials, achieving a highly similar result each time, it is suggested that the CNC lathe intentionally produces this shape rather than due to defective production. Since CNC subtractive manufacturing methods use G codes to generate the pathways to shape the object, it is likely that the software for the Boxford® CNC lathe approximated the non-linear geometry of the capsule into a simple triangle wave of lower amplitude. Furthermore, teflon had a higher surface roughness due to its previously mentioned higher flexibility, which likely induced wobbling and caused a surface burst [55].

There were some key limitations to be taken into account in this experiment. The primary one is that only four slices of the capsule surface were measured, leaving the majority of it unprofiled, which could lead to significant sampling error. Furthermore, more materials could have been tested using the milling and 3D printing processes, which would validate the interpretations made by evaluating them.

Overall, it seems that out of the manufacturing methods tested, the 3D SLA printer was the best at fabricating the intended shape of the capsule. However, it was far from achieving the best surface finish as a result of the layering of the process. The lathe exhibited high precision in cutting a shape, achieving a minimum surface roughness of 2.9 µm. Theoretically, if there were a lathe suitable for cutting out complex geometry at the microscale, it would achieve better results than an SLA printer. Additionally, the difference between lathed and non-lathed capsules is the most significant; therefore, it must be investigated how this impacts the capsule usage in later experiments of this thesis.

4.2 Force Response Through Constriction

4.2.1 Ring Constriction Data

The results in Fig. 4.3 are from data collected using the testing configuration in Fig. 3.22. Data are collected using the previously outlined testing procedure in Section

3.2.1. Each subplot (a), (b), and (c)) in the aforementioned graph represents each type of material tested. As the capsule material becomes more flexible (toward c)), the force required to leave the constriction increases significantly (increasing the tensile force from 1.0 to 2.0 N). Furthermore, the distance required for the tensile testing machine to move the capsule through the restriction increases to approximately 32 mm. The capsule designs from Fig. 3.1 are represented by different colours of the graph line. The segmented design consistently recorded the lowest mid-test force values of 0.5 N or less. The other two designs share the highest recorded mid-test force values of nearly 2.0 N. Furthermore, the smooth design always averaged with the longest required distance, which was always greater than 31 mm across all types of material.

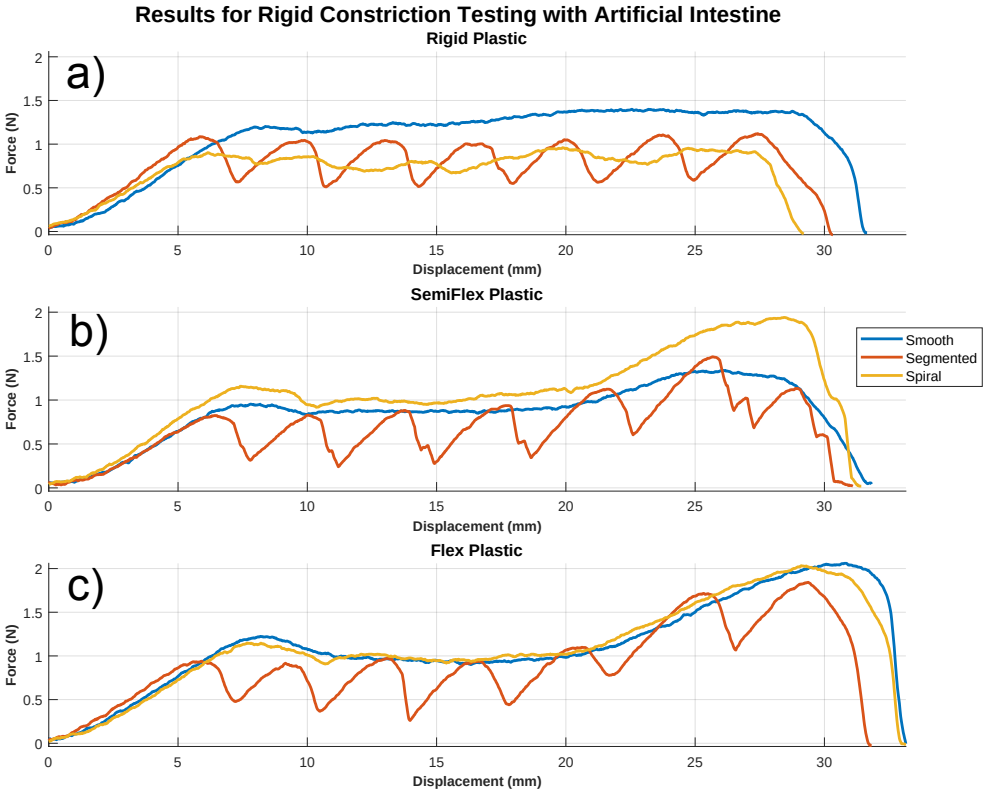

Figure 4.3: These are the force response graphs. The different material types are represented of subplots a), b), and c) (rigid, semi-flex, and flexible, respectively) and each colour of line represents each shape from Fig. 3.1, (smooth, segemented, and spiral). The graph is drawn with a moving average of ten data points

The bar chart in Fig. 4.4, shows the effect of the independent variables of shape and material composition on the work done by the capsule. The work done is the distance intervals in the measurement multiplied by the sum forces, providing a value of how many joules of energy are expended in navigating the synthetic intestine. This dependent variable is the most important because it factors in both the distance required by

the tensile testing machine and the total amount of force. Each bar is an average of three values from each of the categories on the other side of the chart. Chart a) shows that rigid and semi-flex materials require approximately 0.008 J less (24% decrease) to pass than the other two types of materials. However, there is a high degree of overlap between the bars. Chart b) shows that the segmented shape has a significantly lower amount of energy required to pass the capsule, dropping from 0.033 J to below 0.025 J. There is only a small overlap in the error bars between it and the smooth design.

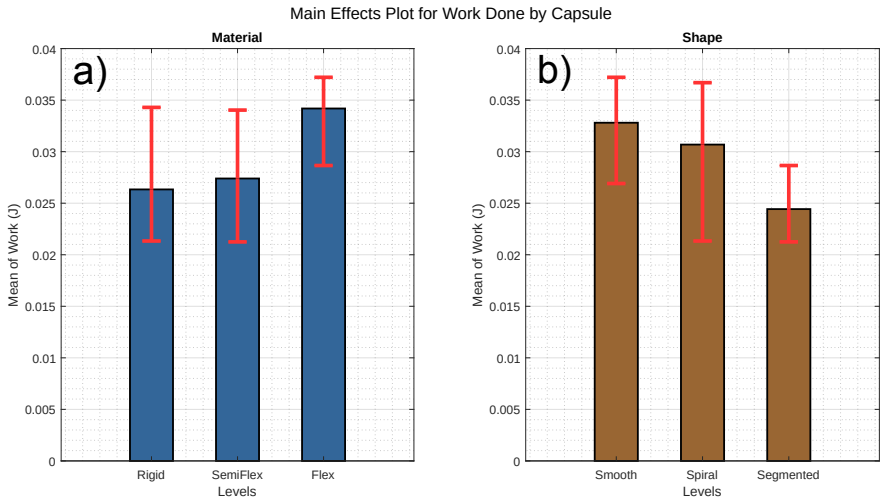

Figure 4.4: The effect that the quantity of ridges in chart a) and depth of cut into capsule body in chart b) have on the work done (force down over a distance) through a rigid constriction. The vertical red bars are error bars and the horizontal red line represents the control data. The error bars are for three data points.

The bar charts in Fig. 4.5 show the effect between the independent variables and the average force recorded during the tensile test. There is a similar relationship to the independent variables in Fig. 4.4. The average force is highest on the flexible (chart a)) and smooth capsules (chart b)) at approximately 1.0 N; and the more rigid capsules (chart a)) with segmented designs (chart b)) are around 0.8 N, which is only approximately 20% less. There is also more overlap between the error bars in the average force charts.

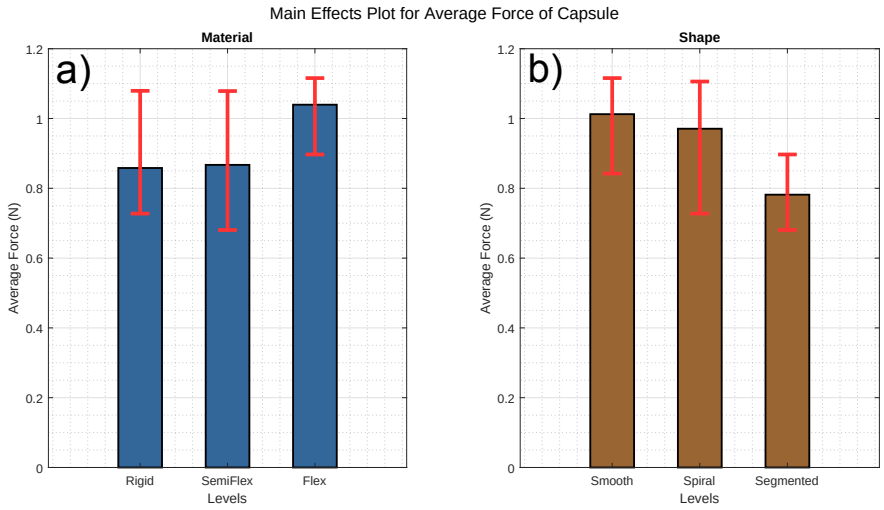

Figure 4.5: The effect that quantity of ridges in chart a) and depth of cut into capsule body chart b) have on the average force measured through a rigid constriction. The vertical red bars are error bars and the horizontal red line represents the control data. The error bars are for three data points.

The bar charts in Fig. 4.6 show the effect between the independent variables and the peak force recorded during the tensile test. In chart a), there is a large increase in peak force when increasing the flexibility of the capsule, decreasing the maximum force from approximately 2.0 N to above 1.2 N (40% decrease). There is also much less overlap between each material type and its error bars. However in chart b), the shape of the capsule does not have a significant effect on peak force; however, the segmented design still has the lowest value of approximately 1.5 N.

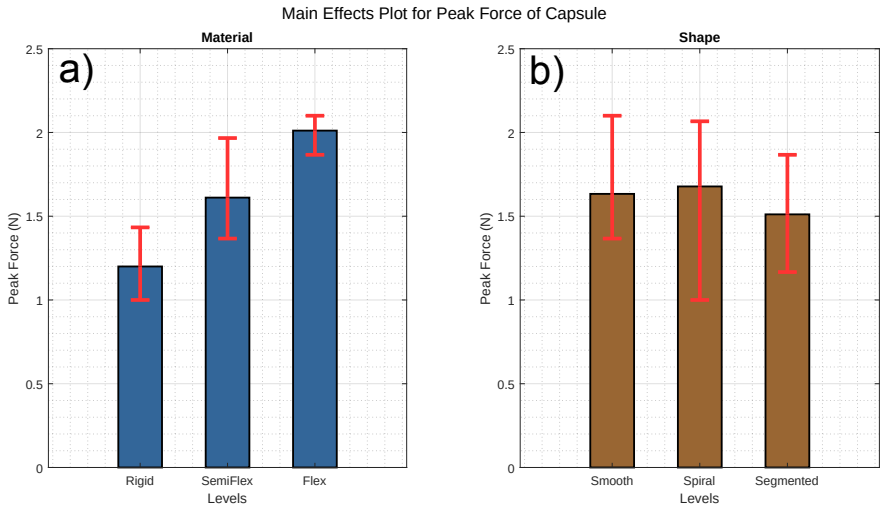

Figure 4.6: The effect that quantity of ridges in chart a) and depth of cut into capsule body in chart b) have on the peak force measured through a rigid constriction. The vertical red bars are error bars and the horizontal red line represents the control data. The error bars are for three data points.

4.2.2 Crohn's Disease (CD) Constriction Data

The results in Fig. 4.7 are from data collected using the testing configuration in Fig. 3.23. Data are collected using the second testing procedure previously described in Section 3.2.1. Each subplot (a, b, and c) in the aforementioned graph represents the number of ridges used in the segmented design selected from previous experimentation. Each solid line colour represents the inward cut depth for the segmented capsules tested, while the dashed purple line compares this to the control design of a smooth capsule with the same external outer dimensions. As the number of ridges increases (toward c), the force response lines shift below the control line, representing a decrease in the measured tensile forces during passage through the moulded stenosis constriction; also, the distance required for the tensile testing machine to pull increases slightly. The differences between the depths of the ridges are not as significant. Additionally, while the number of ridges increases, the graph lines seem to converge and take on a more similar shape to the control line while still remaining below it.

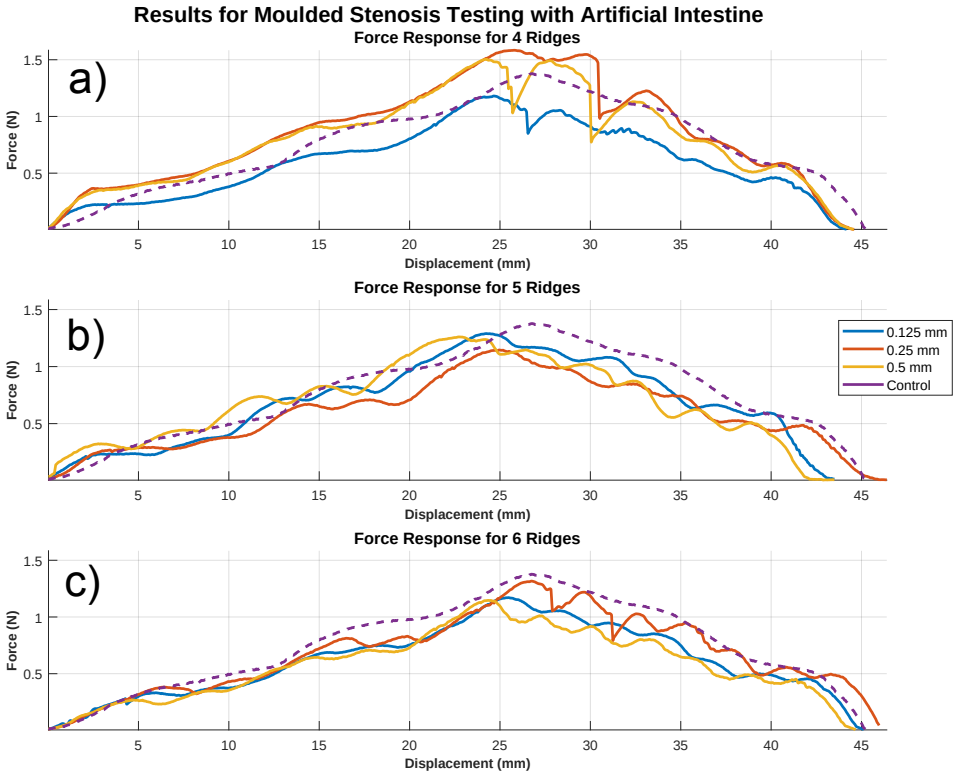

Figure 4.7: These are the force response graphs for each shape configuration of the segmented capsule with each sub-graph (a, b, and c) representing a different number of ridges in the capsule and each line colour representing the depth each ridge has. There is also a control line in all graphs where no surface features are added and has a flat surface like all other standard capsules. The graphs are drawn with a moving average of three data points.

The bar chart in Fig. 4.8, shows the effect of independent variables of the number of ridges and the depth of the ridge on the work needed to pass the constriction. All average values for segmented capsule designs performed better than for the control design. However, some specific configurations are lower than others. In chart a), the capsule with four ridges required 0.034 J to pass while the one with six ridges needed 0.028 J (18% decrease). However, the error bars overlap with each other, yet the five and six ridged-capsule error bars remain below the control line. In chart b), the depth of the ridge has a less significant effect on the work done, for which the 0.125 mm deep capsule requires 0.032 J to pass, while the 0.25 mm capsules require 0.028 J to pass (13% decrease).

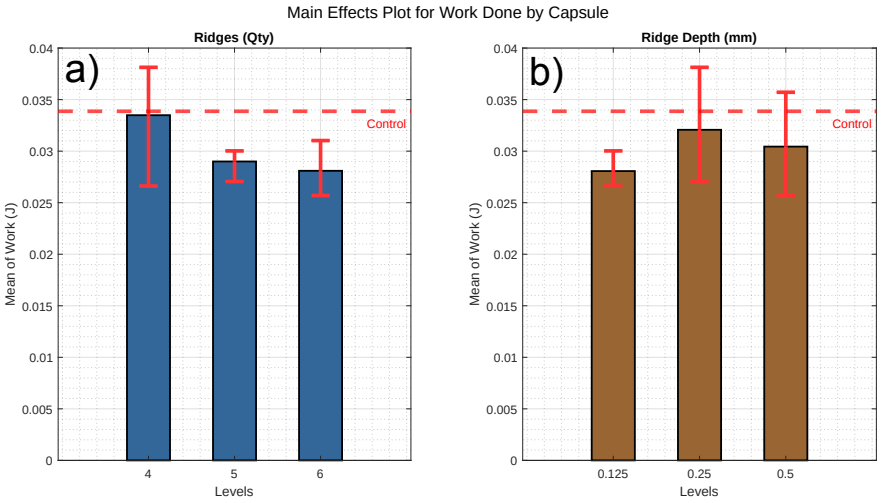

Figure 4.8: The effect that shape (chart a) and material (chart b) have on the work done (force applied over a distance) through the moulded-in stenosis of the synthetic intestine. The vertical red bars are error bars and the horizontal red line represents the control data. The error bars are for three data points.

The bar charts in Fig. 4.9 show the effect between the independent variables and the average force recorded during the tensile test. There is a similar relationship to the independent variables in Fig. 4.8, with no significant differences. In chart a), the six-segment capsule still has the lowest value for average force at 0.62 N and the 0.125 mm deep capsule at 0.64 N.

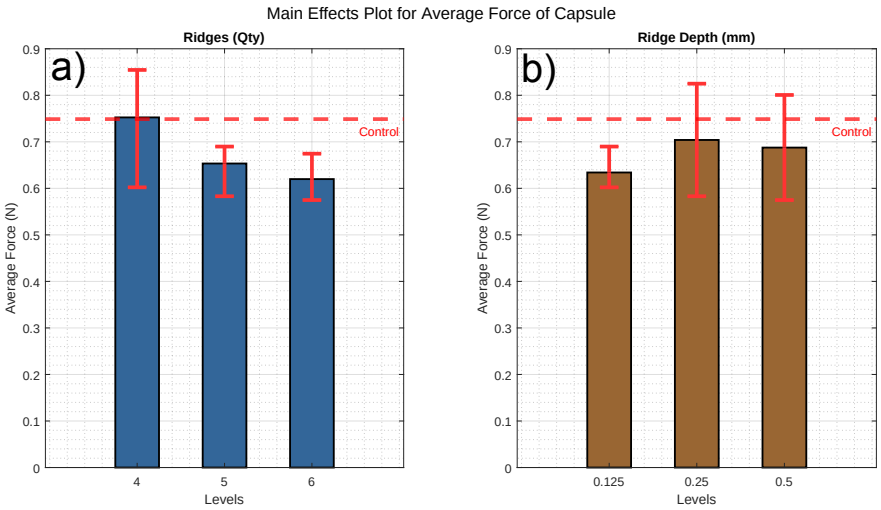

Figure 4.9: The effect that shape (chart a)) and material (chart b)) have on the average force measured through the moulded-in stenosis of the synthetic intestine. The vertical red bars are error bars and the horizontal red line represents the control data. The error bars are for three data points.

The bar charts in Fig. 4.10 show the effect between the independent variables and

the peak force recorded during the tensile test. There is a similar relationship to the independent variables in Fig. 4.8. The values for the different configurations of the capsule have increased. In chart a), the 4-ridged capsule has a peak force of 1.41 N, which is greater than the control of 1.39 N, while the other configurations are approximately 1.2 N (14% decrease), there is also more overlap between the error bars. In chart b), the ridge depth has also shifted upwards with the 0.25 mm bar having a peak force of 1.38 N and the 0.125 mm bar having a peak force of 1.21 N (13% decrease).

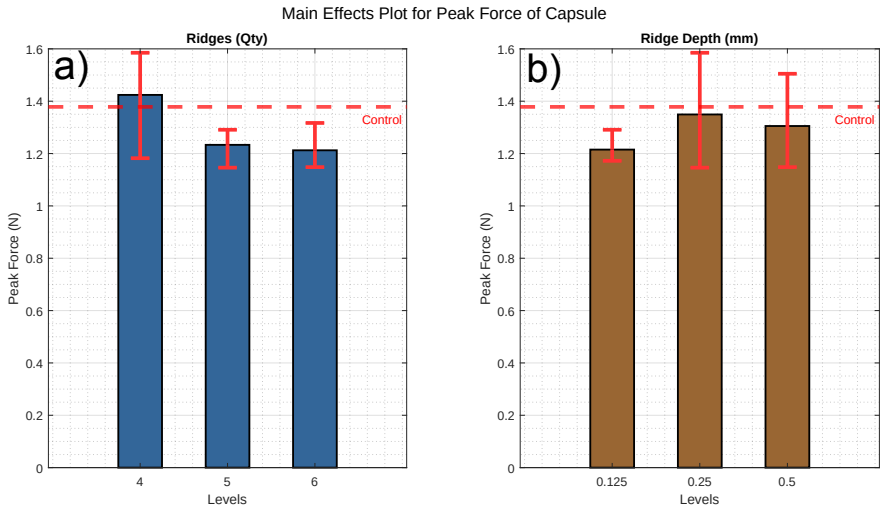

Figure 4.10: The effect that shape (chart a) and material (chart b) have on the peak force measured through the moulded-in stenosis of the synthetic intestine. The vertical red bars are error bars and the horizontal red line represents the control data. The error bars are for three data points.

4.2.3 Materials Testing Data

The results in Fig. 4.11 are from data collected using the testing configuration in Fig. 3.23. Data are collected using the second testing procedure and the materials and equipment from the Materials Testing Subsection, previously described in Section 3.2.1. The aforementioned graph is divided into two subplots; the graph a) shows the differences between the manufacturing types experimented with; and graph b) shows the difference between materials within the same manufacturing type. Both graphs compare the force response from this experiment with the control data from the previous experiment's results in Section 4.2.2.

The strongest difference is between the different types of manufacturing in graph a), with the lathed capsule requiring significantly more force to pull through the moulded-in stenosis. In contrast, the milled and 3D printed capsules have a much lower force response, which is well below the control line from prior experimentation.

The different materials in graph b) are more similar to each other, with acetal

requiring the most force, and the other two materials exhibiting a similar lower force response. For the first 27 mm of distance the capsules exhibit a similar behaviour to the control capsule. From 27 mm to 32/35 mm the force keeps increasing up to 1.8 N on the lathed capsules while the control decreases, then trending down until the capsule leaves the stenosis, taking more 5 mm to complete the experiment.

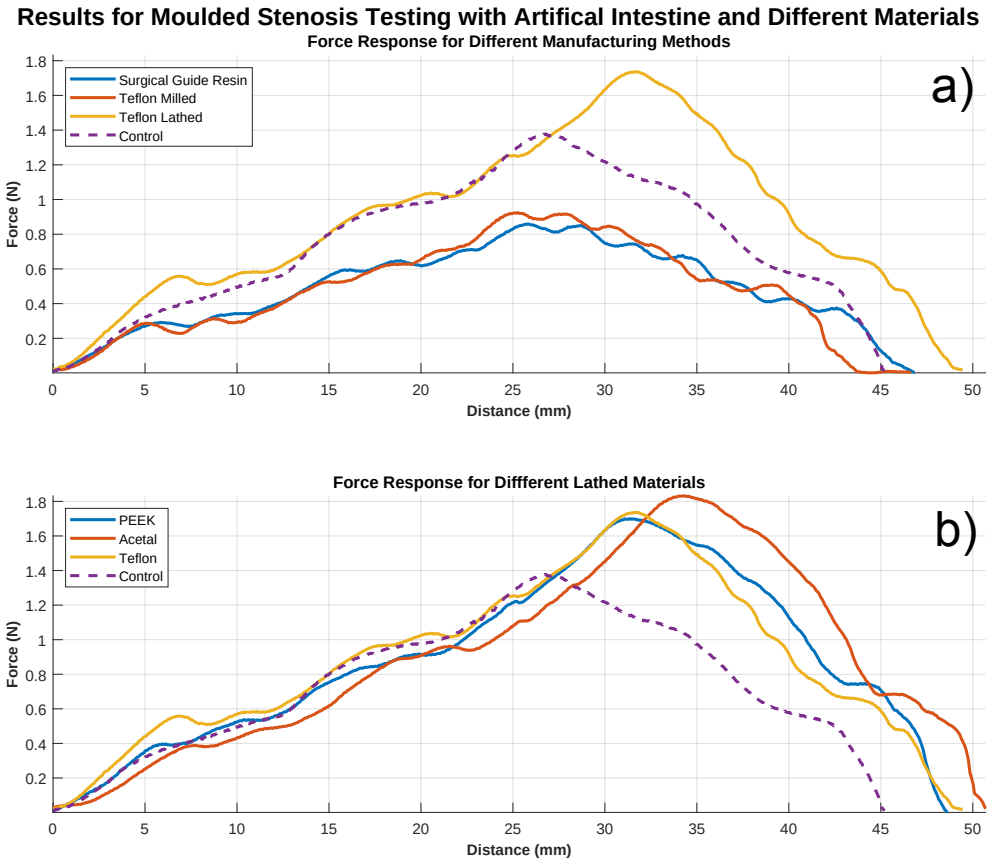

Figure 4.11: These are the force response graphs for capsules of different types of materials which are separated into 2 subplots (a and b). Graph a) is for non-lathed capsules and graph b) is for lathed capsules. The purple line represents the control force response data measured in the previous experiment for the smooth capsule made of FH-1200. The graphs are drawn with a moving average of three data points.

The bar chart in Fig. 4.12, shows the effect of the material and manufacturing method of the capsule on the work needed to pass the constriction. The 3D printed and milled capsules performed significantly better than the control, requiring approximately 0.022 J (35% less) to pass, instead of the 0.034 J of the control. The lathed capsules performed significantly worse, with Teflon and PEEK capsules requiring 0.043 J (26% more) to pass and acetal capsule requiring 0.045 J (32% more) to pass. However, the error bars are larger on the acetal capsule than in the other capsule types.

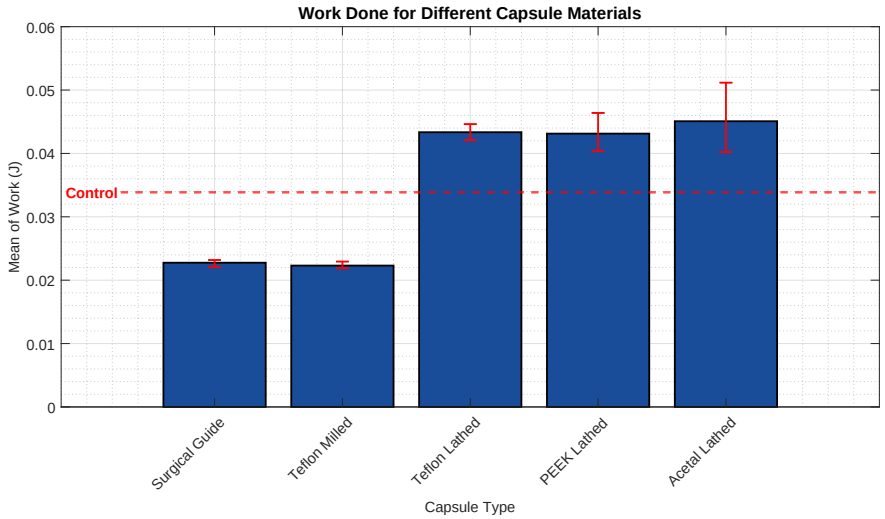

Figure 4.12: The effect that material type has on the work done (force applied over distance) through the moulded-in stenosis of the synthetic intestine. The vertical red bars are error bars and the horizontal red line represent. The control line represents the data measured in the previous experiment for the smooth FH-1200 capsule. The error bars are for three data points.

The bar chart in Fig. 4.13, shows the effect of the material and the capsule manufacturing method on the average force required to pass the constriction. There is no significant difference between the relationship of the non-lathed capsules and the control, with the 3D printed and milled capsules having the lowest average force of approximately 0.48 N (36% less than the control). However, all lathed capsules have a very similar average force of 0.88 N, which is only 17% more than the average control force of 0.75 N.

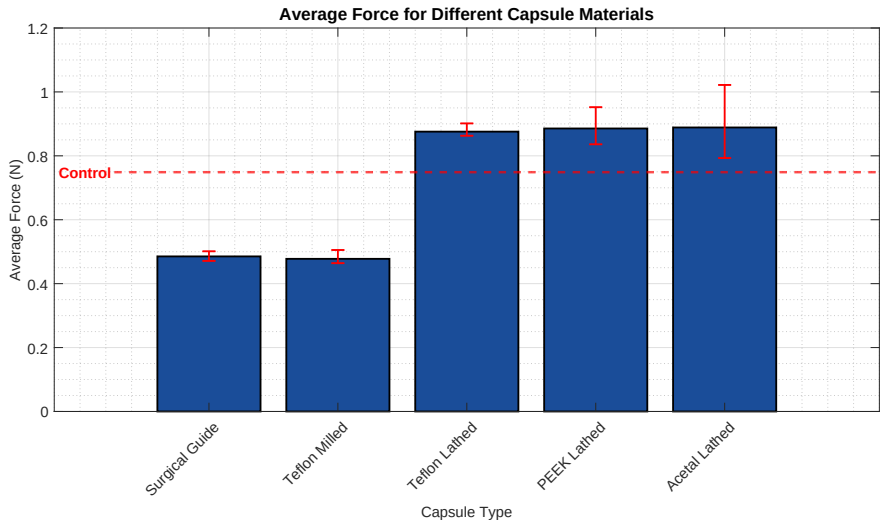

Figure 4.13: The effect material type has on the average force through the moulded-in stenosis of the synthetic intestine. The vertical red bars are error bars and the horizontal red line represent the control line represents the data measured in the previous experiment for the smooth FHD-1200 capsule. The error bars are for three data points.

The bar chart in Fig. 4.14, shows the effect of the material and capsule manufacturing method on the peak force required to pass the constriction. There are no significant differences in the relationship between the lathed capsules and the control value in Fig. 4.12. However, the surgical guide resin capsule now has the lowest peak force of 0.86 N (38% less than the control) and the milled teflon capsule is the second lowest at 0.93 N (33% less than the control). Since the overlap in the range between these values is so small, they are significantly different from each other.

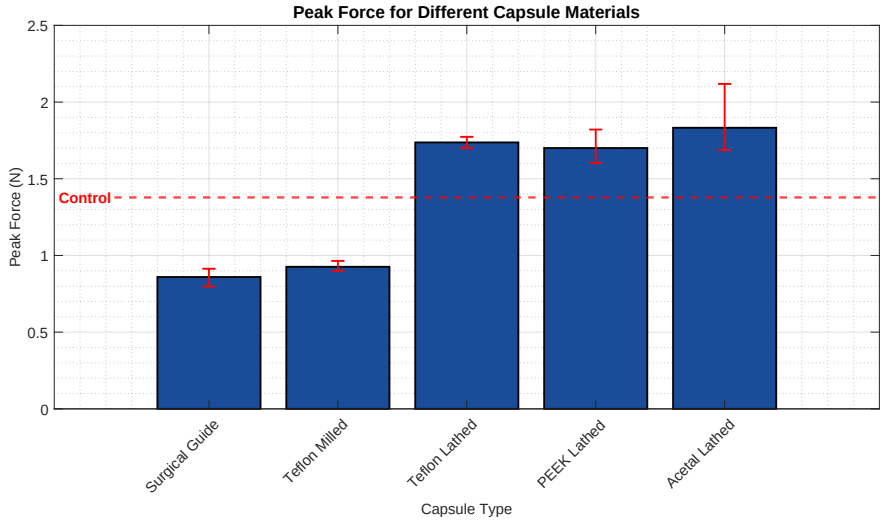

Figure 4.14: The effect that material type has on the peak force through the moulded-in stenosis of the synthetic intestine. The vertical red bars are error bars and the red control line represents the data measured in the previous experiment for the smooth FH-1200 capsule. The error bars are for three data points.

The bar chart in Fig. 4.15, compares the differences between lathed capsules and non-lathed capsules, across all data collected in the Materials Testing experiment. The categories are significantly different from each other in each metric compared in this experiment. The non-lathed capsules are always below the control line, and the lathed capsules are always above it. In graph a) (work) and c) (peak force) the non-lathed capsules are 35/36% below the control line (0.023 J and 0.90 N), while the lathed capsules are only 28/29% above the control line (0.045 J and 1.76 N). There is a slight difference in graph b) (average force), with the non-lathed capsule at 34% less than the control (0.49 N) and the lathed capsule only 19% higher (0.89 N), although its range is still entirely above the control. Additionally, lathed capsule error bars are significantly more spread out than the non-lathed capsules, indicating more variance in the data.

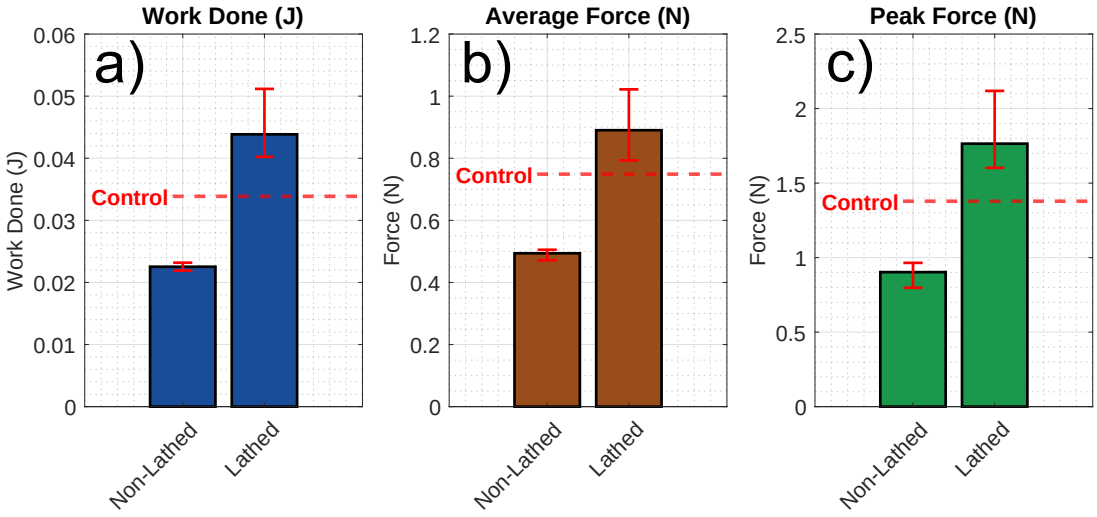

Figure 4.15: Data is combined from the previous 3 graphs to highlight the differences between capsules which were fabricated using the CNC lathe and capsules that were not. a) shows work done (J); b) shows average force (N); and c) shows peak force (N). The control line represents the data measured in the previous experiment for the smooth FH-1200 capsule. The lathed error bars are for nine data points and the non-lathed is for six.

4.2.4 Discussion

The following is a summary of the results presented in this section:

- Section 4.2.1 compares the performance of rigid, semi-flexible, and flexible 3D printed capsules. The results show that flexible capsules require much higher energy and force, making them unsuitable for safe exploration of the GI tract. Furthermore, the segmented capsule design performed better than smooth capsules, demonstrating a significantly lower force response.

- In Section 4.2.2, nine variations of the rigid segmented capsule design were tested, along with a smooth body control capsule. Increasing the number of ridges reduced the force response, lowering the work and the force required to pass. However, changing the depth of the ridge had little effect on the results.

- In Section 4.2.3, a capsule design with six ridges and a depth of 0.125 mm was chosen. Then five capsules were made using different materials and methods. The biggest difference was between lathed and non-lathed capsules; with non-lathed ones needing twice as much force and energy to pass. Although the non-lathed capsules had a lower range than the lathed ones, the prior remained below the control value from the previous experiment. The printed and milled capsules showed similar metrics, except that the printed capsule had a significantly lower peak force.

Analysing all the data collected across the previous three experiments generates a consistent pattern. The shape of the capsule, particularity in the 100 - 1000 µm range has the most significant impact on capsule transit. The segmented design performed consistently better in the majority of all test trials than the standard smooth design prevalent in the field of capsule endoscopy [34]. Furthermore, some specific designs performed better than others. This may be due to how the capsule surface interacts under pressure from a soft tissue analogue. There are many forces that interact, but the two main ones to consider in the context of passive movement are the frictional forces and adhesion forces that interact with the capsule's surface. If the capsule has high friction and naturally adheres to environments similar to the intestinal tract, more force will be required to pass, increasing the risk of retention [50].

The friction and adhesion an object has with a surface is dependent on the area with which it makes contact. If the surface is rough, it will have more friction. However, if two smooth flat surfaces are pressed against each other, they have perfect contact. This leads to more friction, meaning that it is unlikely to slide away. However, if the object is rounded or has a slightly irregular shape, it decreases the contact area, allowing it to roll or slide off the surface with greater ease [83]. Applying this theory to data collected in these experiments, it can be determined that the segmented surface with the right parameters lowers the total contact area the capsule surface has with the synthetic intestine surface. Decreasing the force response as it passes through a constriction, making it more effective in passing through difficult sections of the gut than a conventional smooth-bodied capsule. Furthermore, each segment lets tension be released as it passes through the tightest section, keeping the capsule moving more consistently, as shown in Fig. 4.3.

However, the lathed capsules in Section 4.2.3, performed significantly worse than the segmented capsules and the regular capsules. Another interaction to consider is how the capsule and the lubricating mucus of the intestine interact with each other. Under normal conditions, the surface of an object is fully coated and has a lower friction, allowing it to pass more easily [50]. The profile of the lathed capsules was both 35% flatter and has pointier edges in its triangular profile, this means that as it was pulled into the stricture it behaved more like a smooth-bodied capsule in Fig. 4.11, up to 27 mm. However, when it stopped, the lubrication ran off the sharp points on its surface, causing the capsule surface to dig into the synthetic intestine. This caused the capsule to become temporarily stuck for an additional 5 mm of distance, while the force continued to climb higher. Until it reached a critical point, it freed itself from where it became partially attached, resulting in significantly higher forces and more work to do.

If an increase in surface roughness could lead to more friction against the capsule, then the impact it had on the experimental results needs to be understood. Shown

in Table 4.1, the results for each capsule type tested in Section 4.2.3 are compared with the RMS roughness values in Section 4.1. Based on this table, surface roughness has little effect on the outcome of this experiment. The work and average force values do not change much and the peak force fluctuates randomly between lathed and non-lathed capsules. Therefore, the roughness of the capsule does not have a significant effect during tensile testing.

Table 4.1: Capsule Type Performance Metrics Vs RMS Roughness

Capsule Type	Work Done (J)	Avg Force (N)	Peak Force (N)	RMS (μm)
Surgical Guide	0.0228	0.4852	0.8596	5.41
Teflon Milled	0.0223	0.4776	0.9261	6.42
Teflon Lathed	0.0433	0.8757	1.7369	4.04
PEEK Lathed	0.0431	0.8856	1.7003	2.94
Acetal Lathed	0.0451	0.8887	1.8325	3.09

Additionally, the printed surgical guide resin capsule in the last experiment performed better (0.023 J) than the capsule of the same shape printed with FH-1200 (0.028 J). One possibility could be due to an improvement in the generation and removal of support structures, as well as better calibrated printing parameters, due to repeated practice, leading to higher-quality prints [51, 52]. Another possibility is that surgical guide resin is better suited for navigating confined spaces in a body-like environment than FH-1200 which is designed for plastic jewellery.

There were a few limitations in the tensile testing experiments. The first and later experiments were conducted using different testing rigs with different equipment, which means that their results could vary greatly. Part of this was unavoidable due to the necessity to relocate from Massey to Canterbury, so an opportunity was taken to further improve the testing setup, since perfectly replicating it again would not be possible. In early testing, FHD-1200 resin was used; however, during this project, it was no longer possible to purchase. This required a similar FH-1200 resin to be used instead during the second experiment, the experimental procedure of which was determined by results with the previous resin. This resin could not be used later because it did not meet the biocompatibility requirements. Due to the high number of capsule parameters that needed to be tested, only three replicates for each capsule was tested, which means that some outlying data may influence the results; however, most of the trials were similar to each other. In the first experiment, data was exported to a very low resolution of 0.1 N due to the proprietary software, which required averaging to 10 data points to be legible.

In general, the best capsule in the tensile testing data came from the one printed

using the surgical guide resin; with the target dimensions in Fig. 3.4; using the segmented design. Its results were nearly identical to those of the milled capsule with only a significantly lower maximum force, meaning that it is slightly better than it. It is highly likely that the exact shape of the capsule can have a great impact on transit through constricted environments, as the 20 µm difference between lathed and non-lathed capsules caused a substantial effect on the force response graphs. Therefore, in order to better understand the effects of capsule surfaces, they must be tested in a more realistic environment in the next experiment in this thesis.

4.3 Peristaltic Propulsion

4.3.1 Capsule Propulsion Data

The results in Fig. 4.16 are from data collected using the robotic intestine system in Fig. 3.24. Data are collected using the previously described testing procedure in Section 3.1.3 in ten trials for each material and manufacturing technique and averaged to produce each curve. The purpose of these graphs is to demonstrate how much power is consumed to move differently fabricated capsules through the same constriction in a synthetic intestine. The graph is divided into two subplots; graph a) shows the differences between the manufacturing types experimented with; and graph b) shows the difference between materials within the same manufacturing type. Graph a) shows the strongest differences, and the printed capsule consistently has a lower power consumption, which ranges around 0.010 W. The milled teflon capsule follows a similar trend slightly higher at 0.015 W, while the lathed teflon capsule trends considerably higher at 0.035 W.

In graph b), there are also significant differences between the different lathed materials. All of them go above the 0.030 W mark unlike the non-lathed capsules (ignoring the spike at the end), but at different points of time. The teflon capsule goes above 0.030 W within 20 s, the PEEK capsule within 60 s, and the acetal capsule within 120 s. In general, all lines on graph b) trend above the non-lathed capsules in graph a) . At 160 s all capsules encounter a spike in excess power consumption that consistently goes from 0.030 w to 0.035 W, before trending down to 0 W in excess power consumption when completing the test.

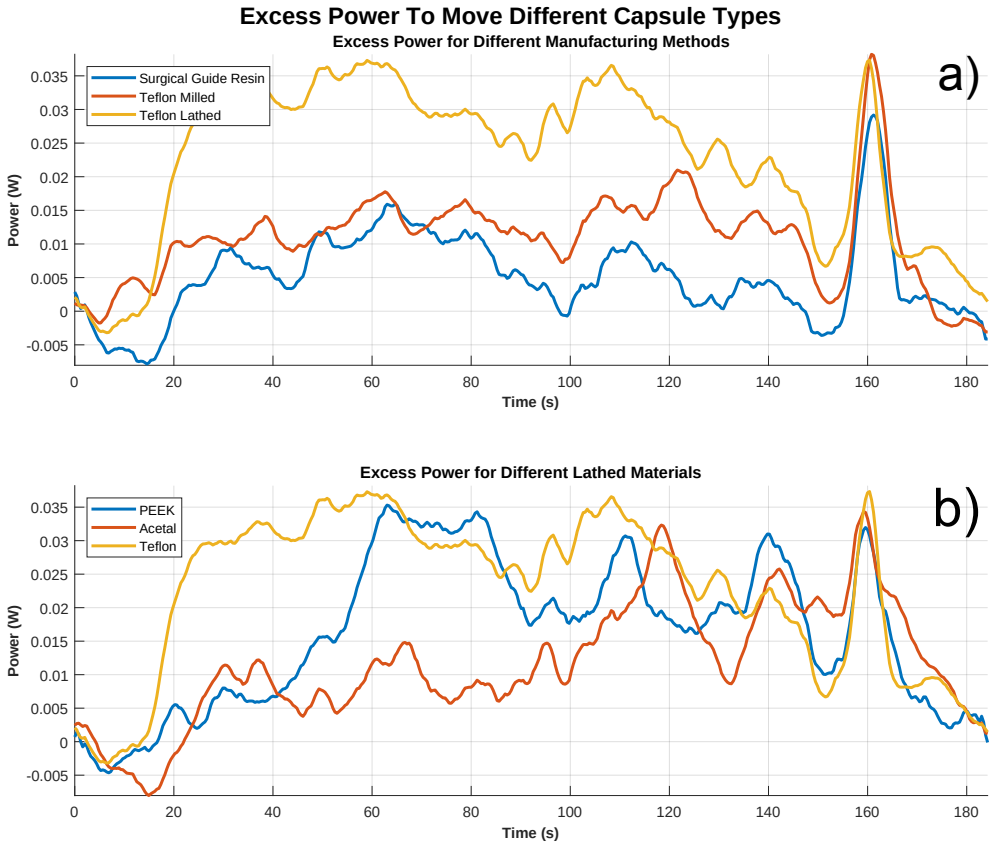

Figure 4.16: These are the power consumption graphs made from logged data from the robotic intestine system while capsules transited through a moulded-in constriction. The power consumed while nothing is inside is factored out. Graph a) shows the difference between manufacturing types and graph b) shows the difference between materials that were lathed. The graphs are drawn with a moving average of three data points.

The box-and-whisker plot in Fig. 4.17 shows the median, quartiles, and range of the area below the lines in the excess power graph in Fig. 4.16, which is calculated by multiplying the time slice by every recorded value and summing every value. Box-and-whisker plots are useful for visualising the distribution and variability of a large set of data points. The horizontal red line in the middle represents the median, which is the lowest in the printed capsule at only 2.33 J, with the milled capsule being very close at 2.39 J. The highest work came from the lathed teflon capsule at 4.80 J with the other lathed capsules sitting above 3.00 J.

The overlap between data sets is assessed by examining how the medians and quartiles intersect each other between capsule types. There is a very strong overlap between the printed and milled capsules, meaning, there is no significant difference between the two. The acetal lathed capsule has a strong overlap with the PEEK lathed and milled capsule; the peek lathed capsule has a strong overlap with the milled and lathed acetal capsule; and the lathed teflon capsule has a strong overlap with the PEEK lathed

capsule. The acetal capsule appears to be significantly lower than the lathed teflon capsule, indicating that there is a difference between materials in this experiment. In addition, the printed capsule has a small overlap with the lathed teflon and acetal capsules, indicating that there is a significant difference in such manufacturing types.

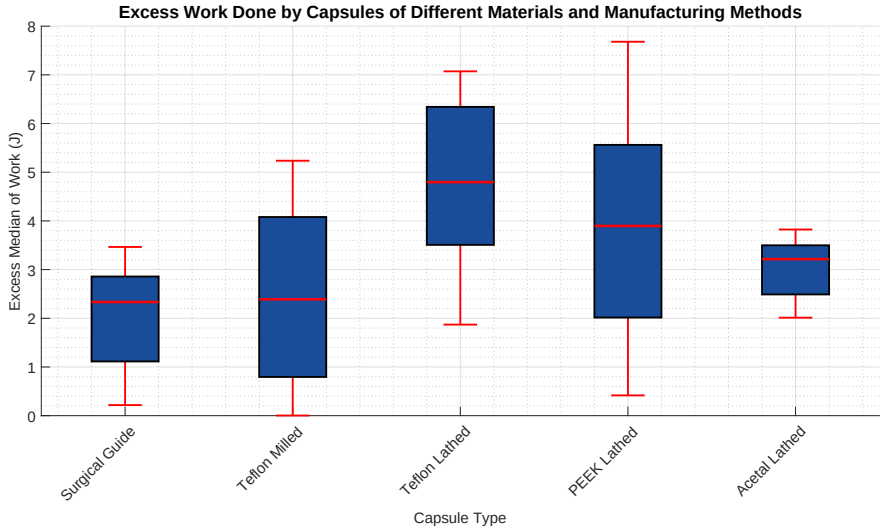

Figure 4.17: The median, quartiles, and range of 10 data points from the area below the lines in the excess power graph in Fig. 4.16. Each box and whisker plot corresponds to each material and manufacturing combination tested.

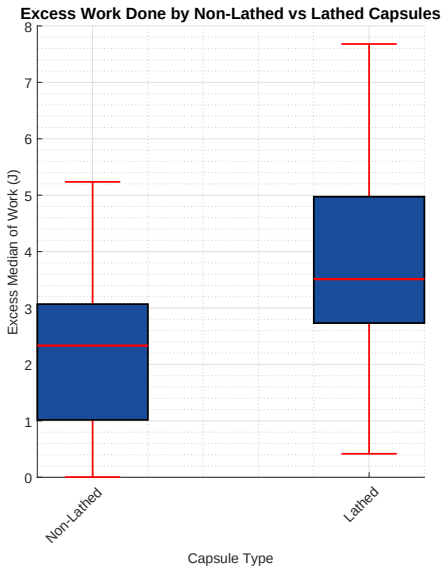

Figure 4.18: The median, quartiles, and range of the area under the excess power graph in Fig. 4.16, with each box and whisker plot representing a different material and manufacturing method. The lathed capsules use 30 data points, while the non-lathed capsules use 20.

The box-and-whisker plot in Fig. 4.18, compares the differences between lathed capsules and non-lathed capsules, in all data collected in the Materials Testing experiment. Both categories are significantly different from each other, with only moderate overlap between the upper quartile on the non-lathed and the lower quartile of the lathed capsules. The non-lathed capsules have a median of 2.33 J while the lathed capsules have a median of 3.51 J. The total range is greater in the lathed capsules, but the quartiles remain similar in spread between both categories.

4.3.2 Discussion

In Fig. 4.16 and Fig. 4.17, it is apparent that there are significant differences between the manufacturing method and the choice of material between the capsules. The printed and milled capsules had the best median results; and the printed capsule had the best average curve. Although all lathed capsules performed worse, there was a difference between materials, with acetal performing best and teflon performing worst.

The most significant difference in the results between the tensile and robotic intestine tests is in the total amount of energy used. In tensile tests, the energy required to pull capsules through the synthetic intestine ranged from a mean of approximately 0.02 to 0.04 J, while the results of the robotic intestine ranged from a median of approximately 2.4 to 4.8 J. When a capsule is pulled by the tensile testing machine in Fig. 3.23, the majority of forces and mechanical interactions occur solely in the vertical direction, while the capsule is suspended weightlessly. Additionally, the capsule is being pulled from its centre of mass, which means the energy transference into the capsule's movement is highly efficient. However, even after factoring in the additional sources of power drain, the energy usage of the capsules in the robotic intestine was much greater. Pushing a capsule with peristaltic-like motion has many more forces interacting with the system. It involves the contraction of muscles behind the capsule, combined with longitudinal progression to propel the capsule forward [13, 14]. As discussed previously, the capsule experiences frictional and adhesion forces on the basis of its properties. When the capsule is lying down rather than suspended in air, it is no longer weightless and gravity begins to influence the capsule. This will naturally lead to increased friction with the surface in response to the weight of the capsules. It will also ensure greater contact with the synthetic intestinal surface, leading to more adhesion forces. Furthermore, peristaltic locomotion can change the way the pressure of the synthetic intestinal material is applied to the body of the capsule [50]. In addition, there would be certain points in the synthetic intestine (such as moulded stenosis) where the capsule would have to work against gravity by moving upward. Taking these forces into account, it can be reasonably determined that the energy required to push the capsule should be much higher than it should be to pull it.

In Fig. 4.16, the main relationship between the variables has been preserved from the tensile test in Fig. 4.11, with a strong correlation of 0.815 between the work values. The largest differences were still between the different manufacturing types and the lathed capsules consistently performed worse than the non-lathed capsules. One feature that stands out is the spike observed at 160 s across all trials, this can be explained by how the data were processed and practical considerations. To determine the excess power used to push the capsule, the power to push nothing had to be subtracted. However, it takes longer to release tension after passing through a constriction with a capsule

inside rather than nothing. Since relative power consumption drops to near zero in the baseline tests at 160 s, nothing is subtracted from the lines, resulting in a relative spike without the capsule being stuck again at the end of the trial. Power consumption tends to increase in the first half and decreases in the second half, as in Fig. 4.11, with the exception of the lathed teflon capsule; and tension is released throughout due to the segmented design. However, the graphs oscillate to a greater extent, which can be explained by the innate variability of the power supply and the motors that drive it.

There is still a significant difference between the non-lathed and lathed capsules shown in Fig. 4.18, however, these values are much closer than in Fig. 4.15. This is likely due to the increase in forces that interact with capsules causing more differences in the spread of data for each capsule type in Fig. 4.17 and subsequently between non-lathed and lathed capsules. This is especially noticeable with lathed capsules that have significant differences from each other when they previously had very similar curves in Fig. 4.14. Therefore, the median work for each type of capsule is compared with the RMS roughness and the mass measured in Table 4.2, since the weight could be a significant factor in this experiment. Within the non-lathed and lathed categories, these values appear to have a relationship with median work. The capsules that performed the worst (the lathed and milled teflon capsules) were the roughest and heaviest. However, the better capsules tended to have lower roughnesses and masses, with the best capsule (the printed one) having the lowest median work in a smaller spread of data. Therefore, it can be determined that a decrease in roughness and mass is likely to decrease the work required to be propelled by peristalsis.

Table 4.2: Peristaltic Testing Data vs Surface Profile and Mass

Material	Median Work (J)	RMS Roughness (μm)	Mass (g)
Surgical Guide	2.33	5.41	1.60
Teflon Milled	2.39	6.42	4.00
Teflon Lathed	4.80	4.04	4.42
PEEK Lathed	3.90	2.94	2.60
Acetal Lathed	3.22	3.09	2.62

There were a few limitations in the robotic intestinal experiment. The main limitation was the high level of variability in the data collected, which required ten trials to be carried out in each capsule before a meaningful result could be obtained. This took a long period of time to complete over multiple days, meaning that uncontrollable variables will likely have influenced the data. Furthermore, the data needed a lot of processing before the information could be extracted from them. The first step involved using a linear trend to approximate the change in power draw without extra work being

done; however, it is possible that non-linear changes between the start and end of the experiment could have occurred, affecting the result. The baseline data could have been inaccurate, affecting the final shape of the graph. Therefore, averaging over ten trials sought to minimise error and establish the relationship between tested variables. Using different materials for milling and printing would have established how their respective masses and roughnesses affected the median work, as it is possible that an acetal milled capsule might perform better than the printed capsule. Adding mass as another factor is not ideal as it makes it harder to determine which effect each variable has on the results. It would be better to see how capsules of different mass behave in the robotic intestine when fabricated with the same method, to better understand how mass and material affect the result separately.

In general, the best capsule from the robotic intestine testing data came from the one printed using the surgical guide resin; with the target dimensions in Fig. 3.4; using the segmented design. It had the lowest median work to pass the constriction in the robotic intestine and its curve had the lowest power consumption throughout the experiment. Its results were more consistent as its data were less spread out in the ten trials. The true shape of a capsule has the greatest effect, causing significant differences between them in the experiment, shown in Fig. 4.18. The type of material affects the passage of the capsules through the robotic intestine, which is likely due to the roughness and mass of the capsules.

4.4 Discussion Summary

Overall, the shape of the capsule has a significant influence on how it passes through a possible constriction within an intestinal environment. Modifying the shape of the capsule from a standard smooth body [34] to a segmented design results in a reduction in the work required to pass a restriction. This improvement can be further enhanced by spacing the ridges 3 mm apart and by using a 3D SLA printer with surgical guide resin. These specifications allow tension to be gradually released throughout its transit and reduce the contact area it has with the intestinal wall, improving its frictional and adhesive properties to reduce the energy required to move it [83]. Specific shapes can also have a significant negative impact on capsule transit, with a 20 µm change in surface height and shape from sinusoidal to triangular leading to a large increase in energy required to transit through tensile tests and robotic intestinal experiments. This is due to the way the surface of the capsule interacts with the intestinal wall, increasing the opposing forces to move it [50]. The magnitude of the data collected with the robotic intestine was significantly higher, due to additional forces interacting with the system due to the increased workload to push the capsule instead of pulling through, also allowing mass and surface roughness to interact more with the experiment [13, 14].

Common limitations include; sampling error in surface profiling; only three trials being conducted in tensile testing; only one material being tested in 3D printing and milling manufacturing methods; repeated changing of the one material used for 3D printed capsules in experiments; high variability in robotic intestine data; and not isolating and testing other variables separately such as roughness and mass. The next chapter will conclude on the findings of this project; what broader impact they could have in the field of capsule robotics; and what recommendations would be made to advance this project beyond the scope of this thesis.

Chapter 5

Conclusions & Recommendations

5.1 Conclusions

The original aim of this work was to improve the safety and motility of CRs within the GI tract and to create new methods to test it. As such, the main objectives for the project were: to create a process for rapidly fabricating a synthetic intestinal environment; develop a test rig using the synthetic intestine to test CRs in static conditions; to develop a robotic intestine to assess CRs in a dynamic environment; to experiment with different exterior shapes, materials, and manufacturing methods; and determine an optimal capsule design. Each of these objectives has been met; however, as discussed in Chapter 4, there were limitations that should be addressed and improvements made.

5.1.1 Key Findings and Objective Criteria

Synthetic intestinal environments were successfully created using a cost-effective 3D printing method for mould production. Silicone resin, degassed in a vacuum chamber and injected from the bottom of the mould, prevented gas buildup and allowed the replication of complex structures, including folds and stenosis. The cores of the mould could be quickly adjusted to mimic different features of the interior surface. The selected resin, similar to those used in previous studies [76] but slightly stiffer, effectively simulated CD within the intestinal tract [23]. This fabrication process fully met the first objective of the project.

A test rig was developed to evaluate the static performance of the capsules. The initial prototype used an unmodified synthetic intestine and a pipe clamp to simulate narrowing with xanthan gum mucus. Although this setup provided interpretable data, the tensile testing machine had low resolution (0.1 N), and the pipe clamp did not realistically replicate stenosis. By refining the synthetic intestinal process and using

higher-precision equipment, a new test rig was created. The improved setup offered precise data (0.001 N) and a fully elastic and realistic interaction with the capsule [76]. Additionally, the cleaner and more centred setup enhanced consistency and comparability, achieving the project's second objective.

A robotic intestine system was successfully created, which involved a standard linear actuator system, combined with a novel aperture mechanism, to replicate longitudinal and circular movements of the peristalsis [13, 14]. This robot combined with control software and a power supply data logger to be able to measure the performance of CRs. However, the simulated environment was not as dynamic as it could have been, movement did not match the peristaltic progression pattern [13, 14] and have a sufficiently long enough area of compression to interface with the capsule [50]. However, a novel robotic system was developed to assess CR performance, which satisfies the third objective of this project.

A wide range of capsule shapes, flexibility types, microstructures, and materials were tested, with 24 unique configurations tested. In all stages, tensile testing was performed, providing robust low-variance data that created informed decisions about the design process. The robotic intestine also validated the final design with a similar relationship between variables, including surface roughness. However, the robotic intestinal data was highly variable and created strong overlaps. In general, the fourth objective was achieved, with the need for a better metric to assess the performance of the capsule in a dynamic environment.

One capsule design achieved the overall best results, which is the six-ridge segmented capsule printed using an SLA 3D printer with Power Resins® Surgical Guide resin. It performed the best in tensile and robotic intestine testing with the lowest recorded force response and excess power values (and their subsequent averages, peaks, and integrals). However, profilometery data revealed significant differences in shape, with lathed capsules having triangular profiles compared to planned sinusoidal ones, which had a detrimental impact on capsule movement [50, 83]. This creates uncertainty, as a more accurate lathe could theoretically produce better performing capsules. Furthermore, the variability in mass could be influencing the results in robotic intestinal testing; which could be further affected by the highly variable data and simple movements of the robot. An improved design has been determined, and the null hypothesis of a standard capsule has been sufficiently rejected. However, an optimal design has not been determined, leaving the fifth objective partially fulfilled.

5.2 Impact

5.2.1 Within Research Group

Meeting the objectives of this research project will have an immediate impact in academia within my research group. Identifying the importance of the capsule shape down to the microscale can be applied to the development of the my groups micro-robotic capsule system for sampling the gut microbiome. Using the improved design will reduce risk retention and improve transit times when performing animal testing with new prototypes. The significant effect of microscale features could be used to improve sample mucus collection by better funnelling it into the collection chamber by improving adhesion to the mucus and increasing the scraping force, while using a lower amount of power. Furthermore, the process of creating a synthetic intestine can be used to create custom testing scenarios for the group to evaluate capsules in a consistent repeatable environment under static conditions. In addition, the robotic intestinal system can also be used to test designs in peristalsis that can be easily monitored and quantified. It will also allow for more testing to occur due to the simple setup process and can be fully customised and controlled in a repeatable manner. Together, these things will ensure that capsule designs are safe, efficient, and effective before being tested in animals or humans, improving overall outcomes [37, 66].

5.2.2 Broader Impact

The findings of this research can benefit other groups developing CR prototypes, enhancing capsule safety and efficiency in GI tract transit. This applies to microbiome sampling capsules, which would benefit from improved shape design and testing methods [68, 69, 70]. Shape optimisation can also help biopsy capsules by improving anchoring mechanisms and allowing controlled testing in static and robotic environments [44, 45, 48]. Similarly, targeted drug delivery capsules could use microscale features to improve drug application by optimising mucosal contact and optimising delivery forces [39, 40, 41]. These advances can extend to capsule endoscopy, where an improved design can reduce the retention rate of 1.1% and 8.4% with known Crohn's disease [58, 59, 60, 61], potentially preventing retention in 1,430 of the 130,000 annual procedures. Patients with Crohn's disease or other high-risk conditions could also benefit from safer procedures, leading to better research opportunities, treatments, and potential cures [6, 34].

5.3 Recommendations

This project provides the foundational work required to improve the safety and performance of CR prototypes. Although capsule designs were improved, they were not optimised, and the created testing equipment requires further improvements to become fully reliable with greater control. Therefore, clear recommendations need to be provided to ensure that the research group further improves the outcomes of this project.

5.3.1 Capsule Optimisation

The constant focus throughout this research project was on what could be done to make capsules more suitable for exploring the GI tract. However, there were many challenges associated with being able to obtain the data to optimise decisions. Only until the later stages of the project was the test equipment ready to collect data, which meant that design decisions were made on limited information. Despite this, the strong correlation of 0.815 between both experiments indicates that they are representative of each other and that the decisions were correctly informed. Among all factors, the shape of the capsule had the greatest impact on measured output, as small variations on the microscale could accumulate to produce substantial effects. More microscale features are recommended to be investigated, as subtle changes (even down to 20 µm) can completely shift response curves during transit. Experimenting with as many shapes as possible can improve understanding of this effect and improve passive control of capsules within the GI tract. Furthermore, further experiments are needed to conduct an in-depth analysis of the differences in mass and roughness separately so that their effect can be understood better compared with more advanced statistical tools. Taking this approach, the field of capsule tribology can be fully understood, leading to more informed design choices in the future.

5.3.2 Test Equipment

The need for reliable test equipment has been apparent since the beginning of this project. CRs are designed to explicitly explore places within the GI tract that are difficult to reach, making it difficult to determine how they would perform. Human and animal experimentation was not feasible within the time frame of this project, so alternative solutions were necessary to complete this project. This shifted the project into the space of bio-mimetic materials and robotics, which resulted in the collection of new metrics to assess capsule performance. However, the uncertainty of being early in this space leads to lower data collection rates and instances of high variability in robotic intestinal studies. More materials and configurations are recommended in the synthetic intestinal environment to better model capsule behaviour and are compared with real

tissue to maximise platform accuracy. Furthermore, the robotic intestine should be improved by employing better technology to assess capsule performance, which could include integrating strain gauges and directly tracking capsule motion relative to the intestine by using positional sensors inside. Using these improvements, more quantitative data can be collected with higher precision, which will further improve the design of capsule exteriors and the testing of entire CR systems themselves.

Appendix A

Parts for Robotic Intestine

Table A.1: Parts for Robotic Intestine

Item Description	Model Number	Quantity
Nema 17 Stepper Motor (1.8°, 1.8 A)	17HS8401	2
5mm to 5mm Motor Shaft Coupling	-	1
6mm Steel Rod (length 200mm)	-	2
6mm Linear Bearing (6x12x19 mm)	LM6UU	2
M5x0.8 Threaded Rod (length 170mm)	-	1
M5x0.8 hex nut	-	5
M3x0.5 socket head screws (length 20mm)	-	12
M3x0.5 socket head screws (length 10mm)	-	15
M3x0.5 socket head screws (length 8mm)	-	4
M3x0.5 socket head screws (length 6mm)	-	10
M3 hex nut	-	5
M3 thread lock hex nut	-	5
ISO 7379 M2X0.5 hex socket head screws (4 mm shoulder, 4 mm thread)	-	5
Tenma Digital-Control DC Power Supply 30V 5A	72-2690	1
Arduino Uno R3	A000066	1
TZT CNC Shield V3	-	1
DRV8825 Stepper Motor Driver	92TC5-A588	2
USB-B to USB-A cable	-	1
2.54 mm Pin Housing 4 Way	-	2
Dupont Terminal	-	8
2.54 mm Pin Jumper	-	3
GT2 Timing Belt Puller 16 tooth 5 mm bore	-	1
GT2 Timing Belt	-	1

Bibliography

[1] Georges Adam, Sagar Chowdhury, Maria Guix, Benjamin V Johnson, Chenghao Bi, and David Cappelleri. Towards functional mobile microrobotic systems. *Robotics*, 8(3):69, 2019.

[2] Pierre E Dupont, Bradley J Nelson, Michael Goldfarb, Blake Hannaford, Arianna Menciassi, Marcia K O'Malley, Nabil Simaan, Pietro Valdastri, and Guang-Zhong Yang. A decade retrospective of medical robotics research from 2010 to 2020. *Science Robotics*, 6(60):eabi8017, 2021.

[3] Tetsuya Nakamura and Akira Terano. Capsule endoscopy: past, present, and future. *Journal of Gastroenterology*, 43:93–99, 2008.

[4] Nikolaj Kofoed Mandsberg, Juliane Fjelrad Christfort, Khorshid Kamguyan, Anja Boisen, and Sarvesh Kumar Srivastava. Orally ingestible medical devices for gut engineering. *Advanced drug delivery reviews*, 165:142–154, 2020.

[5] Gerard Cummins. Smart pills for gastrointestinal diagnostics and therapy. *Advanced Drug Delivery Reviews*, 177:113931, 2021.

[6] Ana-Maria Singeap, Carol Stanciu, and Anca Trifan. Capsule endoscopy: the road ahead. *World journal of gastroenterology*, 22(1):369, 2016.

[7] Leonard R Johnson. *Physiology of the gastrointestinal tract*. Elsevier, 2006.

[8] Jacob Campbell, James Berry, and Yu Liang. Anatomy and physiology of the small intestine. In *Shackelford's Surgery of the Alimentary Tract, 2 Volume Set*, pages 817–841. Elsevier, 2019.

[9] Herbert F Helander and Lars Fändriks. Surface area of the digestive tract–revisited. *Scandinavian journal of gastroenterology*, 49(6):681–689, 2014.

[10] Elizabeth Thursby and Nathalie Juge. Introduction to the human gut microbiota. *Biochemical journal*, 474(11):1823–1836, 2017.

[11] Malin EV Johansson, Henrik Sjövall, and Gunnar C Hansson. The gastrointestinal mucus system in health and disease. *Nature reviews Gastroenterology & hepatology*, 10(6):352–361, 2013.

[12] Jason T Collins, Amanda Nguyen, and Madhu Badireddy. Anatomy, abdomen and pelvis, small intestine. 2017.

[13] Kajal S Patel and Aravind Thavamani. Physiology, peristalsis. In *StatPearls [Internet]*. StatPearls Publishing, 2023.

[14] JD Huizinga, CM McKay, and EJ White. The many facets of intestinal peristalsis. *American Journal of Physiology-Gastrointestinal and Liver Physiology*, 290 (6):G1347–G1349, 2006.

[15] Luke K Ursell, Jessica L Metcalf, Laura Wegener Parfrey, and Rob Knight. Defining the human microbiome. *Nutrition reviews*, 70(suppl_1):S38–S44, 2012.

[16] Jack A Gilbert, Martin J Blaser, J Gregory Caporaso, Janet K Jansson, Susan V Lynch, and Rob Knight. Current understanding of the human microbiome. *Nature medicine*, 24(4):392–400, 2018.

[17] Peter J Turnbaugh, Ruth E Ley, Micah Hamady, Claire M Fraser-Liggett, Rob Knight, and Jeffrey I Gordon. The human microbiome project. *Nature*, 449(7164): 804–810, 2007.

[18] Alessio Fasano and Carlo Catassi. Celiac disease. *New England Journal of Medicine*, 367(25):2419–2426, 2012.

[19] Carlo Catassi and Alessio Fasano. Celiac disease. *Gluten-free cereal products and beverages*, pages 1–I, 2008.

[20] William N Kelley and Vincent T DeVita. *Textbook of internal medicine*. 1989.

[21] David A Warrell, Timothy M Cox, David Weatherall, Edward J Benz Jr, and John D Firth. *Oxford textbook of medicine*. Oxford university press, 2003.

[22] Warren Strober, Ivan Fuss, Peter Mannon, et al. The fundamental basis of inflammatory bowel disease. *The Journal of clinical investigation*, 117(3):514–521, 2007.

[23] Jingbo Zhao, Donghua Liao, Rune Wilkens, Klaus Krogh, Henning Glerup, and Hans Gregersen. Bowel stiffness associated with histopathologic scoring of stenosis in patients with crohn's disease. *Acta Biomaterialia*, 130:332–342, 2021.

[24] Francesco Azzaroli, Laura Turco, Liza Ceroni, Stefania Sartoni Galloni, Federica Buonfiglioli, Claudio Calvanese, and Giuseppe Mazzella. Pneumatosis cystoides intestinalis. *World journal of gastroenterology: WJG*, 17(44):4932, 2011.

[25] Andrew C Dukowicz, Brian E Lacy, and Gary M Levine. Small intestinal bacterial overgrowth: a comprehensive review. *Gastroenterology & hepatology*, 3(2):112, 2007.

[26] Michael C Olson, Patrick J Navin, Christopher L Welle, and Ajit H Goenka. Small bowel radiology. *Current Opinion in Gastroenterology*, 37(3):267–274, 2021.

[27] Angela Cantatore and Pavel Müller. Introduction to computed tomography. *Kgs. Lyngby: DTU Mechanical Engineering*, 2011.

[28] Aladin Carovac, Fahrudin Smajlovic, and Dzelaludin Junuzovic. Application of ultrasound in medicine. *Acta Informatica Medica*, 19(3):168, 2011.

[29] Robert-Jan M Van Geuns, Piotr A Wielopolski, Hein G de Bruin, Benno J Rensing, Peter MA Van Ooijen, Marc Hulshoff, Matthijs Oudkerk, and Pim J de Feyter. Basic principles of magnetic resonance imaging. *Progress in cardiovascular diseases*, 42(2):149–156, 1999.

[30] William E Brant and Clyde A Helms. *Fundamentals of diagnostic radiology*. Lippincott Williams & Wilkins, 2012.

[31] Peter B Cotton and Christopher B Williams. *Practical Gastrointestinal Endoscopy: The Fundamentals*. John Wiley & Sons, 2008.

[32] Vinay Chandrasekhara, B Joseph Elmunzer, Mouen Khashab, and V Raman Muthusamy. *Clinical Gastrointestinal Endoscopy E-Book*. Elsevier Health Sciences, 2018.

[33] Gavriel Iddan, Gavriel Meron, Arkady Glukhovsky, and Paul Swain. Wireless capsule endoscopy. *Nature*, 405(6785):417–417, 2000.

[34] Naoki Hosoe, Kaoru Takabayashi, Haruhiko Ogata, and Takanori Kanai. Capsule endoscopy for small-intestinal disorders: Current status. *Digestive Endoscopy*, 31 (5):498–507, 2019.

[35] Lilli L Zwinger, Britta Siegmund, Andrea Stroux, Andreas Adler, Winfried Veltzke-Schlieker, Robert Wentrup, Christian Jürgensen, Bertram Wiedenmann, Felix Wiedbrauck, Stephan Hollerbach, et al. Capsocam sv-1 versus pillcam sb 3 in the detection of obscure gastrointestinal bleeding. *Journal of clinical gastroenterology*, 53(3):e101–e106, 2019.

[36] Chasyn Enns, Cherry Galorport, George Ou, and Robert Enns. Assessment of capsule endoscopy utilizing capsocam plus in patients with suspected small bowel disease including pilot study with remote access patients during pandemic. *Journal of the Canadian Association of Gastroenterology*, 4(6):269–273, 2021.

[37] Muhammad Rehan, Ibrahim Al-Bahadly, David G Thomas, Wayne Young, Leo K Cheng, and Ebubekir Avci. Smart capsules for sensing and sampling the gut: status, challenges and prospects. *Gut*, 2023.

[38] Ingestible thermometer pill aids athletes in beating the heat. *NASA Spinoff*, 2006.

[39] Pablo Cortegoso Valdivia, Alexander R Robertson, Nanne KH De Boer, Wojciech Marlicz, and Anastasios Koulaouzidis. An overview of robotic capsules for drug delivery to the gastrointestinal tract. *Journal of clinical medicine*, 10(24):5791, 2021.

[40] Marco Beccani, Gregorio Aiello, Nikolaos Gkotsis, Hakan Tunc, Addisu Taddese, Ekawahyu Susilo, Péter Völgyesi, Ákos Lédeczi, Elena De Momi, and Pietro Valdastri. Component based design of a drug delivery capsule robot. *Sensors and Actuators A: Physical*, 245:180–188, 2016.

[41] Sehyuk Yim and Metin Sitti. Shape-programmable soft capsule robots for semi-implantable drug delivery. *IEEE Transactions on Robotics*, 28(5):1198–1202, 2012.

[42] William H Crosby, US Army, and Heinz W Kugler. Intraluminal biopsy of the small intestine: the intestinal biopsy capsule. *The American journal of digestive diseases*, 2:236–241, 1957.

[43] SN Salem, RH Salt, and SC Truelove. Crosby small-intestinal capsule with radio-opaque tube and latex sheath. *Gut*, 6(1):99, 1965.

[44] Kyoung-Chul Kong, Jinhoon Cha, Doyoung Jeon, and Dong-il Dan Cho. A rotational micro biopsy device for the capsule endoscope. In *2005 IEEE/RSJ International Conference on Intelligent Robots and Systems*, pages 1839–1843. IEEE, 2005.

[45] Kyoungchul Kong, Sehyuk Yim, Sunhee Choi, and Doyoung Jeon. A robotic biopsy device for capsule endoscopy. 2012.

[46] Donghoon Son, Hunter Gilbert, and Metin Sitti. Magnetically actuated soft capsule endoscope for fine-needle biopsy. *Soft robotics*, 7(1):10–21, 2020.

[47] Angsagan Abdigazy, Mohammed Arfan, Gianluca Lazzi, Constantine Sideris, Alex Abramson, and Yasser Khan. End-to-end design of ingestible electronics. *Nature Electronics*, 7(2):102–118, 2024.

[48] Hung-Yu Yeh, Hsun-Chin Chao, Shih-Yen Chen, Chien-Chang Chen, and Ming-Wei Lai. Analysis of radiopaque gastrointestinal foreign bodies expelled by spontaneous passage in children: a 15-year single-center study. *Frontiers in pediatrics*, 6:172, 2018.

[49] Yeong Yeh Lee, Askin Erdogan, and Satish SC Rao. How to assess regional and whole gut transit time with wireless motility capsule. *Journal of neurogastroenterology and motility*, 20(2):265, 2014.

[50] Lavinia Barducci, Joseph C Norton, Sunandita Sarker, Sayeed Mohammed, Ryan Jones, Pietro Valdastri, and Benjamin S Terry. Fundamentals of the gut for capsule engineers. *Progress in Biomedical Engineering*, 2(4):042002, 2020.

[51] Ian Gibson. Additive manufacturing technologies 3d printing, rapid prototyping, and direct digital manufacturing, 2015.

[52] Ram K Gupta. *3D Printing: Fundamentals to Emerging Applications*. CRC Press, 2023.

[53] L Eith, RFT Stepto, I Tomka, and F Wittwer. The injection-moulded capsule. *Drug Development and Industrial Pharmacy*, 12(11-13):2113–2126, 1986.

[54] Lucia Zema, Giulia Loreti, Alice Melocchi, Alessandra Maroni, Luca Palugan, and Andrea Gazzaniga. Gastroresistant capsular device prepared by injection molding. *International journal of pharmaceutics*, 440(2):264–272, 2013.

[55] Edward M Trent and Paul K Wright. *Metal cutting*. Butterworth-Heinemann, 2000.

[56] MBADCU Alauddin, IA Choudhury, MA El Baradie, and MSJ Hashmi. Plastics and their machining: a review. *Journal of Materials Processing Technology*, 54 (1-4):40–46, 1995.

[57] Martin Christopher Allen, Simon Lookmire, and Ebubekir Avci. An alternative micro-milling fabrication process for rapid and low-cost microfluidics. *Micromachines*, 15(7):905, 2024.

[58] Feng Li, Suryakanth R Gurudu, Giovanni De Petris, Virender K Sharma, Arthur D Shiff, Russell I Heigh, David E Fleischer, Janice Post, Paula Erickson, and Jonathan A Leighton. Retention of the capsule endoscope: a single-center experience of 1000 capsule endoscopy procedures. *Gastrointestinal endoscopy*, 68(1): 174–180, 2008.

[59] Charlotte M Höög, Lars-Åke Bark, Juan Arkani, Jacob Gorsetman, Olle Broström, and Urban Sjöqvist. Capsule retentions and incomplete capsule endoscopy examinations: an analysis of 2300 examinations. *Gastroenterology research and practice*, 2012(1):518718, 2012.

[60] Artur Nemeth, Gabriele Wurm Johansson, Jörgen Nielsen, Henrik Thorlacius, and Ervin Toth. Capsule retention related to small bowel capsule endoscopy: a large european single-center 10-year clinical experience. *United European Gastroenterology Journal*, 5(5):677–686, 2017.

[61] Hyun Seok Lee, Yun Jeong Lim, Kyeong Ok Kim, Hyun Joo Jang, Jaeyoung Chun, Seong Ran Jeon, Yunho Jung, Ji Hyun Kim, Jae Jun Park, Sun-Jin Boo, et al. Outcomes and management strategies for capsule retention: a korean capsule endoscopy nationwide database registry study. *Digestive diseases and sciences*, 64: 3240–3246, 2019.

[62] Jihong Min, Yiran Yang, Zhiguang Wu, and Wei Gao. Robotics in the gut. *Advanced Therapeutics*, 3(4):1900125, 2020.

[63] Ágnes Varga, Tamás Kovács, and Amulya K Saxena. Analysis of complications after button battery ingestion in children. *Pediatric emergency care*, 34(6):443–446, 2018.

[64] Kristina Leinwand, David E Brumbaugh, and Robert E Kramer. Button battery ingestion in children: a paradigm for management of severe pediatric foreign body ingestions. *Gastrointestinal endoscopy clinics of North America*, 26(1):99, 2016.

[65] Sarker M Parvez, Farjana Jahan, Marie-Noel Brune, Julia F Gorman, Musarrat J Rahman, David Carpenter, Zahir Islam, Mahbubur Rahman, Nirupam Aich, Luke D Knibbs, et al. Health consequences of exposure to e-waste: an updated systematic review. *The Lancet Planetary Health*, 5(12):e905–e920, 2021.

[66] Muhammad Rehan, Ibrahim Al-Bahadly, David G Thomas, and Ebubekir Avci. Development of a robotic capsule for in vivo sampling of gut microbiota. *IEEE Robotics and Automation Letters*, 7(4):9517–9524, 2022.

[67] Felice Schnoll-Sussman and Ketan Kulkarni. Risks of capsule endoscopy. *Techniques in Gastrointestinal Endoscopy*, 10(1):25–30, 2008.

[68] Jose Fernando Waimin, Sina Nejati, Hongjie Jiang, Jake Qiu, Jianghsan Wang, Mohit S Verma, and Rahim Rahimi. Smart capsule for non-invasive sampling and studying of the gastrointestinal microbiome. *RSC advances*, 10(28):16313–16322, 2020.

[69] Peyman Shokrollahi, Yung P Lai, Samrand Rash-Ahmadi, Victoria Stewart, Mohsen Mohammadigheisar, Lee-Anne Huber, Naomi Matsuura, Anna EH Zavodni, John Parkinson, and Eric Diller. Blindly controlled magnetically actuated capsule for noninvasive sampling of the gastrointestinal microbiome. *IEEE/ASME Transactions on Mechatronics*, 26(5):2616–2628, 2020.

[70] Sanghyeon Park, Hyoryong Lee, Dong-in Kim, Hyeonwoo Kee, and Sukho Park. Active multiple-sampling capsule for gut microbiome. *IEEE/ASME Transactions on Mechatronics*, 27(6):4384–4395, 2022.

[71] Itay Abuhav. Iso 13485: 2016: a complete guide to quality management in the medical device industry, 2018.

[72] ASTM International. Recognized consensus standards: Medical devices, 2019. ASTM F1855-00.

[73] ASTM International. Standard specification for implantable polytetrafluoroethylene (ptfe) sheet, tube, and rod shapes fabricated from granular molding powders, 2015. ASTM F754-08.

[74] ASTM International. Standard specification for polyetheretherketone (peek) polymers for surgical implant applications, 2023. Designation: F2026-23.

[75] M Nachman and SE Franklin. Artificial skin model simulating dry and moist in vivo human skin friction and deformation behaviour. *Tribology International*, 97: 431–439, 2016.

[76] Sam Peerlinck, Frauke Willemyns, Dominiek Reynaerts, and Benjamin Gorissen. Biomimetic small intestinal peristalsis simulator using circumferential pneumatic artificial muscles (cirpam). *Advanced Materials Technologies*, 9(4):2301662, 2024.

[77] A Sina Booeshaghi, Eduardo da Veiga Beltrame, Dylan Bannon, Jase Gehring, and Lior Pachter. Principles of open source bioinstrumentation applied to the poseidon syringe pump system. *Scientific reports*, 9(1):12385, 2019.

[78] Steven Dirven, Feijiao Chen, Weiliang Xu, John E Bronlund, Jacqueline Allen, and Leo K Cheng. Design and characterization of a peristaltic actuator inspired by esophageal swallowing. *IEEE/ASME Transactions on Mechatronics*, 19(4): 1234–1242, 2013.

[79] Gregory A Formosa, Joseph Micah Prendergast, Jinghui Peng, Donald Kirkpatrick, and Mark E Rentschler. A modular endoscopy simulation apparatus (mesa) for robotic medical device sensing and control validation. *IEEE Robotics and Automation Letters*, 3(4):4054–4061, 2018.

[80] Grace Ng Cui Fang. *Novel methods to characterise texture changes during food breakdown*. PhD thesis, School of Food and Advanced Technology, Massey University, New Zealand, 2018.

[81] Gaofeng Shi, Hui Jiang, Jianrong Feng, Xian Zheng, Dongjian Zhang, Cuihua Jiang, and Jian Zhang. Aloe vera mitigates dextran sulfate sodium-induced rat ulcerative colitis by potentiating colon mucus barrier. *Journal of Ethnopharmacology*, 279:114108, 2021.

[82] Aude-Marine Paepegaey, Matthew L Barker, David W Bartlett, Miten Mistry, Nicola X West, Nicola Hellin, Louise J Brown, and Philip G Bellamy. Measuring enamel erosion: a comparative study of contact profilometry, non-contact profilometry and confocal laser scanning microscopy. *Dental Materials*, 29(12):1265–1272, 2013.

[83] James A Greenwood and JB Pl Williamson. Contact of nominally flat surfaces. *Proceedings of the royal society of London. Series A. Mathematical and physical sciences*, 295(1442):300–319, 1966.